



Pablo Albuquerque Godoy

**Adsorption behavior of cocamidopropylbetaine
on analogous reservoir rocks at static and
dynamic conditions**

Dissertação de Mestrado

Dissertation presented to the Programa de Pós-graduação em Química of PUC-Rio in partial fulfillment of the requirements for the degree of Mestre em Química.

Advisor: Prof. Aurora Pérez Gramatges
Coadvisor: Dr. Juliana Maria da Fonseca Façanha

Rio de Janeiro
August 2023



Pablo Albuquerque Godoy

**Adsorption behavior of cocamidopropylbetaine
on analogous reservoir rocks at static and
dynamic conditions**

Dissertation presented to the Programa de Pós-graduação em Química of PUC-Rio in partial fulfillment of the requirements for the degree in Mestre em Química. Approved by the Examination Committee.

Prof. Aurora Pérez Gramatges

Advisor
Departamento de Química – PUC-Rio

Dr. Juliana Maria da Fonseca Façanha

Coadvisor
Shell Brasil - Matriz

Prof. Marcio da Silveira Carvalho

Departamento de Engenharia Mecânica – PUC-Rio

Prof. Carla Luciane Manske Camargo

Escola de Química – UFRJ

Rio de Janeiro, August 11, 2023

Todos os direitos reservados. É proibida a reprodução total ou parcial do trabalho sem a autorização do autor, do orientador e da universidade.

Pablo Albuquerque Godoy

Graduou-se em Engenharia Mecânica (PUC-Rio) em 2021. Enquanto cursava sua graduação, foi aluno de Iniciação Científica em Química e estagiário no Laboratório de Físico-Química de Surfactantes (LASURF/PUC-Rio) onde desempenhou atividades de pesquisa em projetos ligados à indústria de óleo e gás, desde o desenvolvimento de software, modelos para previsão de propriedades físico-químicas e simulação de fenômenos em meio poroso, como também análise de imagens. Atual membro do LASURF, realiza pesquisas para o projeto: “Desenvolvimento de formulações contendo surfactantes e nanopartículas para controle de mobilidade de gás usando espumas para Recuperação Avançada de Petróleo”.

Bibliographic data

Godoy, Pablo Albuquerque

Adsorption behavior of cocamidopropylbetaine on analogous reservoir rocks at static and dynamic conditions / Pablo Albuquerque Godoy ; advisor: Aurora Pérez Gramatges ; co-advisor: Juliana Maria da Fonseca Façanha. – 2023.

144 f. : il. color. ; 30 cm

Dissertation (masters)–Pontifícia Universidade Católica do Rio de Janeiro, Departamento de Química, 2023. Includes bibliography

1. Chemistry – Theses. 2. Enhanced Oil Recovery. 3. Colloids. 4. Adsorption. 5. Surfactant. 6. Modelling. I. Pérez Gramatges, Aurora. II. Façanha, Juliana Maria da Fonseca. III. Pontifícia Universidade Católica do Rio de Janeiro. Departamento de Química. IV. Title.

CDD: 540

To my parents, Mauro and Cristina, and my brother Diego.

For all the love and support.

Acknowledgements

I would like to thank my mother, Maria Cristina, for the effort in bringing me to the world and for the greater effort in raising me and my brother Diego, despite all the difficulties. I would be nothing without my family and I love you two. I also thank my aunts Fátima, Glória and Bernadete for all support you gave through life, and my cousins Ana Paula, Leonardo, Fernanda, Roberta and Renata for such nice memories and for all the support.

Thanks to my advisor Prof^a Aurora Perez who had the greatest amount of patience to get me through this master's course and taught a lot to me through the lectures and talks. Thank you for being such an incredible and wise advisor, and for having me on your research group. I'm so grateful for what I learned in all these years in LASURF, since as an undergraduate.

I'm also grateful for the advice and experience of my coadvisor, Dr^a Juliana Façanha, who always encouraged me to do my best and to always criticize my own work in a good and productive way.

A special thanks to all LASURF staff: Felipe Ricardo, Caio Mello, Daniel Vicente, couldn't do anything without their patience to teach me hands-on techniques and to get me through all tasks I needed to do. Also, for the good company throughout all these years.

A thanks to Leandro Lopes and Tatiana Berna, for their company, help and for getting me through the coreflood experiments. Their practical knowledge (especially the help) was essential for me to understating a lot of the HPHT area, where I used to fear operating when I joined LASURF.

A thanks to Luis Maqueira who taught me a lot about chromatography and other analytical techniques, and for the valuable insights and the great company.

A thanks to Bruno Giordano for the help with surface tension measurements and for the spontaneous debates at lunch time.

Also, a great thanks to Francisco from the Laboratorio de Microtomografia de Raios-X, at PUC-Rio, for helping me with the acquisition and treatment of the CT images.

Thanks to Alexandr from Laboratorio de Mecanica de Rochas at PUC Rio for the help with petrophysical measurements.

I also thank to all my LASURF colleagues, and ex-LASURF, who had always been nice to me and for making me feel very welcomed throughout my journey: Alexandre, Júlio, André, Luis Miguel, Alessandra, Lina, Cecília, Beatriz, Vinícius, Brenda, Eduardo, Angela, and Priscilla.

A thanks to my friends: Lucas (Zaca), Luis Andre, Maria Clara, and Lorena, who gave me support on this rough year, with all the great and happy meetings at Zaca's house. Also, to João Alvim, Omar, Patrick and Pedro who gave me so good memories from high school that I could enjoy in difficult times. I could not miss my running partners and friends: Fontes, Ian and Rubens who encouraged me to have such a great hobby. A thanks to Lucas Martins for the friendship and for all the good talks at PUC.

A special thanks to my deceased beloved ones: my friend Mauricio, who inspired me to be a chilled person despite the hostilities of the world, to my grandparents João, Lourdes, Pedro, and Maria, who I carry memories of great love and care. And to my father Mauro who inspired me to seek education, not only to ascend socially, but to help me become a wise person of integrity and character. Despite your flaws, life was always interesting with you.

And, finally, a warm thanks for my love, Beatriz, who always inspired me to be a better version of myself, who is also the greatest company on earth and the one who I have the most gratitude for sharing this life with. Love you so much.

I would like to thank Shell and CNPq for the scholarship provided to me during the work of this dissertation at LASURF.

This study was financed in part by the Coordenação de Aperfeiçoamento de Pessoal de Nível Superior - Brasil (CAPES) - Finance Code 001

Abstract

Albuquerque Godoy, Pablo; Pérez Gramatges, Aurora; da Fonseca Façanha, Juliana Maria. **Adsorption behavior of cocamidopropylbetaine on analogous reservoir rocks at static and dynamic conditions.** Rio de Janeiro, 2023. 144p. Dissertação de Mestrado – Departamento de Química, Pontifícia Universidade Católica do Rio de Janeiro.

The use of zwitterionic surfactants in enhanced oil recovery projects is limited to adsorption on the surface of the reservoir rock, which must be predicted to determine the economic feasibility of these projects. However, there is a lack of models capable of estimating this adsorption and explaining the involved mechanisms. The objective of this study was to provide models that could estimate the adsorption of a zwitterionic surfactant (CAPB) and explain its adsorption mechanisms. Experiments were conducted on carbonate and sandstone rocks using static tests with particulate rock and dynamic tests within rock cores. A methodology was developed to quantify CAPB in brine using high-performance liquid chromatography. As a distinguishing feature, the adsorption was normalized by the specific surface area of the rock, determined through BET analysis (static tests) and microtomography with μ CT-scan (dynamic tests). The results were interpreted with empirical and theoretical models integrated with surface potential estimates. For carbonate, it was observed that the first layer of adsorption follows a homogeneous pattern, limited by electrostatic repulsion with the surface, while the second layer follows heterogeneous adsorption, forming surfactant aggregates mediated by hydrophobic interactions between the tails. For sandstone, both layers exhibit a heterogeneous distribution, explaining the higher adsorption between the two rocks. It was concluded that bilayer models are capable of reliably explaining and estimating adsorption under flow conditions, and the surface area was the most relevant factor in the difference of dynamic adsorption between rocks, favored in sandstone.

Keywords:

Enhanced Oil Recovery, Colloids, Adsorption, Surfactant, Modelling

Resumo

Albuquerque Godoy, Pablo; Pérez Gramatges, Aurora; da Fonseca Façanha, Juliana Maria. **Comportamento de adsorção da cocamidopropil betaína em rochas reservatório análogas em condições estáticas e dinâmicas**. Rio de Janeiro, 2023. 144p. Dissertação de Mestrado – Departamento de Química, Pontifícia Universidade Católica do Rio de Janeiro.

O uso de surfactantes zwitteriônicos em projetos de recuperação avançada de petróleo está limitado à adsorção na superfície da rocha-reservatório, que deve ser prevista para determinar a viabilidade econômica desses projetos. Porém, existe uma falta de modelos capazes de estimar essa adsorção e explicar os mecanismos envolvidos. O objetivo do trabalho foi providenciar modelos que pudessem estimar a adsorção de um surfactante zwitteriônico (CAPB), e explicar seus mecanismos de adsorção. Os experimentos foram realizados em rochas do tipo carbonato e arenito, através de testes com rocha particulada (estáticos) e no interior de núcleos de rocha (dinâmicos). Foi desenvolvida uma metodologia para quantificar o CAPB em salmoura utilizando a cromatografia líquida de alta eficiência. Como um diferencial, a adsorção foi normalizada pela área superficial específica da rocha, através de análise BET (testes estáticos) e microtomografia com μ CT-scan (testes dinâmicos). Os resultados foram interpretados com modelos empíricos e teóricos integrados às estimativas de potencial de superfície. Verificou-se para o carbonato, que a primeira camada de adsorção segue um padrão homogêneo, limitada por repulsão eletrostática com a superfície, enquanto a segunda camada segue uma adsorção heterogênea, onde são formados agregados de surfactante mediados por interações hidrofóbicas entre as caudas. Para o arenito, as duas camadas têm uma distribuição heterogênea, explicando a maior adsorção entre as duas rochas. Concluiu-se que os modelos de dupla camada são capazes de explicar e estimar a adsorção em condições de fluxo de forma confiável e a área superficial foi o fator mais relevante na diferença de adsorção dinâmica entre rochas, favorecida no arenito.

Palavras-chave:

Recuperação Avançada, Coloides, Adsorção, Surfactante, Modelagem

Table of contents

1. Introduction.....	22
1.1 Increasing oil demand.....	22
1.2 Enhanced Oil Recovery (EOR)	22
1.3 Surfactant loss in porous media.....	24
2. Objectives.....	27
3. Main concepts	28
3.1 Surfactants and adsorption	28
3.2 Surfactants aggregation and CMC.....	29
4. Literature review on surfactant adsorption.....	31
4.1 Effects and influence of adsorption parameters on surfactant adsorption	32
4.1.1 Influence of surfactant concentration.....	32
4.1.2 Effect of salinity	34
4.1.3 Effect of temperature	35
4.1.4 Effect of alkalis and pH.....	37
4.2 Static and dynamic adsorption of zwitterionic surfactants.....	39
4.2.1 Static adsorption models	43
4.2.1.1 Langmuir isotherm	43
4.2.1.2 Freundlich isotherm	44
4.2.1.3 Redlich-Peterson isotherm.....	44
4.2.1.4 Sips isotherm	45
4.2.1.5 Alternative isotherms and Bilayer approach..	45
4.2.2 Dynamic adsorption models	49
4.3 Surface complexation model.....	53
5. Materials and Methods	59
5.1 Surfactant, brine and rocks	59
5.1.1 Surfactant characteristics and properties	59
5.1.2 Brine (DSW) composition and properties	60
5.1.3 Rocks characteristics and properties.....	61
5.2 Surfactant characterization and quantification	63

5.2.1 Determination of CAPB critical micelle concentration (CMC).....	63
5.2.2 Determination of CAPB absorption spectrum.....	63
5.2.3 Quantification of CAPB by High performance liquid chromatography (HPLC)	63
5.3 Methodology for Static Adsorption Experiments	64
5.3.1 Preparation of rock samples.....	64
5.3.2 Determination of superficial area by Brunauer-Emmett-Teller (BET) adsorption isotherm.....	65
5.3.3 Methodology for static adsorption test.....	66
5.3.4 Methodology for zeta potential and surface complexation modelling.....	68
5.3.5 Adsorption isotherm fitting for static adsorption results	68
5.4 Determination of dynamic adsorption through flow tests.....	69
5.4.1 Preparation and petrophysical characterization of rock plugs for the experiments	69
5.4.2 Determination of rock cores surface area (pore space) using microtomography	70
5.4.3 Methodology for dynamic adsorption experiments	74
5.4.4 History-matching of experimental dynamic adsorption data	76
6. Results and Discussion	79
6.1 Results of surfactant characterization and quantification	79
6.1.1 Determination of CAPB critical micelle concentration (CMC).....	79
6.1.2 CAPB identification and quantification through HPLC	80
6.1.2.1 Results from determination of CAPB absorption spectrum	80
6.1.2.2 Results from method of quantification of CAPB by HPLC.....	81
6.2 Specific Surface Area (SSA) results for static and dynamic experiments	82

6.2.1 Results of specific surface area from Brunauer-Emmett-Teller (BET) adsorption isotherm	82
6.2.2 Results of specific surface area from μ CT-scan image analysis	84
6.3 Adsorption behavior and mechanisms of CAPB adsorption on sandstone and limestone	85
6.3.1.1 Results of CAPB static adsorption behavior	85
6.3.1.2 Evaluation of static adsorption results by analysis of estimated rock surface potential and speciation	88
6.3.1.3 Fitting of static adsorption results with monolayer models	92
6.3.1.4 Fitting of static adsorption results with bilayer models	96
6.3.2 Results of dynamic adsorption experiments and history-matching of experimental results	101
6.3.2.1 Evaluation of brine-rock interactions through dispersion and ion concentration profile	101
6.3.2.2 Ion profiles on sandstone	101
6.3.2.3 Ion profiles on limestone	103
6.3.3 Determination of dynamic adsorption by comparison of breakthrough curves for CAPB and tracer	105
6.3.4 Evaluation of history-match models for Li ⁺ and CAPB on limestone core	107
6.4 Adsorption estimation in dynamic conditions with the best history-match model	109
7. Conclusions	111
8. Bibliography	113
9. Appendix	125
9.1 Results of selected liquid to solid ratio for static experiments	125
9.2 Results of surface potential at literature conditions for validation of the SCM	126
9.3 PHREEQc script for surface potential and speciation estimates	128
9.3.1 DSW/Calcite	128

9.3.2 DSW/Quartz/Kaolinite.....	129
9.4 Rights and permissions of images utilized	133

List of figures

Figure 1: Incremental oil recovered by EOR project. Adapted from [3]	23
Figure 2: Example of EOR processes. Adapted from [9], Copyright 2023, with permission from Elsevier.....	23
Figure 3: Mechanisms of surfactant retention in porous media	25
Figure 4: Types of surfactants, adapted from Alconox.com [14].....	28
Figure 5: Elements of adsorption on solid-liquid interfaces. Used with permission of Butt, HJ et al., from [16]; permission conveyed through Copyright Clearance Center, Inc.	29
Figure 6: Representation of aqueous surfactant solutions above CMC, depicting the equilibria involving monomers, micelles, and adsorbed surfactant molecules at the interface for zwitterionic surfactant.	30
Figure 7: Other surfactant aggregates. Used with permission of Butt, HJ et al., from [16]; permission conveyed through Copyright Clearance Center, Inc.	30
Figure 8: Common surfactant adsorption mechanisms: (a) ion-exchange, (b) ion pairing, (c) hydrogen bonding, hydrophobic bonding on (d) uncharged surface and (e) oppositely charged surface and (f) dispersion forces on nonpolar surface. Used with permission of Rosen, M.J., from [15], Copyright 2023; permission conveyed through Copyright Clearance Center, Inc.	31
Figure 9: Surfactant adsorption with increase in equilibrium concentration. Adapted from [25]......	32
Figure 10: Adsorption maxima phenomenon in zwitterionic surfactant solutions at different salinities. Adapted with permission from Nieto-Alvarez et al. [32]. Copyright 2023 American Chemical Society.....	33
Figure 11: Adsorption of zwitterionic surfactant (LB-lauryl betaine) on different minerals at 20°C and 80°C. Adapted from [45], Copyright 2023, with permission from Elsevier.....	36
Figure 12: Effect on temperature on carboxylbetaines BW and CA at (a) 100 mg L ⁻¹ and (b) 1000 mg L ⁻¹ surfactant concentration. Adapted with permission from Zhong et al. [35]. Copyright 2023 American Chemical Society.....	37

Figure 13: Effect of pH on the adsorption of different types of surfactants: SDS (anionic), CTAB (cationic) and Tergitol 15-S-7 (non-ionic). Adapted from [48], Copyright 2023, with permission from Elsevier.....	38
Figure 14: Betaine (a) static adsorption and (b) breakthrough curves with different alkali addition. Adapted from [33], Copyright 2023, with permission from Elsevier.	40
Figure 15: Structural formula and static and dynamic adsorption of (a) CAPB and (b) CAO on natural sandstone cores. (a) Used with permission of Dai et al. from [12], Copyright 2023; permission conveyed through Copyright Clearance Center, Inc. (b) Adapted from [52], Copyright 2023, with permission from Elsevier.	41
Figure 16: Structure of micelle, hemimicelle and admicelle. Adapted from [62], Copyright 2023, with permission from Elsevier.....	46
Figure 17: Bilayer model adjusting well breakthrough curves of surfactant in Berea sandstone. Adapted from [64], Copyright 2023, with permission from Elsevier.....	51
Figure 18: Stern layer and Diffusive Double Layer. The largest and smallest white circles are oxygen and hydrogen atoms, respectively, and the black circles represent solvated ions. The inner sphere complexes are formed between the 0-plane and the 1-plane of the stern layer, and the outer sphere complexes are formed at a minimum distance of approach of hydrated ions .Adapted from [75], Copyright 2023, with permission from Elsevier.	54
Figure 19: Surface potentials determination through CD-MUSIC equations. Adapted from Bonto, María et al. [82].....	56
Figure 20: CAPB molecular structure, from [88]	59
Figure 21: Rock cores, adapted from [95]	61
Figure 22: (a) Indiana Limestone and (b) Berea Spider Sandstone cores	62
Figure 23: Schematic of static adsorption methodology	67
Figure 24: The process of image acquisition in a CT-scan.....	71
Figure 25: Core image default and binarized image	71
Figure 26: REV extracted from core 3D image and projections shown in Avizo software	72
Figure 27: Visualization of Centroid Path Tortuosity (CPT), adapted from [105]	73

Figure 28: Example of cropped tortuosity REV in Berea and Indiana cores at 6 μm /pixel of resolution.....	74
Figure 29: Dynamic adsorption setup and methodology.....	76
Figure 30: Surface tension measurements and linear adjustment.....	79
Figure 31: CAPB (tagged as ZW11) absorbance spectrum.....	80
Figure 32: CAPB (tagged as ZW11) chromatogram peak	81
Figure 33: CAPB calibration curves in DSW for HPLC	82
Figure 34: Isotherm plot for N_2 adsorption on Berea Buff sandstone.....	83
Figure 35: Isotherm plot for N_2 adsorption on Indiana limestone	83
Figure 36: SSA_{vol} extrapolation with image resolution	84
Figure 37: CPT extrapolation through μCT -scan image resolution.....	84
Figure 38: Static adsorption of CAPB on (a) Berea Buff Sandstone and (b) Indiana limestone, (c) both per mass of rock and (d) both per BET area .	86
Figure 39: a) Zeta potential estimation from CD-MUSIC built-in PHREEQC for the brine and mineral equilibrium. b) Surface speciation of the quartz/kaolinite equilibrium with DSW per mass of sandstone. v) Surface speciation of the calcite equilibrium with DSW per mass of limestone.	89
Figure 40: CAPB interactions with probable surface species by CD-MUSIC triple layer model	91
Figure 41: Adjusted isotherm models from monolayer approach	92
Figure 42: Best-fit isotherm models, monolayer approach.	93
Figure 43: Monolayer approach proposed mechanisms.....	95
Figure 44: Adjusted isotherm models for bilayer approach.....	96
Figure 45: Best-fit isotherm models, bilayer approach	97
Figure 46: Potential mechanisms of CAPB adsorption on Indiana Limestone	99
Figure 47: Potential mechanisms of CAPB adsorption on Berea Sandstone	100
Figure 48: Monovalent cations profile during adsorption on sandstone..	102
Figure 49: Divalent cations profile during adsorption on sandstone	102
Figure 50: Monovalent cations profile during adsorption on limestone ...	103
Figure 51: Divalent cations profile during adsorption on limestone	104
Figure 52: Breakthrough curves of CAPB and tracer for limestone	105
Figure 53: Breakthrough curves of CAPB and tracer for sandstone	106

Figure 54: History-match of CAPB adsorption and desorption data in limestone core	108
Figure 55: Extended breakthrough curves of CAPB and Li+ (tracer).....	109
Figure 56: CAPB chromatograms peaks with different liquid to solid ratios	125
Figure 57: Variability of liquid to solid ratios in CAPB adsorption on Indiana Limestone.....	125
Figure 58: Zeta potential experimental data vs TL model for calcite [80]	126
Figure 59: Zeta potential experimental data vs TL model for sandstone [81]	127

List of tables

Table 1: Static adsorption isotherm models.....	48
Table 2: Dynamic adsorption models presented in [64].....	51
Table 3: Other dynamic adsorption models developed from classical isotherm models	52
Table 4: PHREEQc sites parameters	57
Table 5: CD-MUSIC parameters on PHREEQc.....	58
Table 6: DSW composition and physical-chemical properties	60
Table 7: Rock subtypes and main characteristics	61
Table 8: Core samples basic petrophysical properties	62
Table 9: Total K_w of each core sample	75
Table 10: Boundary and initial conditions applied for hydrodynamic dispersion equations	77
Table 11: Calibration curves evaluation metrics	82
Table 12: BET Specific Surface Area of the sandstone and limestone powder.....	83
Table 13: REV data for each core	85
Table 14: Calculated pore space properties for each core	85
Table 15: Maximum CAPB static adsorption on static experiments	87
Table 16: Change of solution properties with batch experiments	87
Table 17: Estimated vs measured physical-chemical properties of the equilibrated brine.....	88
Table 18: Estimated surface sites density and polarity.....	90
Table 19: Evaluation metrics of adjusted isotherm models from monolayer approach. Best fit models are highlighted.....	92
Table 20: Sips and Redlich-Peterson isotherms parameters from best fit	93
Table 21: Evaluation metrics of adjusted isotherm models from bilayer approach. Best fit models are highlighted.....	97
Table 22: R-P-Sips and Langmuir-R-P isotherms parameters from best fit	97
Table 23: Transport properties in the pore space for both cores	101
Table 24: Dynamic adsorption from breakthrough curves	106
Table 25: History-match model performance for core effluent data	107

Table 26: Bilayer (kinetic) parameters from best history-match..... 109

List of abbreviations and symbols

q_{∞} : maximum adsorption capacity

q : adsorption per mass of rock

Γ : adsorption per surface area

C_e : equilibrium concentration

> $SiOH$: Silanol surface site

> $AlOH$: Aluminum hydroxide surface site

> $CaOH$: Calcium hydroxide surface site

> CO_3H : Carbonate surface site

Adj-R²: Adjusted R²

ASP: Alkaline Surfactant Polymer

BET: Brunauer-Emmett-Teller

BS: Berea Sandstone

CAPB: Cocamidopropylbetaine

CAO: Cocamidopropyl dimethyl amine oxide

CD: Charge Distribution

CENPES: Centro de Pesquisas e Desenvolvimento Leopoldo Américo Miguez de Mello

CETEM: Centro de Tecnologia Mineral

CMC: Critical Micelle Concentration

CPT: Centroid Path Tortuosity

CT: Computed Tomography

CTAB: Centrimum bromide

PHREEQc: pH-Redox-Equilibrium C-program

DAD: Diode Array Detector

DDL: Diffuse Double Layer

DMAPA: Dimethylaminopropylamine

DSW: Desulfated Seawater

EDL: Electrical double layer

EOR: Enhanced Oil Recovery

FAWAG: Foam-Assisted-Water-Alternating-Gas

GOR: Gas Oil Ratio

HPLC: High Performance Liquid Chromatography
ICP-OES: Inductively Coupled Plasma – Optical Emission Spectrometry
IFT: Interfacial Tension
LABSPECTRO: Laboratório de Espectrometria Atômica
LMR: Laboratório de Mecânica de Rochas
LXS: Linear xylene sulphonate
MATLAB: Matrix Laboratory
MUSIC: Multi-Site Complexation Model
PDI: Potential Determining Ions
PV: Pore Volumes
REV: Representative Elementary Volume
RMSE: Root Mean Square Error
RP: Redlich-Peterson
SA: Surface Area
SCM: Surface Complexation Model
SDS: Sodium Dodecyl Sulfate
SSA: Specific Surface Area
TL: Triple-Layer
TP: Three-Plane model
UV: Ultra-Violet
WSS: Weighted Sum of Squares
ZW: Zwitterionic

“All models are wrong, but some are useful.”

– George E. P. Box

1. Introduction

1.1 Increasing oil demand

Global demand for oil is likely to increase in the coming years. According to the short-term outlook reported in 2022 by the U.S. Energy Information Administration [1], the average consumption of oil and liquid fuels in 2022 is expected to be 99.4 million barrels/day, 2.1 million barrels/day more than the 2021 average. Likewise, it is expected to be an increase of 2.1 million barrels / day in the average consumption for the year 2023 [1]. Thus, to meet the demand, it is necessary to explore new oil reservoirs or increase the production of existing ones. Due to the decrease in natural oil reserves over the last decades and the projected quantities of oil in new reservoirs [2], there are more incentives to develop methods that can extend the productive life of active reservoirs and reduce greenhouse gases emitted by operations. That's when tertiary recovery methods are helpful, making these processes more efficient and sustainable.

1.2 Enhanced Oil Recovery (EOR)

At the beginning of the productive life of a reservoir, the available natural energy is used as the driving energy of recovery, for example: expansion of rock and fluids, influx of water, and solubilization of gases [3, 4]. Because it does not require injection of external fluids, this first recovery process is characterized as primary [3, 4]. In the secondary phase, there is injection of external fluids such as water and/or gas with the intention of maintaining the reservoir pressure and improving the volumetric efficiency of sweeping [4]. The tertiary phase includes any recovery method after the secondary phase. Primary and secondary recovery methods are classified as conventional oil recovery methods, and tertiary methods as Enhanced Oil Recovery (EOR) methods [3].

Enhanced Oil Recovery (EOR) can be defined as the oil recovery that occurs when injecting materials which are not normally present in the reservoir [3,4]. When the rate of oil production declines in a well, reservoir or field, an EOR project is initiated and its success can be determined by the amount of incremental oil recovered, i.e., the difference between oil production after the start of the EOR

project and the forecasted decline in production before the implementation of the project [3], as illustrated in Figure 1.

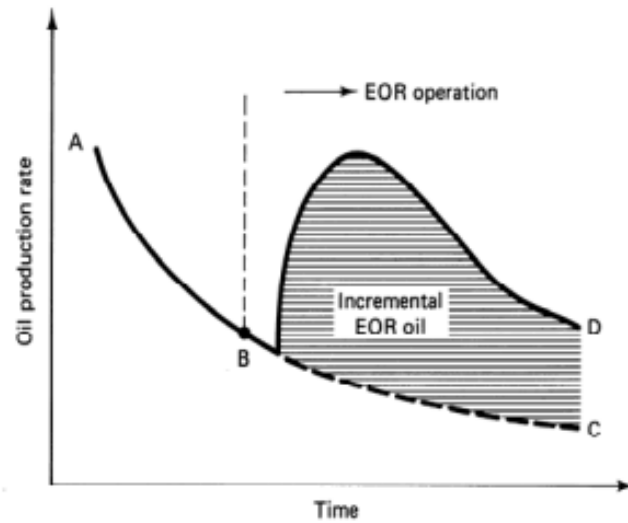


Figure 1: Incremental oil recovered by EOR project. Adapted from [3]

The EOR processes aim at the extraction of oil that would be irrecoverable by conventional methods [3]. For this, thermal energy is applied as well as injected chemicals, or gases (miscible) into the reservoirs (Figure 2).

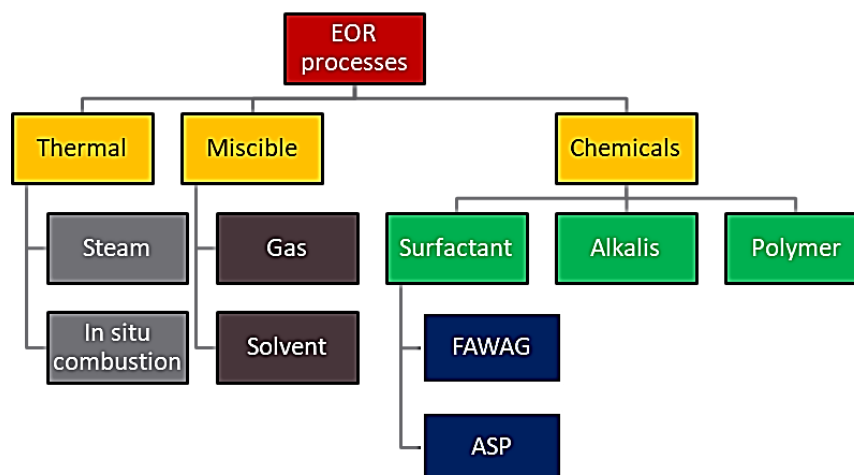


Figure 2: Example of EOR processes. Adapted from [9], Copyright 2023, with permission from Elsevier.

Among the injected chemicals in EOR processes are polymers, alkalis, and surfactants. The application of these substances can also occur through combinations of the three (ASP – Alkaline Polymer Surfactant flooding) [4]. The polymers act mainly in the control of mobility of the injected aqueous phase [4]. Alkalis, such as sodium hydroxide, are responsible for the deprotonation of the organic acids present in the oil (e.g., naphthenic acids) forming surfactant species *in situ* [5]. In the case of surfactants, they can be generated by the injection of alkalis or injected directly, with the purpose of reducing the interfacial tension (IFT) between the oil and the aqueous phase, favoring capillary displacement [4].

Another important type of surfactant application in EOR processes is in Foam Assisted Water Alternating Gas (FAWAG) methods. In this technology, a slug of surfactant is injected at the end of the waterflood, allowing foam to be formed in the reservoir during the gas injection, improving gas conformance control. Gas mobility is improved because when foam is formed, the gas is transported as a dispersed phase within a surfactant-laden continuous liquid phase [110]. Foam is transported as a pseudo-fluid in the pore space because the surfactant retards the coalescence of generated bubbles, and it has been demonstrated that foam selectively reduces gas mobility [6]. Foam mobility is reduced in more permeable zones, trapping the gas phase, and allowing diversion of gas towards less permeable zones. This results in a decrease in the gas/oil ratio (GOR) produced, and in mitigating gas coning near the production wells [7].

Both the ASP and FAWAG applications need the injection of a high quantity of surfactant in the reservoir (surfactant slug). However, this quantity must not be underestimated, to not compromise its effects on recovery, and must not be overestimated to add high production costs, since surfactants are an expensive material to be produced in such scale. This issue demands the prediction of surfactant loss in the porous media, to adjust the required manufactured quantity of surfactant needed to the EOR operation and evaluate its economic feasibility, since the cost of surfactant could reach half or more of the total EOR project cost [4].

1.3 Surfactant loss in porous media

Surfactant can divert from its objective in the porous media by three main mechanisms: precipitation, phase trapping and adsorption [8]. Partitioning will also

occur in the presence of the oil phase [9], where the nonpolar medium will solvate part of the surfactant initially in the aqueous phase because of its hydrophobic characteristics. Neglecting the contact with oil is reasonable at evaluating its loss because the surfactant could go through a lot of oil-empty pores before reaching oil (for lowering IFT purposes) or reaching the high permeability zones (for foaming purposes). Also, precipitation is likely to occur in harsh reservoir conditions of high salinity and temperatures, for example, in the presence of high concentration of divalent cations [10], but it can be minimized with previous surfactant screening, choosing the ones tolerant for high temperature and salinity conditions.

Cocamidopropylbetaine, or CAPB, the surfactant utilized in this work, is highly soluble in water and can resist harsh salinities and temperatures [11,12]. CAPB is also a biodegradable surfactant, and some bacteria found on marine environment are capable of fast and total biodegradation of this compound [91]. This means that CAPB could be a great option for application in subsurface operations by reducing environmental risks.

In terms of the retention mechanisms, only phase trapping and adsorption on pore surface were investigated in this work. Phase trapping, which means dispersion, and diffusivity of the surfactant into dead-end pores, could account for some significant retention. However, surfactant adsorption can account for even more retention, depending on the interfacial phenomena and interactions between the rock surface and the surfactant in aqueous solution. These two mechanisms are illustrated in Figure 3:

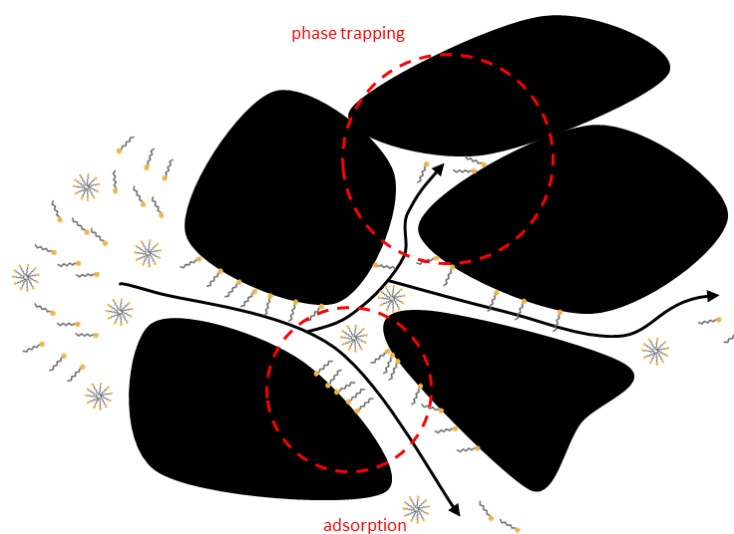


Figure 3: Mechanisms of surfactant retention in porous media

In the end, understanding the main interactions at the surfactant flooding conditions is crucial to the surfactant selection for EOR processes. These interactions can be inferred from retention studies in static and dynamic experiments at the laboratories. The static experiments focus on surfactant being equilibrated with suspended rock powder, and the remaining surfactant concentration is determined for maximum adsorption calculation as a function of the total concentration. In the dynamic experiments, the surfactant solution is continuously injected through the rock (as cores), and the effluent concentration is quantified at different injection volumes for adsorption determination.

Despite the ways of determining surfactant adsorption, this phenomenon needs to be predicted with reliable models to not compromise the economic feasibility of EOR projects associated with the application of surfactants.

There is a lack of models that represent the adsorption behavior of surfactants on rocks under static and dynamic conditions and could explain the complexity of this phenomenon. The models should account for the most important interactions of the surfactant molecules with the surface and with each other molecules, but most of the literature attributes only electrostatic interactions as the main mechanism of adsorption of zwitterionic surfactants, and that could not be the case.

2. Objectives

Having presented the reasons to evaluate surfactant adsorption, this work aims to provide models that could explain the mechanisms of adsorption of a zwitterionic surfactant on the surface of rocks analogue to oil reservoirs and estimate it in a reliable manner for dynamic conditions.

To accomplish this objective, a set of specific objectives need to also to be accomplished:

- Develop a methodology to precisely quantify the low adsorption values of CAPB in the equilibrated solutions from static tests and in the effluent samples from dynamic tests.
- Develop a methodology for static and dynamic adsorption experiments.
- Measure the surface area of the adsorbent under particulate and core forms, through nitrogen gas adsorption isotherm analysis (BET) and microtomography images (μ CT-scan), for normalization of adsorption results.
- Integrate adsorption results with estimates of surface potential and surface speciation through a validated surface complexation model, as the experimental conditions of salinity do not allow for direct surface potential measurements.
- Finally, compare static and dynamic adsorption and verify if it has the same behavior in such different conditions.

3. Main concepts

3.1 Surfactants and adsorption

Surfactants, derived from combining the terms: *surface active agents*, are compounds that significantly reduce interfacial tension (IFT) and easily adsorb at interfaces, that is, compounds that demonstrate activity in the region between two immiscible phases [15]. They are organic compounds that have a nonpolar structural group, called the lipophilic group, or simply tail, and a polar group, called the hydrophilic group or simply head.

Depending on the nature of the polar group, surfactants are classified as: anionic, cationic, zwitterionic (which are also amphoteric), and non-ionic (Figure 4). Anionic surfactants have a negative charge in a portion of the molecule, while cationic ones have a positive charge. Zwitterionics have both charges in their polar group. Finally, non-ionic ones have no ion charge, making the polarity more dependent on the formation of dipoles.

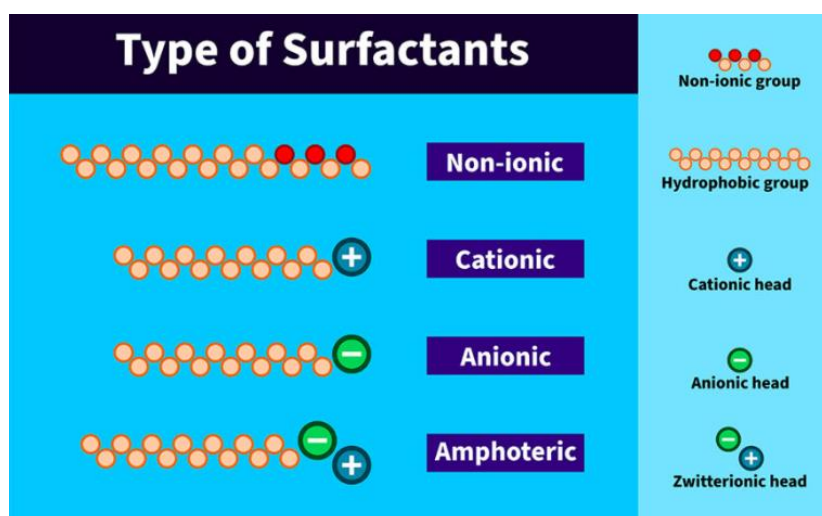


Figure 4: Types of surfactants, adapted from Alconox.com [14]

Because its structural groups have affinity for different types of solvent (polar and nonpolar), when inserted into water (polar solvent), the nonpolar group distorts the structures of the solvent, adding energy to the system by breaking the hydrogen bonds and guiding the water molecules in the vicinity of this group [15]. The system reacts in a way that reduces contact between the nonpolar group and

the water molecules. As a result, surfactant molecules are expelled from the bulk and adsorb at the interfaces, both processes occurring spontaneously [15]. In the process of adsorption on solid-liquid interfaces, the surfactant adsorbed is called the adsorbate (before adsorption is called adsorpt) and the material in which it is adsorbed is called the adsorbent (Figure 5).

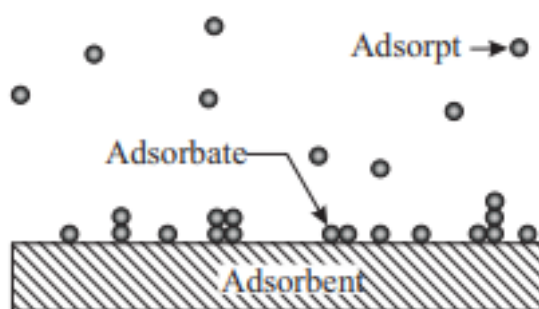


Figure 5: Elements of adsorption on solid-liquid interfaces. Used with permission of Butt, HJ et al., from [16]; permission conveyed through Copyright Clearance Center, Inc.

The main aspect of investigating surfactant adsorption is to quantify the amount of surfactant left in the interface by means of experiments, and to use models to adjust this data in order to explain its behavior at constant temperature (isotherms).

3.2 Surfactants aggregation and CMC

At low concentrations, surfactants act as individual monomers with interfacial activity. However, as the concentration rises, these surfactant monomers start to aggregate, aligning their hydrophilic heads outward towards the surrounding solution and their hydrophobic tails inward away from the water. This rearrangement is driven by the goal of minimizing the system's free energy (and maximizing entropy). The specific concentration at which this aggregation takes place is referred to as the critical micelle concentration (CMC), and the resulting aggregates are termed micelles (Figure 6). As a phenomenon of surfactant aggregation, micelle formation significantly changes the physical-chemical properties of a surfactant solution. Therefore, it is important to determine the concentration at which micelle formation starts to occur, i.e., the critical micelle

concentration (CMC), because the concentrations of surfactants slugs in EOR applications are often far above this number, so the adsorption experiments must attend this condition.

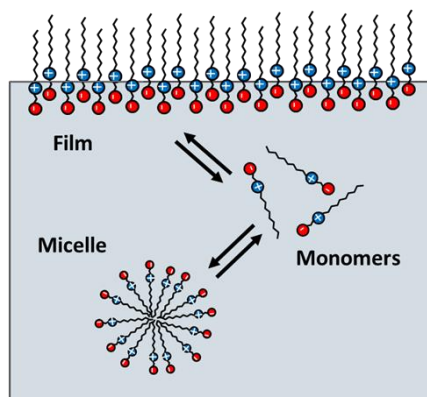


Figure 6: Representation of aqueous surfactant solutions above CMC, depicting the equilibria involving monomers, micelles, and adsorbed surfactant molecules at the interface for zwitterionic surfactant.

Surfactants in solution can also form other types of aggregates, which depend on specific factors, such as temperature, salinity, concentration, and surfactant structure [16,17]. From these diverse forms (shown in Figure 7) some like micelle and bilayers will be important for visualizing some of the mechanisms related to adsorption of surfactants in this work, since they might influence the adsorption of the zwitterionic surfactant.

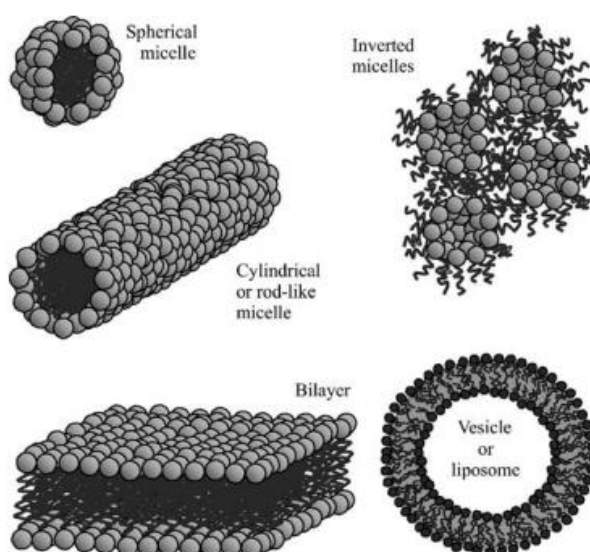


Figure 7: Other surfactant aggregates. Used with permission of Butt, HJ et al., from [16]; permission conveyed through Copyright Clearance Center, Inc.

4. Literature review on surfactant adsorption

Surfactant adsorbs on surfaces as monomers rather than micelles [18] and a considerable number of authors had presented a range of mechanisms responsible for adsorption on mineral surfaces. Dang [19], Paria and Khillar [20], Somansundaran and Huang [21], Zhang and Somansudaran [22], have shown mechanisms where ion exchange, ion association or pairing, hydrophobic bonding, polarization of π electrons, and dispersion forces play a major role in surfactant adsorption (Fig. 8). Commonly, the overall mechanisms are derived from electrostatic and van der Waals interactions, which arise between the proximity of the solid surface and the surfactant molecules [10].

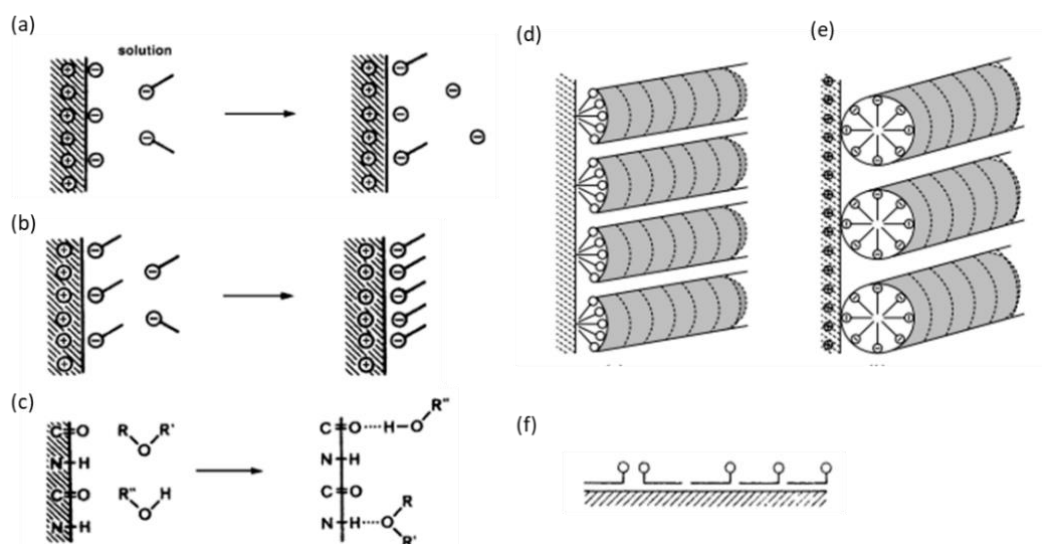


Figure 8: Common surfactant adsorption mechanisms: (a) ion-exchange, (b) ion pairing, (c) hydrogen bonding, hydrophobic bonding on (d) uncharged surface and (e) oppositely charged surface and (f) dispersion forces on nonpolar surface. Used with permission of Rosen, M.J., from [15], Copyright 2023; permission conveyed through Copyright Clearance Center, Inc.

For applications involving chemical flooding, the surfactant adsorption on reservoir rock is the most important parameter [23, 24], and this phenomenon depends on a variety of physical-chemical conditions related to both the surfactant and the rock surface, such as surfactant concentration, water salinity, pH, and temperature [15, 24]. The next sections will discuss in greater detail the influence of these parameters, focusing on the behavior of ionic and zwitterionic surfactants (such as the one used in this work).

4.1 Effects and influence of adsorption parameters on surfactant adsorption

4.1.1 Influence of surfactant concentration

Adsorption is directly affected by surfactant concentration, where the more available surfactant molecules in bulk, the more adsorbed molecules are found at the solid-liquid interface. This can occur until a certain level of surfactant concentration (CMC) is reached, when the monomers start to aggregate and associate themselves forming micelles rather than to adsorb (Figure 9).

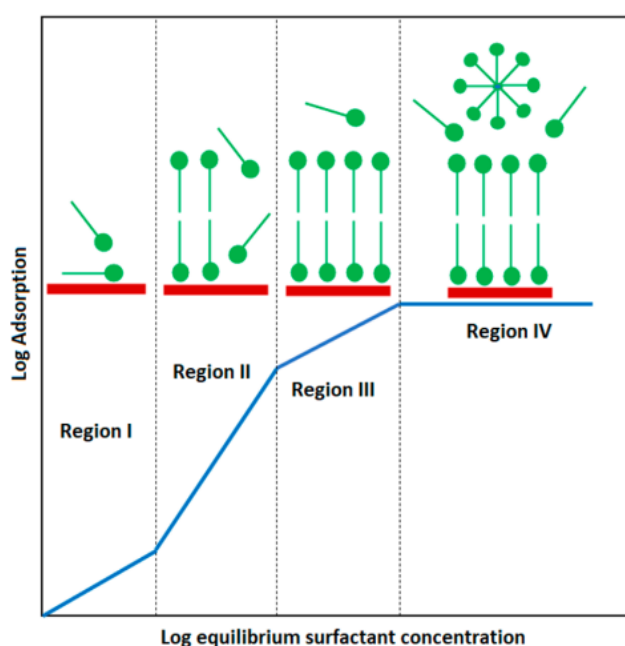


Figure 9: Surfactant adsorption with increase in equilibrium concentration. Adapted from [25].

Each of the four regions labeled in the image exhibits a distinct adsorption behavior, typical of ionic surfactants on surfaces with opposite charges. The Four-Region theory, developed upon the work of Somasundaran and Fuerstenau [26], explains that in Region I, at low concentrations, the surfactant adsorbs solely by electrostatic interactions [20] and usually obeys Henry's law [25]. In region II, the sudden increase in the adsorption occurs due to lateral interactions, resulting in surface aggregation of surfactants (hemimicelles [20]). Region III shows a slower rate of adsorption compared to region II, and finally, region IV is the plateau region

above the CMC [20]. In the plateau, micelles are formed in solution, and the adsorption density does not vary further, and the main driving force behind adsorption is the lateral hydrophobic interaction between hydrocarbon chains [25].

Adsorption maxima could occur within this four-region regime [20,27]. The occurrence of these maxima, rather than a plateau typical of surface saturation, is a phenomenon not well understood yet, and the main explanation is that surface active impurities could be adsorbed below CMC, and solubilized in micelles above CMC, decreasing the adsorbed amount [28]. Troguis et. al [29] showed that adsorption maxima can also occur in surfactant mixtures, even if each surfactant has simple adsorption behavior, such as obeying Henry's law. The absence of adsorption maxima could indicate, according to Arnebrant et. al [30], that surfactant samples do not contain impurities with higher affinity for the adsorbent surface.

Additionally, adsorption can decrease past CMC values in the case of non-ionic surfactants [27,31], anionic [27,30], cationic [28,30], surfactant mixtures [29] and, more recently, zwitterionic surfactants [32] (Figure 10) at pH 8 (seawater) and pH 6 (connate water), with CMC on the 180-300 ppm range.

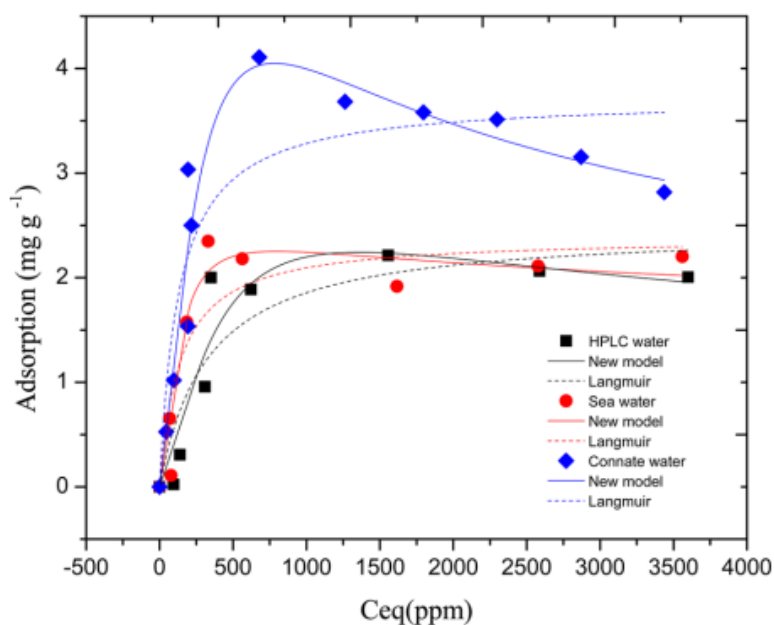


Figure 10: Adsorption maxima phenomenon in zwitterionic surfactant solutions at different salinities. Adapted with permission from Nieto-Alvarez et al. [32]. Copyright 2023 American Chemical Society.

A few works have demonstrated also that adsorption of zwitterionic surfactant increases with equilibrium concentrations above CMC in a variety of salinity and temperature conditions [12, 32-35]. This could be attributed to the lack of CMC measurements in the presence of the solid interface from the adsorbent, where the measurements typically occur with only liquid-gas interfaces.

These works also demonstrate the complex behavior of zwitterionic surfactant adsorption on rocks related to reservoir formations.

4.1.2 Effect of salinity

Salinity is another important factor that influences surfactant adsorption, and its effect is complex. Depending on the nature of the surfactant, the rock surface, and the surfactant concentration, salinity has different effects due to various interactions occurring on the interface. One example is the decrease of repulsive forces arising between surfactant molecules and the rock surface, with an opposite charge, because of increased salinity [10, 23], which will lead to a higher adsorption. This was explained in the case of anionic and cationic surfactants in oppositely charged surfaces at high surfactant concentrations by Lee et. al [36]: as the ionic strength rises, mutual head group repulsion is reduced, thus, adsorption is increased.

The influence of salinity on non-ionic surfactant adsorption occurs as the solubility, surface activity, and aggregation properties change with the increase in electrolyte concentration [15]. Denoyel and Rouquerol [37] found out that the CMC decrease of a non-ionic surfactant in the presence of electrolytes produced a shift of the adsorption plateau to lower concentrations, therefore increasing adsorption in certain concentration range. This was explained by the increase in lateral interactions between the polar groups as salinity increases. However, Nevskaja et. al [38] showed that non-ionic surfactant adsorption can decrease or increase with salinity depending on the nature and quantity of the surface hydroxyl groups from the solid.

Salinity alterations can affect in an even more complex way the zwitterionic surfactant adsorption mechanisms. Mannhardt et. al [39] demonstrated that increasing salinity slightly increased and shifted the adsorption plateau of a betaine surfactant towards low equilibrium concentrations in limestone. The same

could not be affirmed for sandstone, where the increase in salinity decreased adsorption, and shifted the plateau towards higher equilibrium concentrations. Li et. al [34] showed quite a similar adsorption behavior of betaines in quartz sand. Low NaCl concentrations (1 wt%) in the brine implied higher adsorption for sulfobetaine, as also NaCl concentrations up to 30 wt%, but middle concentrations presented the lowest adsorption values. The same behavior occurred for the carboxylbetaine between 1% and 10% wt.% NaCl concentrations, but the adsorption was very much higher at the high salinity condition. Nieto-Alvarez et. al [32] presented an adsorption increase of sulfobetaine in limestone with increased salinity. Zhong et. al [35] also presented this result for a sulfobetaine in Bakken-Formation minerals which has different surface charge nature compared to limestone at the tested conditions. In the later work, adsorption seemed to decrease with salinity for the carboxyl betaine.

In summary, salinity is a factor that, combined with the mineralogy of the rock and pH, could alter adsorption behavior in a complex manner for every type of surfactant, and deserves a more cautious approach to generalize its effects in surfactant-brine-rock systems.

4.1.3 Effect of temperature

In general, adsorption of surfactants is an exothermic process ($\Delta H > 0$) and thus tends to decrease as the temperature increases [24]. However, some works showed that the influence of temperature depends on whether the process is enthalpy- or entropy-driven [10, 40-42]. As Kamal et al [10] pointed out, based on the works of Hirasaki et. al [40, 41] and Tackie-Otoo et. al [42], if the process is enthalpy-driven, as it is the case for surfactants with low adsorption density, adsorption increases with temperature. If the process is entropy-driven, in the case of a surfactant with high adsorption density, the reverse happens, and a temperature increase decreases adsorption.

Non-ionic surfactants adsorption typically increases with temperature due to solvation effect at high adsorption [43]. Liu et. al [24] explained that the increase in temperature progressively dehydrates the head groups of surfactants, rendering it to be less hydrophilic and more compact, and therefore increases the surface activities and adsorption amount. This type of surfactant could have their adsorption

lowered with temperature increase at low concentrations, and the opposite was found for high concentrations [44]. Liu et. al [24] also pointed out, based on Azam's work [23], that anionic surfactant adsorption seemed to be reduced by temperature as at high temperatures the relatively high kinetic energy contributes to destabilize aggregate organizations.

In the case of a zwitterionic surfactant, Mannhardt et al [11] reported no alteration in the surfactant adsorption on Berea sandstone with significant temperature difference, while an anionic surfactant had its adsorption lowered with the same temperature increase.

Jian et. al [45] also reported that temperature seemed to have no significant effect on the adsorption of zwitterionic surfactants in calcite, dolomite, silica, and kaolin with deionized water (Figure 11). However, temperature was responsible for the increase in one of the zwitterionic surfactants (carboxylbetaine) studied in Zhong et. al [35] at low initial concentration (Figure 12 (a)), but when concentration was 10 times the latter (Figure 12 (b)), the temperature effect was the opposite, resulting in less adsorption. The conclusion about the latter work could be also that temperature effect was also not clear because of the close adsorption values may laying inside an experimental error range, and the lack of replicates corroborates to that conclusion.

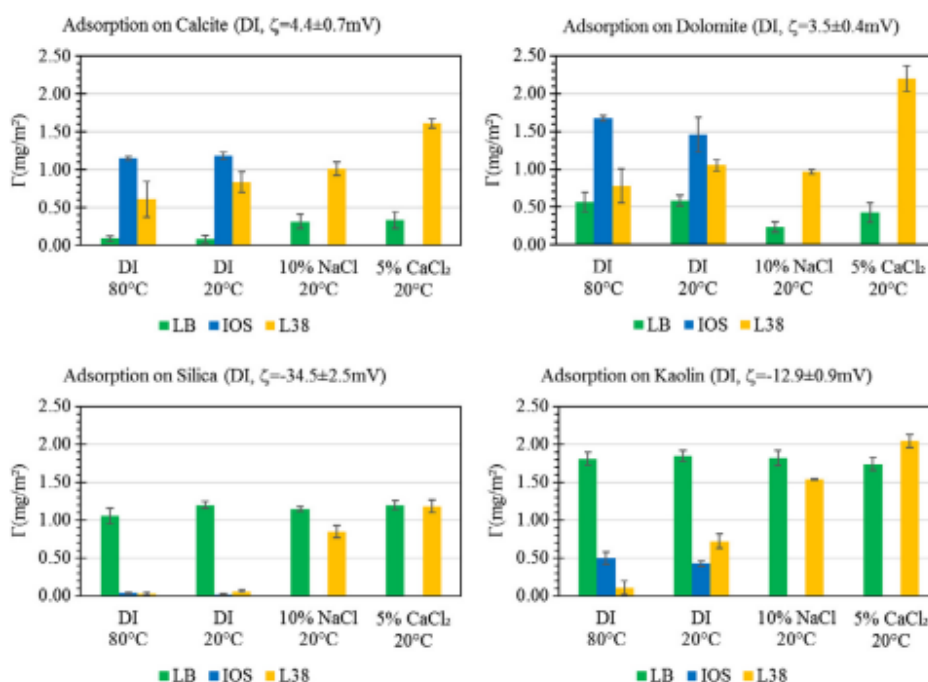


Figure 11: Adsorption of zwitterionic surfactant (LB-lauryl betaine) on different minerals at 20°C and 80°C. Adapted from [45], Copyright 2023, with permission from Elsevier.

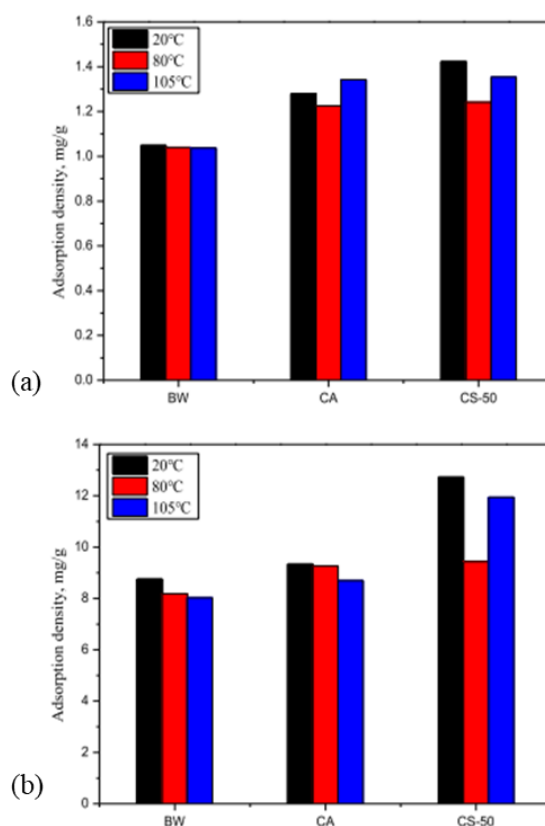


Figure 12: Effect on temperature on carboxylbetaines BW and CA at (a) 100 mg L⁻¹ and (b) 1000 mg L⁻¹ surfactant concentration. Adapted with permission from Zhong et al. [35]. Copyright 2023 American Chemical Society.

4.1.4 Effect of alkalis and pH

The addition of alkaline species and variation of pH can significantly modify surface properties and, thus, the surfactant adsorption behavior at solid-liquid interfaces. More specifically, surface charge is influenced by salinity and pH of the surfactant solution, which has a direct effect on surfactant adsorption [15].

The use of alkaline species is related to *in situ* soap generation, as less surfactant is needed to be injected. However, as Weinfeng et. al [33] demonstrated, it reduces adsorption of anionic and zwitterionic surfactants by increasing pH, thus increasing the number of negative sites in kaolinite. The zwitterionic surfactant behavior pointed out by Weifeng et. al [33], in this case the used betaine, is totally anionic in the alkaline conditions because of deprotonation of the quaternary

ammonium present in the surfactant molecule, so a more negative surface would difficult its adsorption via electrostatic interactions. Alkalis are also more sensitive to divalent cations, and its capability of sequestering Ca^{+2} and Mg^{+2} in the solution limits its application onto low salinity/hardness waters [15, 24]. This capability reduces divalent ion interactions with the charged surface sites, which become less positive.

As reviewed by Belhaj et. al [15], pH increase alters the magnitude of adsorption by reducing the number of hydroxyl groups in the surface. Thus, hydrated mineral oxides on solid surface, e.g., silica oxides/silanol, become negatively charged. At low pH, the mineral hydroxyl groups become protonated, acquiring a positive charge. In the case of anionic surfactants, as demonstrated by Somasundaran et. al [46, 47], higher pH makes the surface more negative and decreases its adsorption, while the opposite happens for cationic surfactants.

Bera et. al [48], pointed out that, in the case of a non-ionic surfactant, adsorption decreases to neutral pH, and is almost constant at alkaline pH range. As explained by Bera et. al [48], the lone pair of electrons of the oxygen atom in the ethylene oxide group is attracted to the positive surface, thus increasing adsorption at low pH, where the surface is more positive. Figure 13 shows the effect of pH on adsorption for anionic (SDS), cationic (CTAB) and non-ionic (Tergitol 15-S-7) surfactants, as reported by Bera et al [48].

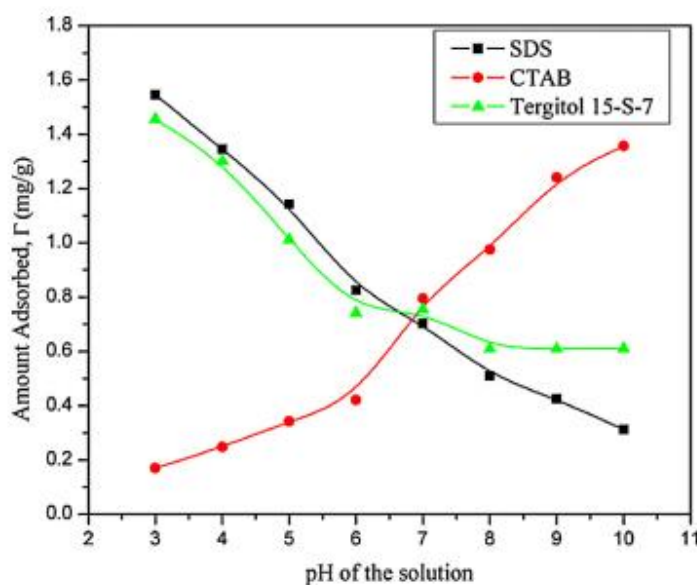


Figure 13: Effect of pH on the adsorption of different types of surfactants: SDS (anionic), CTAB (cationic) and Tergitol 15-S-7 (non-ionic). Adapted from [48], Copyright 2023, with permission from Elsevier.

4.2 Static and dynamic adsorption of zwitterionic surfactants

Surfactant adsorption is often measured in two types of experiment: static and dynamic (coreflood). The latter type has a lower liquid to solid ratio (mL of liquid / g of rock) compared to the former (static), even though the dynamic approach has more difficulties in order to determine adsorption, it simulates the reservoir conditions better than static tests. Because of this, many researchers choose to infer static adsorption data from dynamic experiments. Satter et. al [50], Novosad et. al [51] and Mannhardt et. al [11, 39, 49] have reported this approach in surfactant adsorption studied, based on good dynamic adsorption models that adjusted well the experimental data.

Betaine, the type of zwitterionic surfactant utilized in this dissertation, had its dynamic adsorption studied by Mannhardt et. al [39, 49] on limestone and sandstone cores, at different salinities. They demonstrated that betaine-type surfactant adsorbs more on Berea sandstone than on Indiana limestone, and this adsorption is considerably increased in the presence of divalent ions on both types of rocks. It is worth noting, that the brine utilized in this work [39] was composed only by Na^+ and Ca^{2+} cations, distancing from the desulfated sea water composition, which is more representative of operations and, more importantly, because they did not make the static test, nor measured the surface area of the adsorbents, comparison between the two methods was not analyzed. The inference of such static parameters from dynamic data should not represent the adsorption due only to interactions, because data was obtained through flow conditions which could alter the mechanism. This hypothesis will be tested through this work.

More recently, other authors like Weifeng et al [33], studied betaine adsorption through dynamic and static experiments, in 10 g L^{-1} NaCl solution and neutral pH. They showed that the maximum dynamic adsorption ($\sim 3.2 \text{ mg g}^{-1}$), using the initial concentration of the static adsorption plateau, was lower than that obtained in the static tests ($\sim 4.3 \text{ mg g}^{-1}$), even though a sand pack was used in dynamic case and 100% kaolinite powder in the static case. Also, they concluded that alkali addition and pH increase lowered the static adsorption plateau (Figure 14 (a)), and the breakthrough curves shifted to low PVs (Figure 14 (b)).

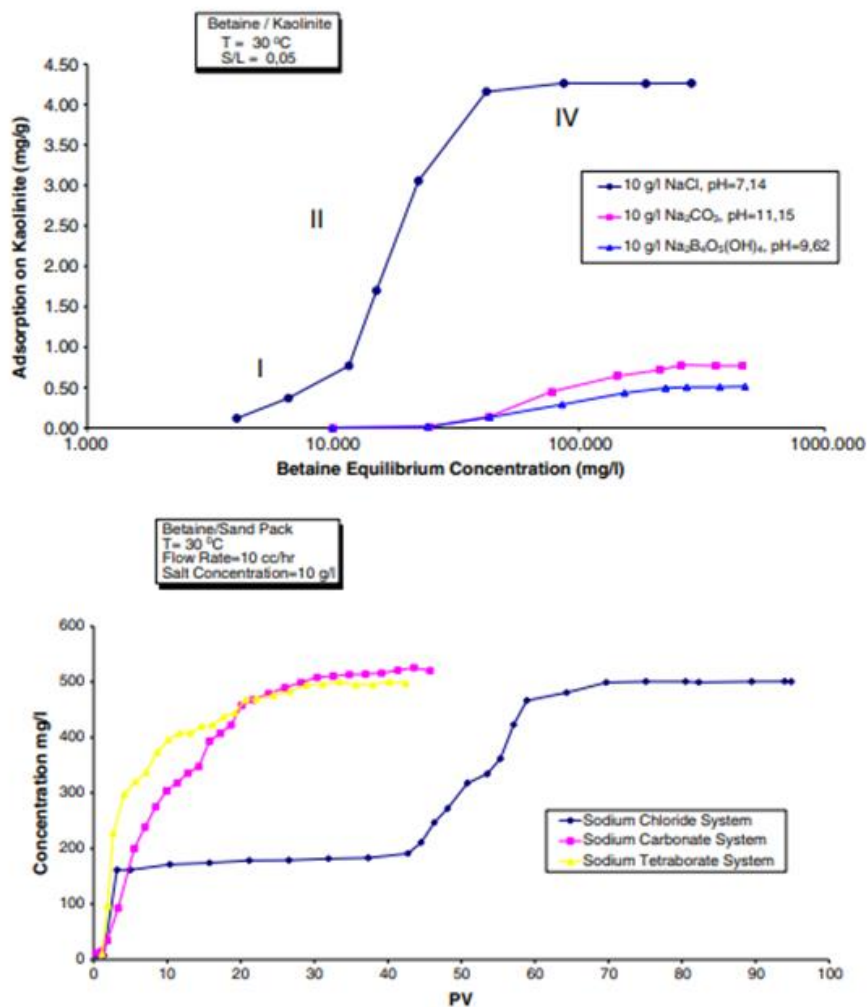


Figure 14: Betaine (a) static adsorption and (b) breakthrough curves with different alkali addition. Adapted from [33], Copyright 2023, with permission from Elsevier.

Dai et. al [12] studied CAPB adsorption with static and dynamic experiments at high temperature and salinity. Zhao et. al [52] studied, at the same conditions of Dai, the adsorption of cocamidopropyl dimethyl amine oxide (CAO) under static and dynamic conditions. It should be noticed that the molecular formula of CAO is slightly different from CAPB, as the head group of the former does not have a terminal carboxylic group. Despite the difference in the surfactants, both studies demonstrated that static adsorption was considerably higher than the dynamic results, and CAO showed almost the double amount of adsorption compared to CAPB with the same adsorbent, at same salinity and temperature conditions. Despite this, dynamic adsorption was higher for CAO than CAPB, but the magnitude of the difference was considerably lower than static adsorption.

Figure 15 (a) and (b) showed the static and dynamic results for CAPB and CAO respectively, from the works of Dai et. al [12] and Zhao et. al [52].

Both authors concluded that the adsorption of CAPB and CAO were too high, and they assigned the possibility of multilayer adsorption of these surfactants to explain the results.

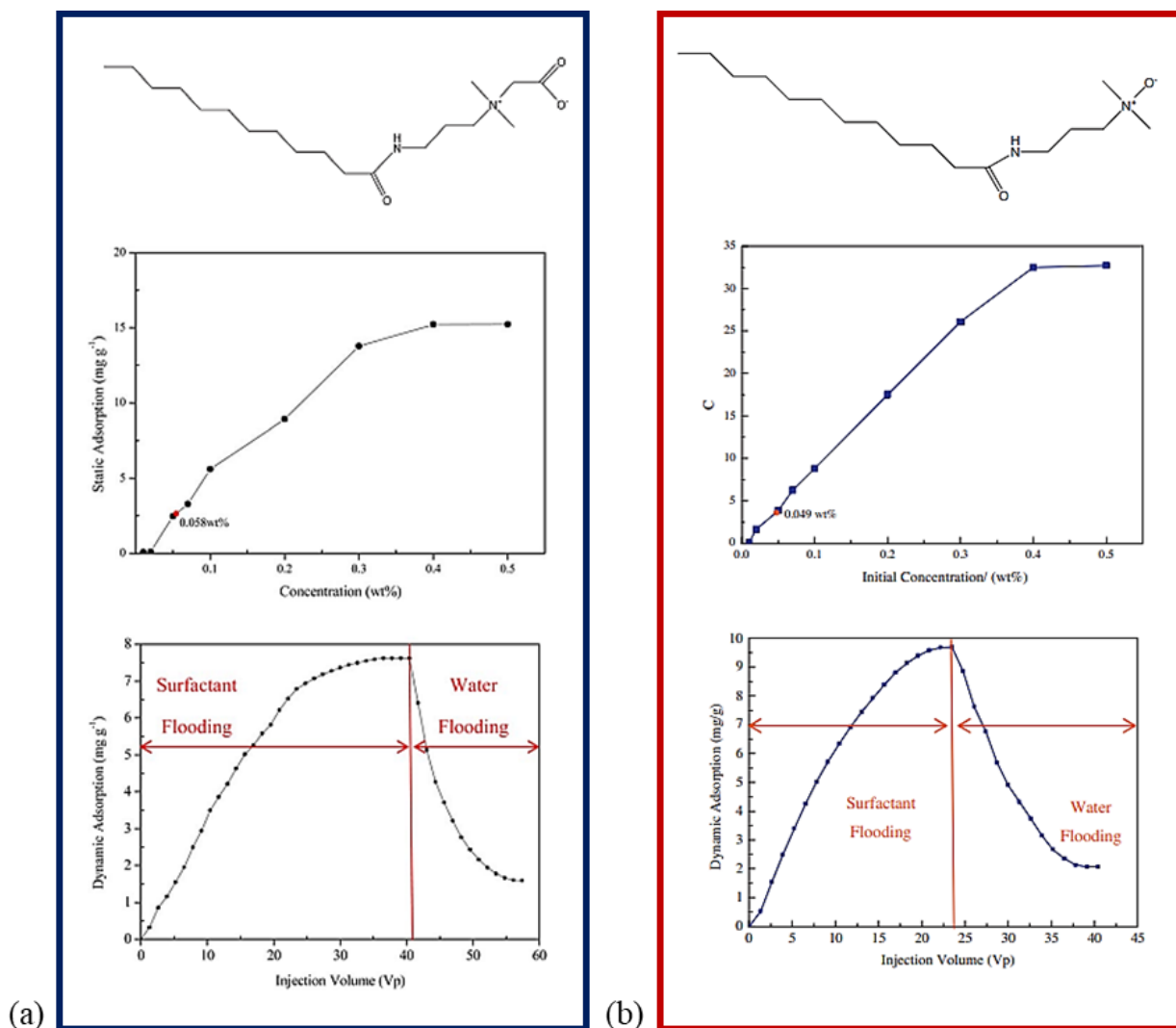


Figure 15: Structural formula and static and dynamic adsorption of (a) CAPB and (b) CAO on natural sandstone cores. (a) Used with permission of Dai et al. from [12], Copyright 2023; permission conveyed through Copyright Clearance Center, Inc. (b) Adapted from [52], Copyright 2023, with permission from Elsevier.

These works that approached the static and dynamic adsorption of zwitterionic surfactants clearly showed that adsorption of zwitterionic surfactants is higher at static conditions, but none of them explained the possible mechanisms

of adsorption for the static tests results by isotherm modelling, given that without the mechanisms the improvement of such models, and then reliable estimates for adsorption, does not progress.

Although some authors have focused on the static adsorption of zwitterionic surfactants on mineral surfaces [32, 34, 35, 45, 53], only a few described isotherm modelling to explain possible mechanisms of static adsorption [32, 35, 53]. Li et. al [34] evaluated static adsorption of carboxyl and sulfo betaines on quartz sand with carbon chain number varying from 16 to 18 at different salinities. They demonstrated that maximum static adsorption of the carboxylbetaine could range from 4 to 23 mg g⁻¹ depending on the salinity and surfactant concentration, and 2 to 5.5 mg g⁻¹ for the sulfobetaine.

Nieto-Alvarez et. al [32], found out that a sulfobetaine in connate/formation water adsorbs on limestone (~4 mg g⁻¹) almost two-fold compared to adsorption with sea water (~2 mg g⁻¹). This is one of the few works that show a decrease of adsorption in such a system, and the authors explained this effect regarding the micelle-vesicle equilibrium in a theoretical framework, introducing a new model resembling Langmuir isotherm, and with images of vesicles that proves its existence in connate water.

Jian et. al [45] evaluated the static adsorption of lauryl betaine on two carbonate minerals: calcite and dolomite and two silicate ones: silica and kaolin. The betaine adsorption was determined separately and blended with anionic surfactants. They showed that the betaine adsorbs on silicate minerals in the range of 1 to 2 mg m⁻² and in the carbonate minerals on the range of 0.1 to 0.5 mg m⁻². These experiments consider changes in salinity and temperature. The authors concluded that the blending with anionic surfactant increased adsorption on calcite and decreased on dolomite.

Zhong et. al [35], found out maximum static adsorption values of two carboxylbetaines on calcite and clay were in the range of: 1 to 2 mg g⁻¹ for calcite and 10 to 15 mg g⁻¹ for clay, with high salinity brine. They also obtained an adsorption maximum between 4 and 5 mg g⁻¹ for Berea sandstone with the same brine. Kumar et. al [53], also compared the adsorption of betaine in carbonate and sandstone surface with deionized water. In this case, adsorption on carbonate was considerably higher in the carbonate rather than in the sandstone.

4.2.1 Static adsorption models

Surfactant adsorption behavior can be described by physical or empirical isotherm models which were applied on many works in the literature. As explained by Wang et. al [55]: “isotherm refers to the relationship between the equilibrium adsorbate concentration in the liquid-phase and the equilibrium adsorption amount on the solid-phase at certain temperature”. So, equilibrium adsorption data can be modelled by isotherms to obtain information about mechanisms, maximum adsorption capacity and other properties of the adsorbents.

Kalam et. al [25] and Liu et. al [24] listed a huge set of isotherm models that are usually applied to adjust static adsorption curves of surfactants. There is no evidence of application of some of these models in the case of zwitterionic surfactant adsorption, but a handful of the classical isotherms developed by Langmuir, Freundlich, Redlich-Peterson and Sips, have been already applied for modelling surfactant adsorption data of every type of surfactant [48,53].

Each isotherm will be explained next on its original mathematical form (not the linear one) because, as pointed out by Foo et. al [54] and Wang et. al [55] reviews, propagated errors are generated in the linearization process, leading to inaccurate estimation of parameters or to bias in adsorption data.

4.2.1.1 Langmuir isotherm

The Langmuir isotherm is one of the most used isotherm models and it was initially developed to represent gas-solid adsorption [56], but it was also used for various adsorbents [25]. It is a theoretical model based on kinetic principles, which balances the relative rates of adsorption and desorption. Equation (1) shows how the adsorption density (q [mg g⁻¹]) is related to equilibrium concentration (C_e [g L⁻¹]) in the Langmuir model:

$$q = \frac{q_{\infty} K_L C_e}{1 + K_L C_e} \quad (1)$$

Where K_L ($L g^{-1}$) is the Langmuir equilibrium constant, C_e ($g L^{-1}$) is the equilibrium concentration and q_∞ is the maximum adsorption capacity of the adsorbent in $mg g^{-1}$.

This model assumes that: adsorption in monolayer fashion, sites are homogeneous and have constant adsorption energy, and there are no lateral interactions between the adsorbed molecules.

4.2.1.2 Freundlich isotherm

Unlike Langmuir, Freundlich isotherm can be used to represent multiplayer adsorption behavior on heterogeneous sites, and it's described by equation (2) [57]:

$$q = b C_e^{1/n} \quad (2)$$

In this case b is the adsorption capacity term in $L g^{-1}$ and $1/n$ is adsorption intensity or surface heterogeneity. The main assumption is that adsorption heat distribution and affinities toward the heterogeneous surface are nonuniform [25].

4.2.1.3 Redlich-Peterson isotherm

Redlich-Peterson isotherm was developed to fit adsorption data related to molecular sieves [58], but it appeared to be a combination of the Langmuir and Freundlich isotherms. The authors of the original paper found a relation where at low adsorbate concentrations, the adsorption approaches the Langmuir regime and at high concentrations the Freundlich regime. Its isotherm is described by the equation (3):

$$q = \frac{K_r C_e}{1 + \alpha_r C_e^{\beta_r}} \quad (3)$$

Where K_r ($L g^{-1}$), α_r ($L m^{-1}g$) are empirical constants, and β_r is an empirical adjusted exponent. The mechanism of adsorption is a mix of the previous two adsorption models and does not follow ideal monolayer adsorption.

4.2.1.4 Sips isotherm

The Sips isotherm is also a combination of the Langmuir and Freundlich isotherms, but it overcomes the limitation of indefinite adsorption of the Redlich-Peterson model at increasing concentrations. Its mathematical description is as follows [59]:

$$q = \frac{K_s C_e^{\beta_s}}{1 + \alpha_s C_e^{\beta_s}} \quad (4)$$

The adjusted Sips isotherm model constant are K_s ($L g^{-1}$) and α_s ($L m^{-1}g$). β_s is the Sips isotherm exponent. This model is suitable for explaining and predicting adsorption on heterogeneous surfaces. At low concentrations the model has a Freundlich regime, and at high concentrations the Langmuir regime is reached giving it a S-shape curve with a maximum adsorption density plateau.

4.2.1.5 Alternative isotherms and Bilayer approach

Ayawei et. al [60] and Wang et. al [55] showed a vast set of isotherm models and its mechanisms that could be added to surfactant adsorption investigation. Some works on literature even applied multi-site, or multi-layers, models for gas-solid adsorption, describing multi-layer adsorption models with the already presented isotherms, where the total adsorption is the sum of the adsorption on each layer or site [61].

In this work, a considerable range of isotherm models were fitted to experimental data. These models were categorized in single layer isotherm models and bilayer models. Because of hydrophobic nature of the surfactant chain, surfactants can interact laterally on the surface to form hemimicelles and interact vertically forming bilayers or admicelles (Figure 16). This motivates the use of the bilayer approach which states that surfactant adsorbs in two layers: one

corresponding to surface surfactant interaction and the other to surfactant-surfactant interactions. The bilayer models used in this work were also composed of a novel description where surfactant adsorption behavior is represented by different isotherm models for each layer.

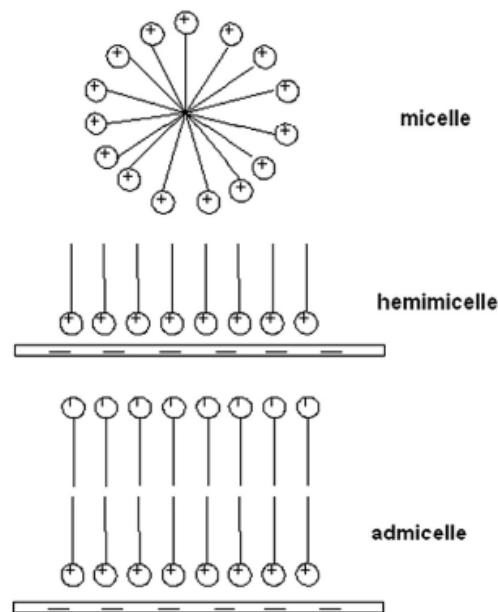


Figure 16: Structure of micelle, hemimicelle and admicelle. Adapted from [62],
Copyright 2023, with permission from Elsevier.

Some works have already used bilayer models for surfactant adsorption in static [63] and dynamic experiments [64] with relative success. In the case of the static case, they were limited to Langmuir and Langmuir-Freundlich type isotherms for both adsorption layers, the latter isotherm has the same mathematical description as the Sips isotherm. In this work, some combinations of the previous isotherm models were applied, and the results were interpreted according to each layer proposed model/behavior premises.

The bilayer approach to model adsorption data considers the total adsorption as a sum of each layer and the expression for the second layer is dependent on the first one (Equation (5)):

$$q = q_1 + q_2(q_1) \quad (5)$$

The deduction of the general bilayer isotherm model could be understood assuming that there is a maximum adsorption capacity for each layer: q_{∞_1} and q_{∞_2} and a fraction term, representing the related isotherm behavior for the surface coverage fraction in each layer, which depends on the equilibrium concentration: $f_1(C_e)$ and $f_2(C_e)$. Because it's considered adsorption in bilayers, the adsorbed amount on the second layer is proportional to the quantity already adsorbed on the first layer or first sites, according to Koresh et. al [65]. The model could be re-written on the following form:

$$q = q_{\infty_1}f_1 + q_{\infty_2}f_2 \quad (6)$$

And:

$$q_{\infty_2} = \alpha q_1 \quad (7)$$

Where α is a constant of proportionality. So, the overall formula for the bilayer approach is:

$$q = q_{\infty_1}f_1(1 + \alpha f_2) \quad (8)$$

The terms f_1 and f_2 can be substituted for similar terms of the presented isotherm models. The general equation for bilayer adsorption model is then:

$$q = q_{\infty_1} \frac{b_1 C_e^{n_1}}{1 + b_2 C_e^{n_2}} \left(1 + \alpha \frac{b_3 C_e^{n_3}}{1 + b_4 C_e^{n_4}} \right) \quad (9)$$

Where, depending on the combination and values of the model parameters different interpretations of these terms could arise, e. g., the α term could be interpreted as how much maximum adsorption capacity is available on the second layer per quantity adsorbed on the first layer.

Langmuir, or abbreviated to “Lang, Redlich-Peterson, “RP”, and Sips isotherms, also, its combinations included: Lang-Lang, RP-RP, Sips-Sips, Lang-

RP, RP-Lang, Lang-Sips, Sips-Lang, RP-Sips and Sips-RP. Are resumed in table 1 on the single layer and bilayer approach:

Model	Equation	Approach
Langmuir	$q = \frac{q_{\infty} K_L C_e}{1 + K_L C_e}$	Single layer
Freundlich	$q = b C_e^{1/n}$	
Redelich-Peterson	$q = \frac{K_r C_e}{1 + \alpha_r C_e^{\beta_r}}$	
Sips	$q = \frac{K_s C_e^{\beta_s}}{1 + \alpha_s C_e^{\beta_s}}$	
Lang-Lang	$q = \frac{q_{\infty_1} K_{L_1} C_e}{1 + K_{L_1} C_e} \left(1 + \alpha \frac{K_{L_2} C_e}{1 + K_{L_2} C_e} \right)$	Bilayer
RP-RP	$q = \frac{q_{\infty_1} K_{r_1}^* C_e}{1 + \alpha_{r_1}^* C_e^{\beta_r}} \left(1 + \alpha \frac{K_{r_2}^* C_e}{1 + \alpha_{r_2}^* C_e^{\beta_r}} \right)$	
Sips-Sips	$q = \frac{q_{\infty_1} K_{s_1}^* C_e^{\beta_s}}{1 + \alpha_{s_1}^* C_e^{\beta_s}} \left(1 + \alpha \frac{K_{s_2}^* C_e^{\beta_s}}{1 + \alpha_{s_2}^* C_e^{\beta_s}} \right)$	
Lang-RP	$q = \frac{q_{\infty_1} K_L C_e}{1 + K_L C_e} \left(1 + \alpha \frac{K_{r_2}^* C_e}{1 + \alpha_{r_2}^* C_e^{\beta_r}} \right)$	
RP-Lang	$q = \frac{q_{\infty_1} K_r^* C_e}{1 + \alpha_r^* C_e^{\beta_r}} \left(1 + \alpha \frac{K_L C_e}{1 + K_L C_e} \right)$	
Lang-Sips	$q = \frac{q_{\infty_1} K_L C_e}{1 + K_L C_e} \left(1 + \alpha \frac{K_s^* C_e^{\beta_s}}{1 + \alpha_s^* C_e^{\beta_s}} \right)$	
Sips-Lang	$q = \frac{q_{\infty_1} K_s^* C_e^{\beta_s}}{1 + \alpha_s^* C_e^{\beta_s}} \left(1 + \alpha \frac{K_L C_e}{1 + K_L C_e} \right)$	
RP-Sips	$q = \frac{q_{\infty_1} K_r^* C_e}{1 + \alpha_r^* C_e^{\beta_r}} \left(1 + \alpha \frac{K_s^* C_e^{\beta_s}}{1 + \alpha_s^* C_e^{\beta_s}} \right)$	
Sips-RP	$q = \frac{q_{\infty_1} K_s^* C_e^{\beta_s}}{1 + \alpha_s^* C_e^{\beta_s}} \left(1 + \alpha \frac{K_r^* C_e}{1 + \alpha_r^* C_e^{\beta_r}} \right)$	

Table 1: Static adsorption isotherm models

The isotherm constants with superscript * represents the initial presented constant of each related isotherm, but without physical or chemical units, because the model already assumes a term of maximum capacity the other terms compose the separate coverages and don't need have any units.

Each bilayer approach isotherm model on table 1 has different premises related to the intrinsic mechanisms of surfactant adsorption, most of them divided into homogeneous/heterogeneous and monolayer m⁻¹utilayer adsorption behavior.

4.2.2 Dynamic adsorption models

Dynamic adsorption modelling is based on the adjustment and prediction of breakthrough curves from species that travel through the porous media. Because of the aqueous phase flow and diffusion, solutes who behave like a tracer, which does not interact with the rock matrix, can travel in the capillaries of the rock and its quantity in the effluent, in this case, concentration, can be described mathematically by the hydrodynamic dispersion equation. This model is commonly called the convection-dispersion equation and has been used for a long time in describing breakthrough curves from non-adsorbing species ([66], [67], [50], [68], [51], [69], [64], [70] and [71]). Its deduced formulation is found in Bear [72]:

$$\frac{dC}{dt} = D \frac{d^2C}{dx^2} - V \frac{dC}{dx} \quad (10)$$

Where D is the coefficient of dispersion in $\text{cm}^2 \text{min}^{-1}$ and V is average interstitial velocity (cm min^{-1}) of the solute in porous media. Solutions of this equation are often used as the tracer model for breakthrough curves. However, it can be used for adsorbed species if the adsorption term is added to the equation as Troguis et. al [73] and Kwok et. al [64] formulated:

$$\frac{dC}{dt} = D \frac{d^2C}{dx^2} - V \frac{dC}{dx} - \frac{\rho_b}{\phi} \frac{d\Gamma}{dt} \quad (11)$$

The term added depends on the bulk density of the rock (ρ_b), the porosity (ϕ) and the adsorption of the transported species (Γ). When adsorption is

considered to reach the equilibrium faster, the effluent concentration is considered the equilibrium equation $C = C_e$ and adsorption becomes a function of that concentration $\Gamma(C_e)$. As pointed out by Satter. et. al [50], the adsorption rate term could be substituted by:

$$\frac{d\Gamma}{dt} = \frac{d\Gamma}{dC} \frac{dC}{dt} = \frac{d\Gamma}{dC_e} \frac{dC_e}{dt} \quad (12)$$

The term $\frac{d\Gamma}{dC_e}$ means the derivative of the isotherm model with respect to equilibrium concentration. Thus, the reformulated model becomes:

$$\left(1 + \frac{\rho_b}{\phi} \frac{d\Gamma}{dC_e}\right) \frac{dC}{dt} = D \frac{d^2C}{dx^2} - V \frac{dC}{dx} \quad (13)$$

The term $\left(1 + \frac{\rho_b}{\phi} \frac{d\Gamma}{dC_e}\right)$ is known to be the retardation factor of the breakthrough curve [72]. When the equilibrium is not assumed, the rate of adsorption becomes described by kinetic models.

Kwok et. al [64] listed a couple of simple and effective models capable of adjustment and prediction of surfactant the breakthrough curves when equilibrium and non-equilibrium is assumed:

Expression adsorption term	Model -type
$\frac{d\Gamma}{dC_e} = K_H$	Henry - Equilibrium
$\frac{d\Gamma}{dC_e} = \frac{q_{\infty} K_L}{(1 + K_L C_e)^2}$	Langmuir - equilibrium
$\frac{d\Gamma}{dt} = k_a C(\Gamma_{\infty} - \Gamma) - k_d \Gamma$	Langmuir - Kinetic
$\frac{d\Gamma_1}{dt} = k_{a_1} C(\Gamma_{\infty_1} - \Gamma_1) - k_{d_1} \Gamma_1$ $\frac{d\Gamma_2}{dt} = k_{a_2} C(\Gamma_{\infty_2} - \Gamma_2) - k_{d_2} \Gamma_2$	Two-site - Kinetic

$\frac{d\Gamma_1}{dt} = k_{a_1}C(\Gamma_{\infty_1} - \Gamma_1) - k_{d_1}\Gamma_1$ $\frac{d\Gamma_2}{dt} = k_{a_2}C\left(\frac{\Gamma_{\infty_2}}{\Gamma_{\infty_1}}\Gamma_1 - \Gamma_2\right) - k_{d_2}\Gamma_2$	Bilayer - Kinetic
--	-------------------

Table 2: Dynamic adsorption models presented in [64]

The bilayer and the two-site kinetic models performed very well on adjusting and predicting breakthrough curves in Kwok et. al [64] (Figure 17), despite this advantage of kinetic models, some works reported good agreement of equilibrium models on fitting surfactant breakthrough curves such as in Novosad et. al [51].

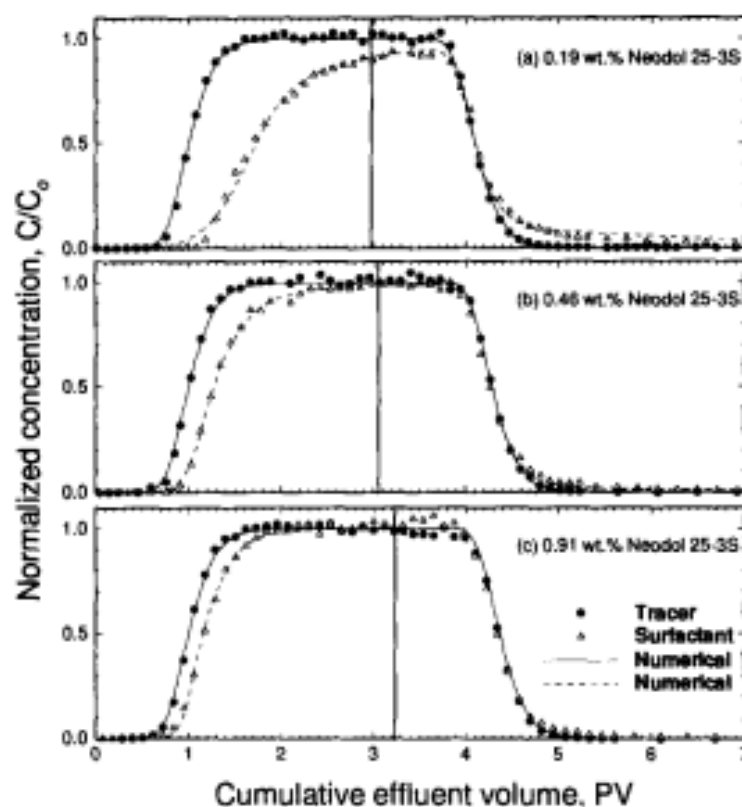


Figure 17: Bilayer model adjusting well breakthrough curves of surfactant in Berea sandstone. Adapted from [64], Copyright 2023, with permission from Elsevier.

For the sake of comparison between isotherm models in static and dynamic form, another isotherm models can be added besides the equilibrium models already cited:

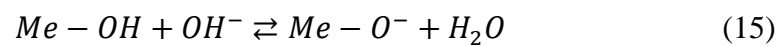
Expression adsorption term	Model -type
$\frac{d\Gamma}{dC_e} = \frac{b}{n} C_e^{\frac{1}{n}-1}$	Freundlich - Equilibrium
$\frac{d\Gamma}{dC_e} = \frac{K_r(1 + (1 - \beta_r) \alpha_r C_e^{\beta_r})}{(1 + \alpha_r C_e^{\beta_r})^2}$	Redlich-Peterson - Equilibrium
$\frac{d\Gamma}{dC_e} = \frac{K_s \beta_s C_e^{\beta_s-1}}{(1 + \alpha_s C_e^{\beta_s})^2}$	Sips - Equilibrium

Table 3: Other dynamic adsorption models developed from classical isotherm models

4.3 Surface complexation model

As seen in the review of literature on surfactant adsorption, salinity and pH could significantly alter the adsorption behavior of every type of surfactant species. This happens mainly because it modifies the surface sites which the surfactant molecules can adsorb, whether deprotonating and protonating surface species or exchanging ions, thus changing the potential of the surface. Yet, for solid particles or surfaces to acquire surface electric charges, the contact with a polar medium is sufficient.

Electrostatic and van der Waals interactions always arise between surfactant molecules and sites; the latter are mostly metal hydroxide with hydroxyl groups for the minerals of this work. They can be found protonated, deprotonated (equations 14 and 15) or in their natural form. As presented by surface charge basic theory in Shaw [74], hydrogen and hydroxyl are potential determining ions (PDI) because their concentration determines the electrical potential of the solid particle surface. Therefore, pH is a major factor in the surface potential determination.



Considering that the aqueous phase in contact with the surface always has solvated electrolytes species, they tend to adsorb on the surface of these protonated or deprotonated hydroxyl groups through ion exchange and ion-ion interactions mechanisms. This ion-adsorption proceeds to form layers of ions and counterions and complexation may occur as different ions adsorb in different distributions (Figure 18). The layers of adsorbed ions are situated in two different regions: the closest to the surface, mostly referred to as Stern layer, and the most outer region called the Diffuse Double Layer (Figure 18).

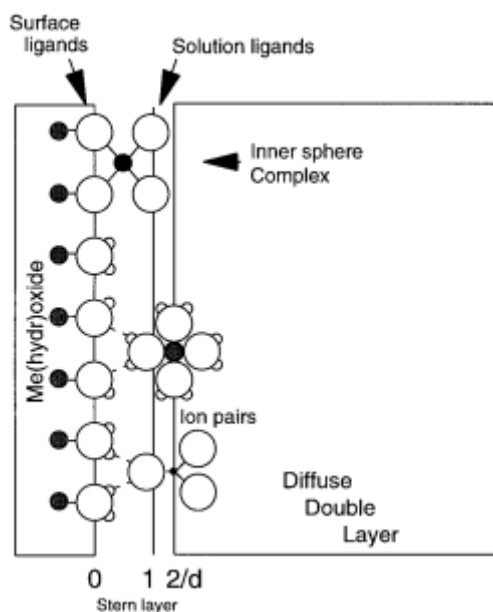


Figure 18: Stern layer and Diffusive Double Layer. The largest and smallest white circles are oxygen and hydrogen atoms, respectively, and the black circles represent solvated ions. The inner sphere complexes are formed between the 0-plane and the 1-plane of the stern layer, and the outer sphere complexes are formed at a minimum distance of approach of hydrated ions .Adapted from [75], Copyright 2023, with permission from Elsevier.

The structure of these adsorbed ion layers is often constructed based on a three-plane model (TP) [75] commonly called triple layer model by other authors ([76], [77] and [78]). In this approach, three electrostatic planes exist at the surface of the solid: 0-, 1- and 2- or d planes, the latter divides the two regions of the Stern Layer and the Diffuse Double Layer (DDL), both constitute the electrical double layer (EDL).

The ionic species interact with the hydroxyl sites and form complexes in the inner sphere and outer sphere. The location of the central ionic species of the complexes closest to the surface is between the 0- and 1- plane (inner sphere) where the ligands shared with the surface are in the 0- plane. The other ligands are located in the 1- plane, where other central ions adsorb between the 1- and 2- or d plane. (outer sphere) [75]. As Rahnemaie et. al [77] pointed out, the outer ion complexes do not have common ligands with surface groups (Figure 19).

Because many ions can form inner sphere complexes with surface groups, one or more ligands of the adsorbed ion are common with the surface, other ligands are oriented towards the solution. These differences in orientation lead to

differences in the distance from the surface, and then the compact part of the EDL, i.e., the Stern Layers, will have a distribution of charge. This is the charge distribution (CD) principle of the TP model presented by Hiemstra and van Riemsdijk [75]. For each defined surface reaction, e.g., dissociation and adsorption, there is a charge distribution Δz_i in each plane ($\Delta z_0, \Delta z_1, \Delta z_2$) which must be imputed to the model.

Besides the charge location, another that need to be imputed is the capacitance of the Stern Layer, which is calculated from the combination of the capacitance of the inner (C_1) and outer sphere (C_2):

$$\frac{1}{C} = \frac{1}{C_1} + \frac{1}{C_2} \quad (16)$$

Where each capacitance depends on the relative dielectric permittivity of the medium ϵ_r , in this case, water (78.5 at 25°C), and the distance of the planes from the surface (d_i), as shown in equation (16):

$$C_i = \frac{\epsilon_0 \epsilon_r}{d_i} \quad (17)$$

The ϵ_0 is the dielectric permittivity of the vacuum (8.854×10^{-12} F m⁻¹) and the distances of the planes are adjustable with experimental data.

The charge distribution approach needs to be accompanied by a multi-site complexation model (MUSIC) since there are different metal oxides and other surface groups in the minerals in this work. This was first introduced by Hiemstra et. al [79], because of the different proton affinities of the metal oxides on the solid Liquid interface. Combined with the concepts of charge distribution, the CD-MUSIC complexation model is then assumed to be the triple-layer model utilized for surface charge, potential and speciation in this work. This conceptual framework proved to be effective in predicting surface potentials and adsorption phenomena ([75], [77], [78], [80], [81]).

According to Bonto et. al [82] review's, CD-MUSIC model can determine the surface potentials (Ψ_i) through the charge density (σ_i) of each plane (Figure 19). Surface potentials are assigned for the three planes and their values decrease

with the distance from the surface towards the bulk until reaching zero. In the inner sphere and outer spheres, the potential decreases linearly with distance and proportional to the capacitance of each compressed layer. Entering the DDL domain the potential decreases rapidly because charge density decreases almost exponentially.

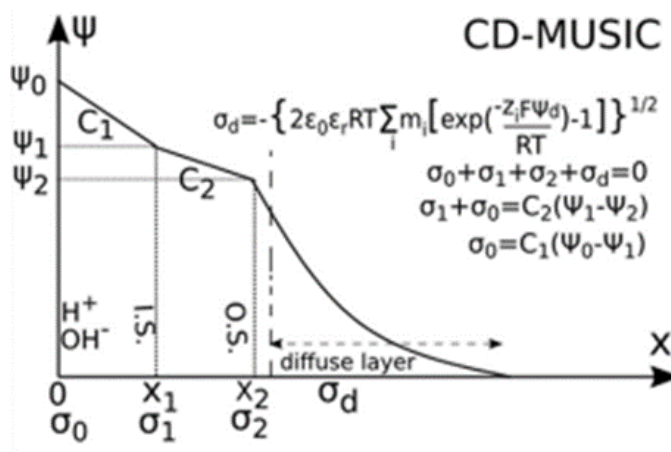


Figure 19: Surface potentials determination through CD-MUSIC equations. Adapted from Bonto, María et al. [82]

The zeta potential represents the potential at the boundary between stagnant and mobile ions, or commonly known as the slip or shear plane [82] and it is an effective indicator of electrostatic forces on the solid-liquid interface. As Bonto et. al [82] stated, prediction zeta potential with surface complexation models (SCM), such as CD-MUSIC, necessarily involves assumptions for the distances of the electrostatic planes, x_i (Figure 19) or d_i . The shear plane is considered an adjustable variable, but it provoked contrasting values in the literature in the case of calcite-brine interface [96]. To reduce the number of adjustable parameters is often assumed that the zeta potential coincides with the potential at 2-, d- or outer sphere plane Ψ_2 or Ψ_d .

Therefore, changes in que molar quantities of the adsorbed ions derived from the brine-rock equilibrium will alter the charge density of the planes, thus the zeta potential estimation. Software with a database of species involved in the equilibrium, as well the equilibrium constants, is necessary to develop such estimations and determine the polarity and magnitude of the zeta potential of sandstone and limestone.

The geochemical simulation software PHREEQc has built in its code the proper implementation of the CD-MUSIC model. Charge distribution, capacitance of the compressed layers and reactions involving dissociation, protonation or complexation of sites need to be defined before the calculations. In this case the works of Takeya et. al [78],[80], Elakneswaran et. al [81] defined the parameters which adjusted experimental data of zeta potential for the brine-calcite and brine-sandstone systems where the utilized brine is sea water with closer concentration to the brine utilized in this work.

Table 4 and 5 show all ion adsorption, dissociation or protonation reactions and parameters assumed on the works of Takeya and Elakneswaran which performed well on adjusting to experimental data.

	Limestone	Sandstone
sites (site density [sites m ⁻² rock])	> CO ₃ H (4.95)	quartz > SiOH (2.95)
	> CaOH (4.95)	kaolinite > SiOH (0.32)
		kaolinite > AlOH (0.32)
specific surface area [m ² g ⁻¹]	1.23	1.37
C1 [F m ²]	3.098	3.098
C2 [F m ²]	0.65	0.2

Table 4: PHREEQc sites parameters

Site density was corrected for the sandstone since the original values from Elakneswaran et. al [81] were related to each mineral surface area, and in this work only the rock surface area as a role was obtained. The site density was then pondered by its quantity in 1 g of rock based on the reference composition and specific surface area values for each mineral on sandstone. Had the site quantity in 1 g of sandstone being estimated, the determined specific surface is of sandstone in this work was used to correct the values from site per mineral surface area to site per rock surface area.

The capacitance of the inner sphere was defined based on the size of the largest ion adsorbed (calcium) for both interfaces. The outer sphere capacitance was calculated for the calcite case, as the sum of the Stern layers distance was 13Å [80]. In the case of the outer sphere capacitance for quartz and kaolinite surface, the

values assigned are based on Leroy et. al [76]. Finally, the PDI's considered in this work are H^+ , OH^- , Ca^{2+} , Mg^{2+} and SO_4^{2-} .

Reactions	Δz_0	Δz_1	Δz_2	$\log(K)$ [25°C]
Calcite-Brine interface				
$> CO_3H \rightleftharpoons > CO_3^- + H^+$	-1	0	0	-7.3
$> CaOH + H^+ \rightleftharpoons > CaOH_2^+$	1	0	0	15
$> CO_3H + Ca^{2+} \rightleftharpoons > CO_3Ca^+ + H^+$	-1	2	0	-6.45
$> CO_3H + Mg^{2+} \rightleftharpoons > CO_3Mg^+ + H^+$	-1	2	0	-6.15
$> CaOH + H^+ + SO_4^{2-} \rightleftharpoons > CaOH_2SO_4^-$	1	-2	0	14.75
Quartz-Brine interface				
$> SiOH + H^+ \rightleftharpoons > SiOH_2^+$	1	0	0	-1.75
$> SiO^- + H^+ \rightleftharpoons > SiOH$	-1	0	0	6.75
$> SiOH + Ca^{2+} \rightleftharpoons > SiOCa^+ + H^+$	-1	2	0	-5.70
$> SiOH + Mg^{2+} \rightleftharpoons > SiOMg^+ + H^+$	-1	2	0	-5.70
Kaolinite-Brine interface				
$> SiOH + H^+ \rightleftharpoons > SiOH_2^+$	1	0	0	0.80
$> SiO^- + H^+ \rightleftharpoons > SiOH$	-1	0	0	7.00
$> SiOH + Ca^{2+} \rightleftharpoons > SiOCa^+ + H^+$	-1	2	0	-6.00
$> SiOH + Mg^{2+} \rightleftharpoons > SiOMg^+ + H^+$	-1	2	0	-5.55
$> AlOH + H^+ \rightleftharpoons > AlOH_2^+$	1	0	0	0.80
$> AlO^- + H^+ \rightleftharpoons > AlOH$	-1	0	0	7.00
$> AlOH + Ca^{2+} \rightleftharpoons > AlOCa^+ + H^+$	-1	2	0	-6.00
$> AlOH + Mg^{2+} \rightleftharpoons > AlOMg^+ + H^+$	-1	2	0	-5.55

Table 5: CD-MUSIC parameters on PHREEQc

Some other works utilized models with slightly different formulations and parameters for quartz [83] and calcite [84], but the works previous mentioned in table 5 accounts for experiments at conditions like the ones of this dissertation and

used the same model for the two types of rocks (considering limestone as calcite and sandstone as quartz and kaolinite), thus maintaining assumptions.

5. Materials and Methods

5.1 Surfactant, brine and rocks

5.1.1 Surfactant characteristics and properties

The zwitterionic, or zwitterionic, surfactant utilized in this work was Cocamidopropyl betaine (CAPB), obtained as a gift from Oxiteno (Brazil) in the form of a commercial formulation (Oxitaine CP 30 APH) containing 30 wt.% of the active compound. This surfactant is commonly used in EOR-oriented research [85, 86], and its molecular formula and molecular weight are, respectively, $C_{19}H_{38}N_2O_3$ and 342.5 g mol^{-1} . The chemical structure is represented in Figure 20.

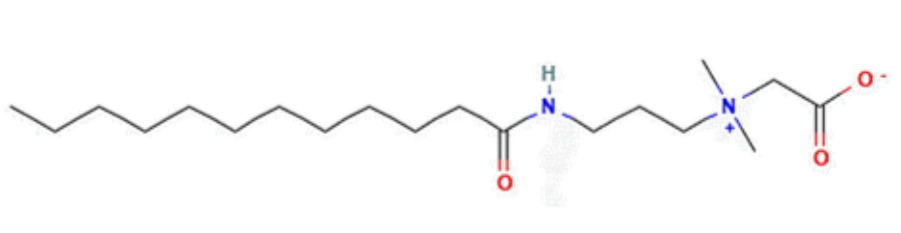


Figure 20: CAPB molecular structure, from [88]

CAPB is obtained from the reaction between coconut oil fatty acids and 3,3-dimethylamine propylamine (DMAPA) in aqueous solution, where an intermediate product (cocamidopropyl dimethylamine) is reacted with sodium monochloroacetate to produce the intended betaine [87].

This surfactant can be present in two forms, depending on pH, which confers its zwitterionic character. At acidic pH (below isoelectric point 3.34 [89]), the carboxylic acid moiety is protonated, and the cationic form is predominant. At higher pH values occurs deprotonation of the acid, and at $\text{pH} > 6$ most surfactant molecules are in the zwitterionic form [90]. Therefore, in the tested conditions of this work ($\text{pH} > 7$) the zwitterionic form is the sole one.

5.1.2 Brine (DSW) composition and properties

The brine used in this work had similar composition to desulfated seawater (DSW), often used as injection water in offshore environments [93,94]. The dissolved salts utilized on the making of the DSW were: NaCl, CaCl₂-2H₂O, MgCl₂-6H₂O, KCl, NaHCO₃ and Na₂SO₄, all from Sigma Aldrich, Brazil with >99% purity. The DSW was prepared by adding the appropriate mass of salt to deionized water to the concentration shown on Table 6:

Composition	
Ions	Concentration [mg L ⁻¹]
Na ⁺	11,000
Ca ⁺²	132
Mg ⁺²	151
K ⁺	393
Cl ⁻	17,937
SO ₄ ⁻²	23
HCO ₃ ⁻	72
Physical-Chemical Properties	
Salinity [mg L ⁻¹]	30,529
Ionic Strength [mol kgw ⁻¹]	0.517
pH*	7.86 ± 0.10
Conductivity* [mS cm ⁻¹]	45.58 ± 0.02
Viscosity [mPa.s]	0.90

*average between static and dynamic tests brine

Table 6: DSW composition and physical-chemical properties

The pH and conductivity of this brine was measured with a calibrated Metrohm pH Meter/Conductometer at ambient temperature, resulting in the respective values of 7.95 and 45.55 mS cm⁻¹ for the static adsorption tests and 7.76 and 45.60 mS cm⁻¹ for the coreflood tests. For the brine mixed with surfactant was added LiCl to a concentration of 2 g L⁻¹. Brine viscosity at 30°C was 0.90 mPa.s, measured with a HAAKE MARS Rheometer.

5.1.3 Rocks characteristics and properties

The adsorption tests were conducted in two types of outcrop rocks mimicking composition of carbonate and sandstone reservoir rocks. Two subtypes of sandstones cores were obtained: Berea Buff and Berea Spider; as also one subtype of limestone core: Indiana. The Indiana core is a carbonate that originated from the Mississippian formation and the two sandstones came from the Upper Devonian formation. Both types of rocks were analogue to oil reservoirs and were supplied in cylindrical shape by Kocurek Inc. (Figure 21).



Figure 21: Rock cores, adapted from [95]

The main difference between the sandstones compositions is that the limestone is predominantly constituted of calcite (CaCO_3) and the sandstones of quartz (SiO_2). However, the clay content (kaolinite, illite, chlorite, smectite, and muscovite) may vary between Berea Buff and Spider subtype, being considerably higher for Berea Spider. Table 7 shows sandstones and limestone composition obtained from works in the literature, as well as physical properties of the cores.

Rock subtype	Diameter [cm]	Length [cm]	Main mineral (%)	Clay content (%)
Berea Buff	2.54	15	Quartz (>83%)*	5%**
Berea Spider			Quartz (>90%)**	7.6%**
Indiana			Calcite (>99%)***	0%***

* ([97], [98], [81]) ** [97] *** ([99],[100],[101])

Table 7: Rock subtypes and main characteristics

For the dynamic experiments, cylindrical rock plugs of Berea Spider sandstone (Figure 22 (b)) and Indiana limestone (Figure 22 (a)) were separated for dynamic adsorption experiments. Its petrophysical properties are described in table 8.

The methodology which was utilized to determine the basic petrophysical properties of the cores is detailed in Section 5.4.1 Preparation and petrophysical characterization of rock plugs for the experiments.



Figure 22: (a) Indiana Limestone and (b) Berea Spider Sandstone cores

The measured petrophysical properties are shown on Table 8.

Core sample	Porosity [%]	Gas Permeability [mD]	Pore Volume [cm ³]	Bulk Volume [cm ³]	Mass [g]	Bulk density [g cm ⁻³]
Limestone	15.22 ± 0.14	180.10 ± 14.80	11.47 ± 0.10	75.38	167	2.22
Sandstone	19.52 ± 0.04	207.58 ± 17.35	14.78 ± 0.04	75.77	158	2.08

Table 8: Core samples basic petrophysical properties

5.2 Surfactant characterization and quantification

5.2.1 Determination of CAPB critical micelle concentration (CMC)

The critical micelle concentration of CAPB was determined from surface tension measurements. The tensiometer Kibron Ez-Pi Plus was used for all the measurements. Prior to the tests, the equipment was calibrated utilizing deionized water which has a known surface tension of 72 mN m^{-1} . CAPB solution's surface tension was measured at ambient temperature ($25 \text{ }^\circ\text{C}$).

To calculate the CMC of the surfactant solutions, it is considered that the interfacial tension, or superficial tension if it is an air-liquid interface, does not change significantly with concentration past a certain point, which is the CMC itself [15]. Thus, the calculation involves fitting a straight line on two regions of the plot, the first one lies on the decrease in surface tension with the logarithm of the concentration and the second one is the region of constant surface tension.

5.2.2 Determination of CAPB absorption spectrum

The absorbance spectra of CAPB range were determined to optimize analytical methods suited for its detection, as in the case of High-Performance Liquid Chromatography (HPLC) with a UV-lamp. There is a need to adjust the wavelength of the light source to get maximum absorbance and improve selectivity while injecting in the chromatography column.

One of the prepared CAPB solutions was evaluated in the Agilent 1260 Infinity II HPLC apparatus utilizing a Diode Array Detector (DAD). The spectrometer bandwidth is limited to a 190 nm-950 nm range.

5.2.3 Quantification of CAPB by High performance liquid chromatography (HPLC)

To determine surfactant adsorption in static and dynamic experiments, an analytical method capable of detecting and quantifying the CAPB molecules needed to be implemented. The method consists of injecting a mobile phase of variable volumetric ratio of Acetonitrile (CH_3CN) from Supelco e (for HPLC

Gradient Analysis) and Ammonium Acetate (NH_4OAc), also from Supelco (for HPLC LiChropur) at acidic pH, using a UV-lamp source to create an absorbance spectrum. Then the samples are drawn to be analyzed.

This gradient approach for mobile phase injection led to a tilted baseline for the spectrum during sample analysis. In comparison to a standard isocratic injection of mobile phase (50:50 volume of Acetonitrile and Ammonium Acetate), a good separation was obtained between the peaks from species from the matrix (brine/DSW) and the analyte itself (CAPB) with de gradient injection.

The utilized method was applied with a chromatographer (Agilent® 1260 Infinity II) and a suitable column for the analyte (Acclaim Surfactant Plus; 250 x 4.6 mm, 5 μm). Samples were previous filtered with .22 μm hydrophilic filter before injection into the column.

5.3 Methodology for Static Adsorption Experiments

5.3.1 Preparation of rock samples

The preparation for the static adsorption experiment started by preparing the rock powder as adsorbent. It was prepared by crushing two core samples provided by Kocurek: one from Berea Buff Sandstone and another from Indiana Limestone. Both cores were brought to CETEM (Centro de Tecnologia Mineral - Ilha do Fundão) where they were crushed utilizing a jaw crusher followed by a disc crusher, resulting in a thin powder which was collected and labeled afterwards.

The collected powder was sieved in an electromagnetic sieve utilizing 32 and 150 MESH size for 30 minutes with vibration intensity set to 10 (maximum). The sieving was executed until we had enough powder to fill a single 50 ml Falcon tube for each rock. A 32 MESH allows particles with diameter below 518 μm , used for larger debris from the core crushing step, and a 150 MESH allows particles with 111 μm of diameter or lower.

After sieved, both materials were cleaned through a Soxhlet apparatus. The glassware was assembled over a bowl of glycerin with a heating plate beneath. A magnetic stirrer was inserted into the round flask and the bowl, the latter supported the temperature sensor for the glycerin bath.

Toluene was left to cycle in the Soxhlet within 1 day at 150 °C and then substituted by methanol to cycle within the same period at 90°C. As soon as the cycles were completed, the remaining material was dried in a vacuum oven at 90°C and 0.1 bar. At last, each powder was collected and stored in a Falcon tube.

5.3.2 Determination of superficial area by Brunauer-Emmett-Teller (BET) adsorption isotherm

Determining the surface area of the adsorbent (rock powder) is necessary to evaluate the mechanism of adsorption for CAPB on the rock surface. Hence, a representative sample of the cleaned rock powder obtained during preparation was sampled and sent to BET analysis for specific surface area quantification. The BET analysis consisted in evaluating N₂ adsorption on samples of Berea Buff and Indiana after the drying step. The samples were sent to CENPES (PDAB/TFCC division) where roughly 0.3 g of each rock was submitted to a -195°C bath for analysis. N₂ adsorption was calculated in relation to relative pressure (current pressure and vapor pressure ratio) to create an isotherm plot. The equilibration elapsed time was around 1 hour and 40 minutes for both samples.

The BET equation (18) for linear adjustment of the N₂ isotherms is demonstrated below [102].

$$\frac{1}{Q \left[\frac{P}{P_0} - 1 \right]} = \frac{1}{Q_m C} + \frac{C - 1}{Q_m C} \left(\frac{P}{P_0} \right) \quad (18)$$

Where Q is the amount of gas molecules adsorbed per mass of adsorbent, Q_m is the coverage of the first layer (considered a monolayer), P is the actual gas pressure, P_0 is the N₂ vapor pressure and C is an isotherm parameter. By plotting $\frac{1}{Q \left[\frac{P}{P_0} - 1 \right]}$ versus $\frac{P}{P_0}$, a straight line is adjusted and the slope $\frac{C-1}{C Q_m}$ determined. As the value C is usually very large, the slope becomes $\frac{1}{Q_m}$ [102]. The surface is calculated from equation (19):

$$S = Q_m N_A a_m \quad (19)$$

Where N_A is the Avogadro number and a_m is the molecular projected area of the N_2 [102].

5.3.3 Methodology for static adsorption test

The static adsorption of CAPB on Berea Buff Sandstone and Indiana Limestone was evaluated through a batch experiment (Figure 23) where crushed rock powder was contacted with a known concentration surfactant solution (prepared with DSW) under agitation. Prior to performing experiments with different surfactant concentration to determine adsorption isotherm, an evaluation of the optimum liquid to solid ratio was done to determine the appropriate mass of rock and volume of surfactant solution needed for the experiments.

One of the points to consider in the methodology adopted in the static adsorption studies is the ratio between solid and liquid phases in the batch experiment. As shown in Section 6.1.2.2 Results from method of quantification of CAPB by HPLC, the chromatograms showed a significant peak of surfactant, and the difference between the area of the chromatogram peak from initial solution and from the equilibrated solution needed to be greater than the quantification error. Therefore, three liquid-to-solid ratios were tested prior to adsorption experiments to select the one with least variation in the results due quantification error (see Appendix 9.1 Results of selected liquid to solid ratio for static experiments)

The ratios changed in relation to the solid quantity, as the volume was set to 10 mL and the adsorbent masses were: 0.5, 1.0 and 2.0 grams. The 5:1 liquid to solid ratio was selected among the other two because of the significant adsorption. To use less adsorbent material in the tests, the 5 to 1 ratio was maintained with 5 mL of solution 1 g of adsorbent material. Then, it was tested in Indiana limestone against other ratios (20 to 1 and 10 to 1) in triplicate to ensure the conclusion taken on the first chromatograms in Appendix 9.1 Results of selected liquid to solid ratio for static experiments.

After the optimum liquid to solid ratio was determined the experiments were performed. They began by placing 1 g of the prepared adsorbent material into

a vial containing 5 mL of a known concentration CAPB solution. Afterwards, the vial was closed with a cap and securely placed on the orbital shaker. This step was done simultaneously for all 9 concentrations ($0.05 - 1.00 \text{ g L}^{-1}$) evaluated in this work. All the experiments were performed with an agitation of 300 rpm and temperature of 30°C . To assess repeatability of the data, all the experiments were carried out in triplicates. All the experiments were carried out for 24 hours to allow the system to reach equilibrium, that is, no change in surfactant concentration in the aqueous phase.

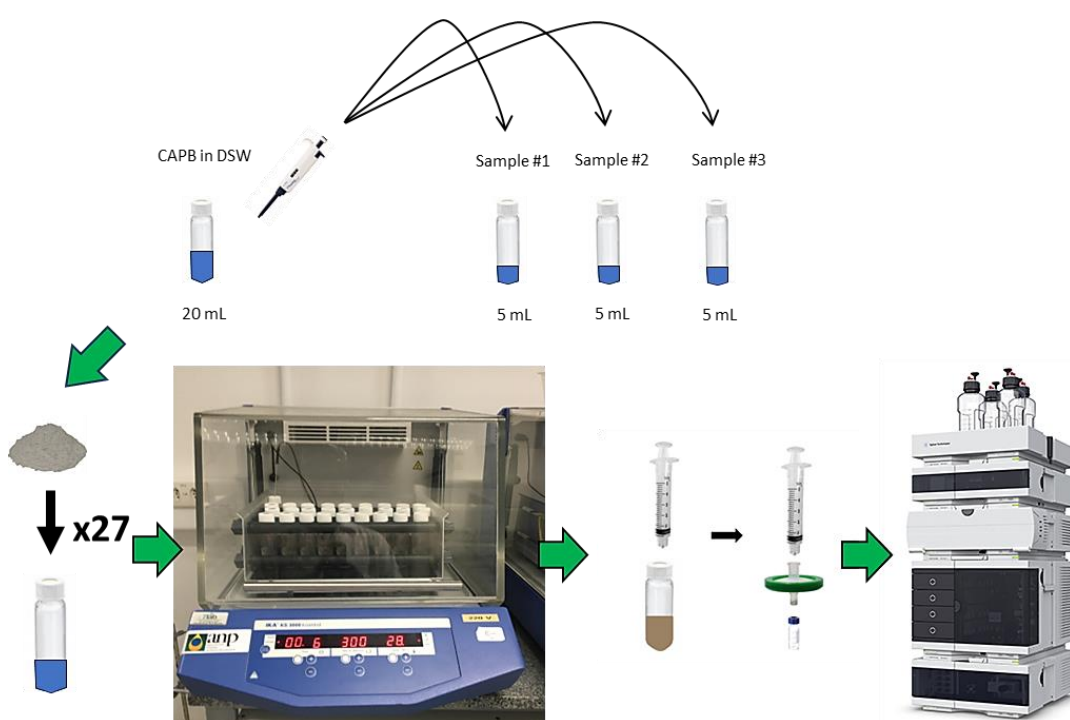


Figure 23: Schematic of static adsorption methodology

After that time, a process of transferring and filtering the sample with a $0.22 \mu\text{m}$ filter to a 2 mL HPLC flask was executed. The filtered samples were quantified by HPLC-UV utilizing an optimized chromatographic condition previously presented. (Figure 23). The quantification results were then computed into a spreadsheet where the adsorption could be calculated with two formulas, one standing for mass of surfactant per mass of rock ($q, \text{mg/g}$) and per BET surface area ($\Gamma, \text{mg/m}^2$):

$$q = \frac{(C_0 - C_e)V}{m_{rock}} \quad (20)$$

$$\Gamma = \frac{(C_0 - C_e)V}{m_{rock} A_{s,BET}} \quad (21)$$

Where C_0 and C_e are, respectively, the initial and equilibrium concentrations of the CAPB (g L^{-1}), V is the volume of the solution (mL), m_{rock} as the mass of adsorbent weighted before (g) the test and $A_{s,BET}$ is the specific surface area ($\text{m}^2 \text{g}^{-1}$) of each rock powder determined by BET analysis.

The pH and conductivity of the brine were measured before and after the experiment to assess any changes that might have occurred.

5.3.4 Methodology for zeta potential and surface complexation modelling

To calculate zeta potential of the system: DSW-limestone and DSW-sandstone without surfactant, a script on the geochemical simulator PHREEQc was written, firstly, to match the experimental data obtained by Takeya et. al [80] and Elakneswaran et. al [81] and the calculated potential zeta value utilizing their parameters and conditions.

After validation, the DSW composition, ion concentrations, pH, quantities of liquid and solid phase and specific surface area from BET were inputted to the PHREEQc code to match the conditions of the static adsorption experiments. Then the equilibrium conditions were calculated using the defined reactions and parameters on Section 4.3 Surface complexation model on the literature review.

5.3.5 Adsorption isotherm fitting for static adsorption results

The adsorption isotherm models applied for fitting the static adsorption, per mass of rock (q) data were selected from the literature (Section 4.2.1 Static adsorption models) based on previous documented applications and some were based on combinations of common applied isotherm models for two layers [63]. These bilayers combinations were implemented to be tested on its capacity of describing surfactant adsorption phenomena in comparison to monolayer models.

A monolayer approach differs from bilayer approach because the latter assumes two layers of adsorption. They also could differ, or agree, in underlying mechanisms of adsorption, where each layer is modelled with different, or equal, isotherm types. The two approaches were compared with each other with respect to its performance adjusting the experimental data.

The model adjustment was implemented in a MATLAB script with the *fit* function, which applies the non-linear squares method. This method was chosen primarily over linearization of the isotherms and linear regression because the latter could add bias to the fitted parameters errors [54,55]. The Trust-Region algorithm was utilized in the static adsorption isotherm fitting.

Also, a method of randomized reinitialization of the parameters vector was applied until its values converge within a tolerance range: the parameters are updated with a deviation σ_j with magnitude greater or equal to $|a_i + a_{i+1}|$, where a_i is the initial set of parameters (initial guess) and the a_{i+1} is the resulted set of parameters from the fitting [106].

Fit evaluation has been made with two metrics: adjusted R^2 and RMSE (Root Mean Square Error), as described in [55]. Therefore, best fit will be the one with R^2 closest to one and lowest RMSE.

After selecting the best fit models of each set, the parameters were interpreted based on described mechanisms appointed in the literature review section for each model. Then, the two sets, monolayer and bilayer approach models, were compared in performance. A potential mechanism was detailed and illustrated for CAPB adsorption on each rock surface.

5.4 Determination of dynamic adsorption through flow tests

5.4.1 Preparation and petrophysical characterization of rock plugs for the experiments

Prior to the experiments, the cores were cleaned using Soxhlet extraction. The procedure was very similar to the rock powder preparation but, cycling only methanol at 90°C, instead of toluene followed by methanol. After one day cycle, both cores were dried in the same vacuum oven of the rock powder preparation step, also at 90°C.

Had the cores been cleaned and dried, their petrophysical properties such as permeability and porosity were measured. Gas permeability was measured with nitrogen using a permeameter (Ultraperm®610), and porosity and pore volume were measured using a helium porosimeter (UltraPore®600). Both measurements were performed in the LMR (Laboratório de Mecânica de Rochas) at PUC-Rio, before and after adsorption experiments. Also, both measurements were performed using a confining pressure of 138 bar, which is the same used for the dynamic adsorption experiments.

5.4.2 Determination of rock cores surface area (pore space) using microtomography

A significant part of the surfactant transport characteristics depends on the pore space properties, such as dispersion with tortuosity [72]. Hence, some of these were analyzed through a computed tomography scan, in the micro scale (μ CT-scan). More importantly, a representative specific surface area was determined from CT images for understanding the dynamic adsorption behavior as a function of rock chemical composition and structure.

A ZEISS Xradia 510 Versa X-ray microCT scanner from the Laboratorio de Microtomografia de Raios-X, at PUC-Rio, was utilized to acquire images from the pore space of the Berea Spider and Indiana core samples, after the experiments in two different resolutions: 35 and 6 μ m per pixel, both acquisitions performed with voltage set to 140 kV. As shown in Figure 24, to obtain the 3D images of the pore space the sample is exposed to an X-ray source in a rotating platform with a detector behind the sample, aligned with the light source. 2D projections are obtained from the light intensity profiles acquired with the detector, and through a series of computer methods and transformations, 2D images are converted to cross sectional images of the core. Finally, these cross-sectional images are compiled in a single 3D image.

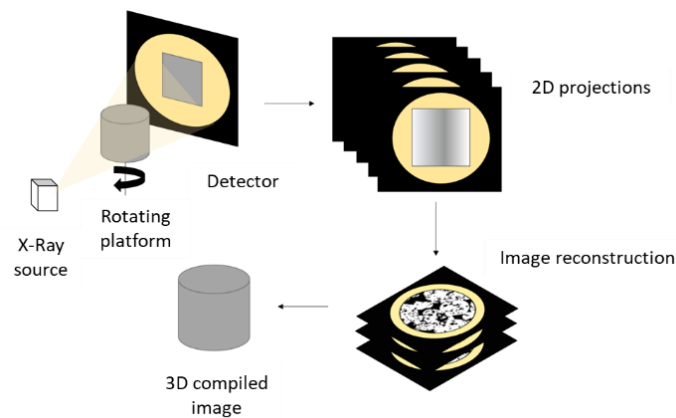


Figure 24: The process of image acquisition in a CT-scan

After image acquisition with the micro-CT scanner, the images were processed to enhance the image quality and to segment its regions into pore space and everything that is not void, utilizing software such as ImageJ, DragonFly, MATLAB Image Processing Toolbox and Avizo. The segmentation step involves a binarization of the image pixels assigning values of 1 to pore space and 0 for everything else (Figure 25). This binarization is achieved with Otsu's algorithm [104].

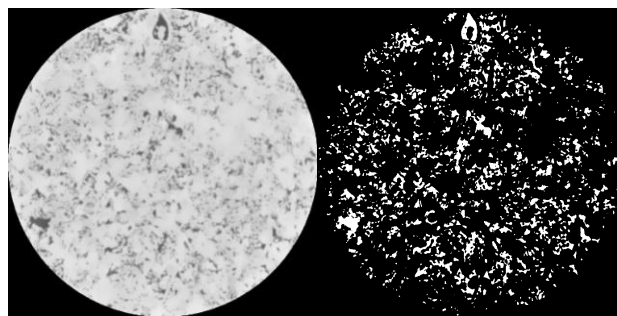


Figure 25: Core image default and binarized image

As the output binary images do not represent entirely the core properties, random Representative Elementary Volumes (REV) were cropped from the entire composition of images related to the measured porosity of each sample (Figure 26) with different edge lengths ranging randomly between 200 to 300 pixels and calculated porosity close to the measured for the entire core.

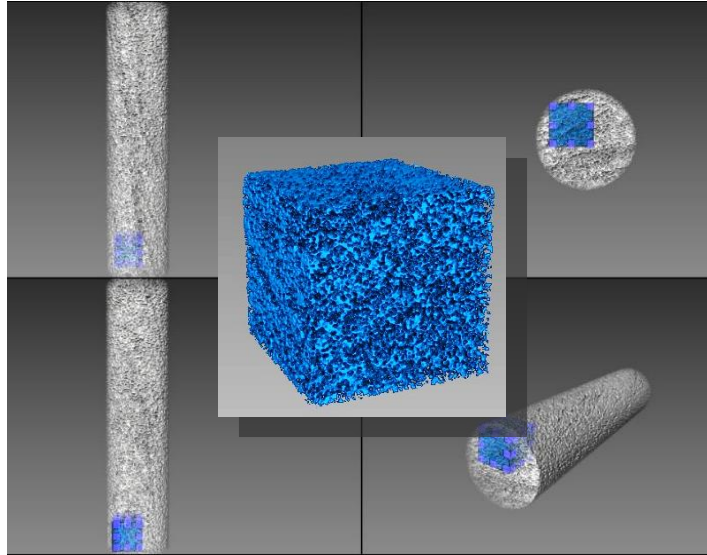


Figure 26: REV extracted from core 3D image and projections shown in Avizo software

REV porosity was determined by calculating the ratio of pixels with assigned value one to the total volume of the REV:

$$\phi_{REV} = \frac{\text{total pixels of pores}}{\text{total pixels of REV}} \quad (22)$$

The REV specific surface was determined with the *Object Specific Surface* module which calculates the superficial area of the pore space (*area3d*) and normalizes by its volume (*volume3d*):

$$SSA_{vol} = \frac{\text{area3d}}{\text{volume3d}} \quad (23)$$

Each resolution had a different SSA_{vol} , so it was observed a direct relationship between SSA_{vol} and the resolution of the acquired digital images, because new small pores start to appear with increased resolution. The final SSA_{vol} will be the extrapolation to the limit where resolution tends to the value of zero.

To calculate the final superficial area, and therefore the SSA ($\text{m}^2 \text{g}^{-1}$) of each core sample, the measured pore volume is multiplied by average SSA_{vol} of the randomly selected REV's and then normalized by the core mass (equations 24 and 25).

$$SA_{core} = SSA_{vol} * Pore Volume \quad (24)$$

$$SSA = \frac{SA_{core}}{m_{core}} \quad (25)$$

Finally, the REV tortuosity was determined by *Centroid Path Tortuosity* (CPT) module which calculates the tortuosity of path created by the centroid of each cross section through the core length (Equation 26 and Figure 27). Since tortuosity is a property of the porous media that influences dispersion phenomena it is fundamental to calculate it, and CPT is an efficient way of give it a value.

$$Tortuosity = CPT = \frac{\sum_{i=1}^{H-1} d_i}{H} \quad (26)$$

Where d_i is the distance between centroids of consecutives cross sections, and H is the total number of cross sections or planes which the centroid was calculated. Figure 27 shows a representation of the features involved in this metric:

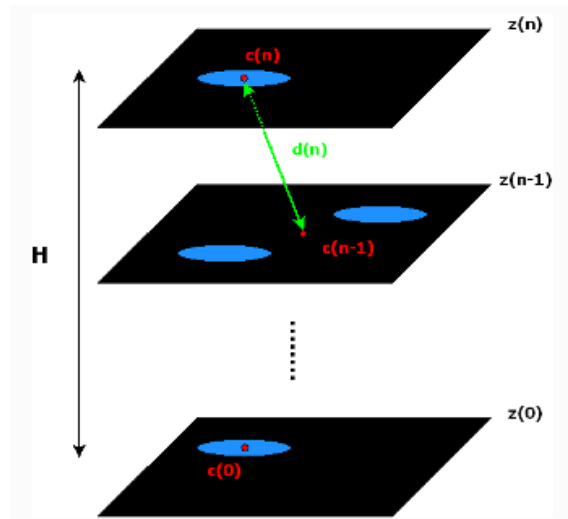


Figure 27: Visualization of Centroid Path Tortuosity (CPT), adapted from [105]

In this case, REV were cropped throughout the entire length of the 3D images for centroid path tortuosity (CPT) calculation (Figure 28).

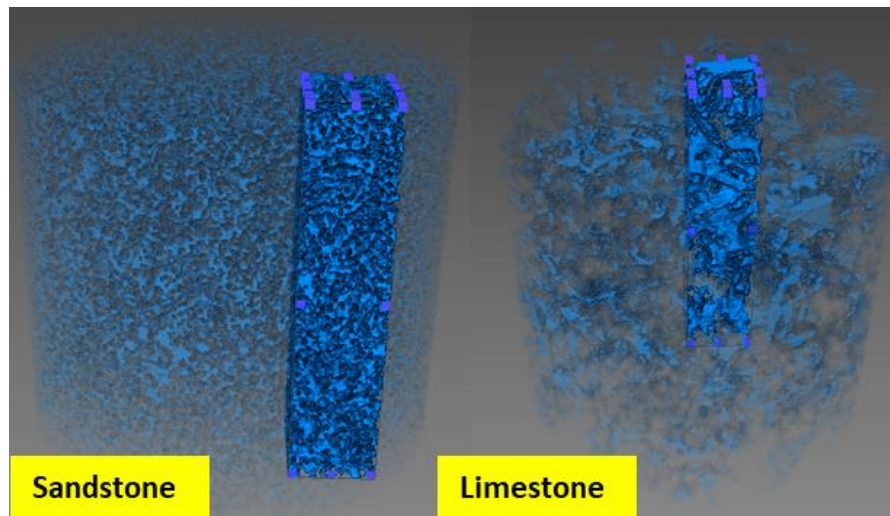


Figure 28: Example of cropped tortuosity REVs in Berea and Indiana cores at 6 $\mu\text{m}/\text{pixel}$ of resolution

5.4.3 Methodology for dynamic adsorption experiments

Three solutions were prepared for the dynamic adsorption studies: brine (DSW), 1.0 g L⁻¹ CAPB solution in DSW. The surfactant solution was doped with lithium chloride (2.0 g L⁻¹), and the lithium was used as a non-reactive tracer. A third solution consisting of 50:50 DSW: methanol was used to clean the core after the experiments. After the preparation, the three solutions were propped stored in the accumulators of the core flood system with proper caution to not generate bubbles or considerable air in the solution.

The system is mainly composed of: three accumulators which storage the solutions to be injected; the core holder, where the core is confined at high pressure; a series of differential pressure transducers linked to the core holder entrance, middle and exit sections; a system of automatic valves for isolating the core and permitting the flow of the liquids of interest; a system of syringe pumps to control flow rate and injection and confinement pressures; a back pressure system utilized to maintain the working pressure during the experiment; an oven with a thermocouple (core holder entrance) and temperature control; and finally, a fraction collector which collects produced effluent samples.

To prepare for dynamic adsorption tests, first, the system lines were cleaned with pure methanol and dried by blowing synthetic air through the lines. Then the

core was mounted in the Hassler type coreholder and connected to the closed accumulators. Afterwards, a confining pressure of 34.5 bar was applied to the core, and it was saturated with DSW under vacuum. After saturation of the core, all the lines were filled with brine. The pressure transducers were also purged during this process to make sure they could make accurate readings. Once the system was filled with brine, the core's pore pressure and the confining pressure of the system were raised to 100 bar and 172.4 bar, respectively. Brine was slowly injected overnight to make sure the core was saturated. The temperature of the system for the whole experiment was 30°C. Prior to the adsorption experiments DSW was through the core at five different flowrates, while recording pressure drop along the core. The core's brine permeability was determined using Darcy's law (see Table 9).

Core	Total (mD)
Sandstone	168.5 **
Limestone	260.1 **
** Test 3 with only dp2 and dp3 sections	

Table 9: Total K_w of each core sample

The odd result where limestone has more permeability related to the aqueous phase than gas phase could have occurred due to lack of the pressure drop measurement on the first segment of the core, which could assign a lower value for its entrance and reducing overall permeability.

After the K_w determination, the dynamic adsorption tests were performed in triplicates for each core at 0.7242 cm³ min⁻¹ (6.8 ft/day) flow rate, 30°C, 100 bar of working pressure. For the test, 5 PV of 1000 ppm CAPB surfactant solution dopped with lithium was injected (breakthrough/adsorption curve) followed by injection of 7 PV of DSW (elution/desorption curve).

During both stages, samples of the effluent were collected with the aid of a fractional collector (1.88 mL for limestone and 2.35 ml for sandstone). The effluent samples were filtered with a hydrophilic 0.22 μm diameter filter and surfactant concentration in the sample was determined from chromatographic analysis (HPLC) (see Figure 29).

For measurement of non-reactive tracer concentration (Li^+) in the effluent, the samples were diluted (1 to 100) and sent to elementary analysis through ICP-OES at LABSPECTRO (PUC-Rio). After the experiments 10 PV of a methanol/DSW mixture was injected (overnight injection) to remove all remaining surfactant from the core surface. Samples at 3 PV and at 10 PV were taken and surfactant concentration was also measured by HPLC.

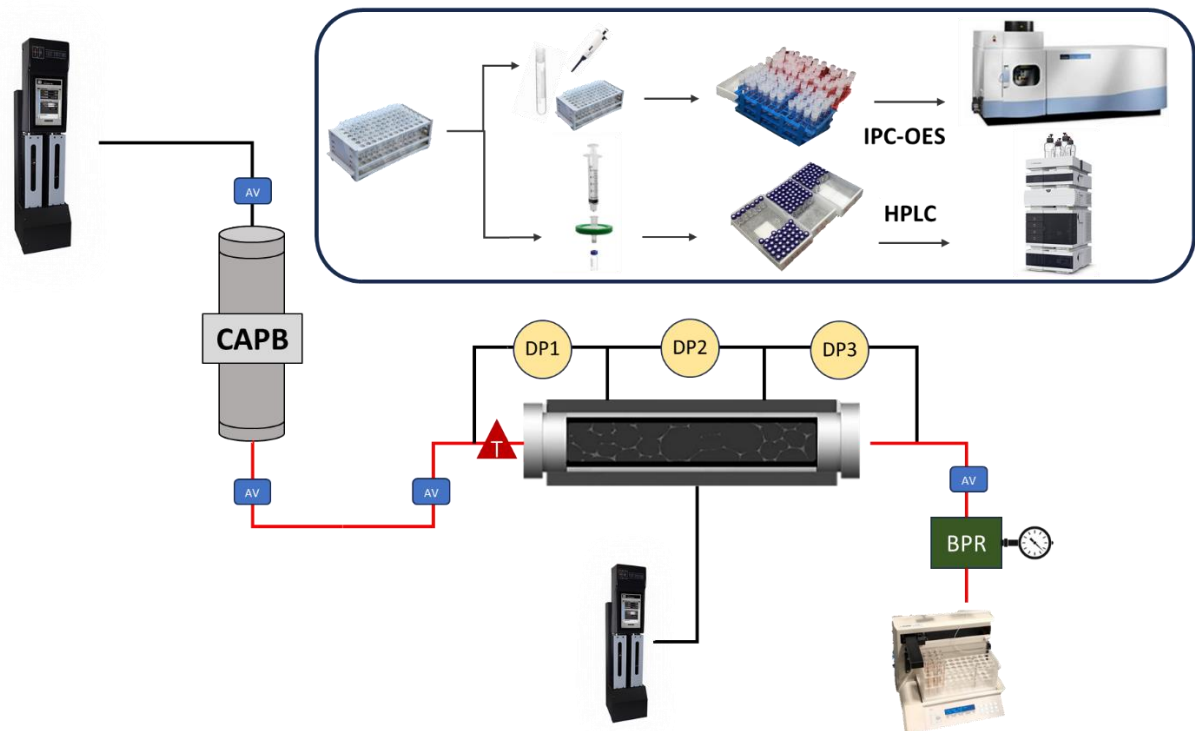


Figure 29: Dynamic adsorption setup and methodology

The dead volumes (red lines in Figure 29) of the surfactant injection corresponding to the line path of the accumulator to the core entrance and from the core exit to the fraction collector, were subtracted from the breakthrough curves and pressure drop data. With this adjustment, the PVs now represent the effective fluid quantity injected through the core samples.

5.4.4 History-matching of experimental dynamic adsorption data

Differently from the static adsorption behavior model adjustment, the dynamic adsorption behavior depends on the transport characteristics of the

surfactant solution in the porous media, and it is rather impossible or very much time and resource consuming to derive analytical solutions to surfactant breakthroughs. A more practical approach is implementing a numerical model which accounts for the hydrodynamic dispersion of the solutes coupled with adsorption kinetics or isotherm models and solve its parameters until a satisfactory fit is obtained. As the adjustment is numerically determined to match coreflood production data, the procedure is called history-matching.

As seen in Section 4.2.2 Dynamic adsorption models, the equations of the Advection-Dispersion model and Advection-Dispersion-Adsorption model are solved for the tracer and surfactant respectively, utilizing functions of the MATLAB Partial Differential Equation Toolbox, such as *pdepe*. The boundary and initial conditions are shown in table 10:

Expression	Condition
$C(x, 0) = 0$	Initial condition
$C(x_{inlet}, t) = C_0 \quad 0 < t < t_{inj}$ $C(x_{inlet}, t) = 0 \quad t > t_{inj}$	Boundary condition at inlet
$\frac{dC(x_{outlet}, t)}{dt} = 0$	Boundary condition at outlet

Table 10: Boundary and initial conditions applied for hydrodynamic dispersion equations

The solutions were evaluated in the last cell of the discretized space and the model breakthrough curves are interpolated in the interval of time of experimental data for purposes of comparison with coreflood data. The adjustment is also performed utilizing the non-linear squares method, with low tolerance, randomized reinitialization of parameters and adjustable parameters boundaries for seeking better solutions when convergence is biased to lower or upper boundaries.

The same metrics of the isotherm adjustments were applied for evaluation of the breakthrough curves and the experimental ones, and the best match was chosen based on highest adjusted R^2 and lowest RMSE.

6. Results and Discussion

This section is divided into four main subsections 6.1, 6.2, 6.3 and 6.4. 6.1 and 6.2 related to specific objectives and 6.3 and 6.4 related to the main objectives results. Subsection 6.1.2 shows the results from the developed method of CAPB quantification at the concentration interval of interest. The 6.2 subsection presents the specific surface area determination from BET and μ CT analysis for the rock samples in static and dynamic experiments. In the subsection 6.3, theoretical models were used to fit the data and gain further understanding of the dominating mechanisms of adsorption. These fittings were integrated to surface potential and speciation estimates to determine which active sites were available for adsorption on the rock surface, giving further insights on adsorption mechanisms. And finally, in section 6.4, the chosen history-match model from the dynamic adsorption results is used for estimating CAPB adsorption in limestone under dynamic equilibrium.

6.1 Results of surfactant characterization and quantification

6.1.1 Determination of CAPB critical micelle concentration (CMC)

Both fits of the respective regions are shown in Figure 30. The CMC is the intercept point of the two linear adjustments.

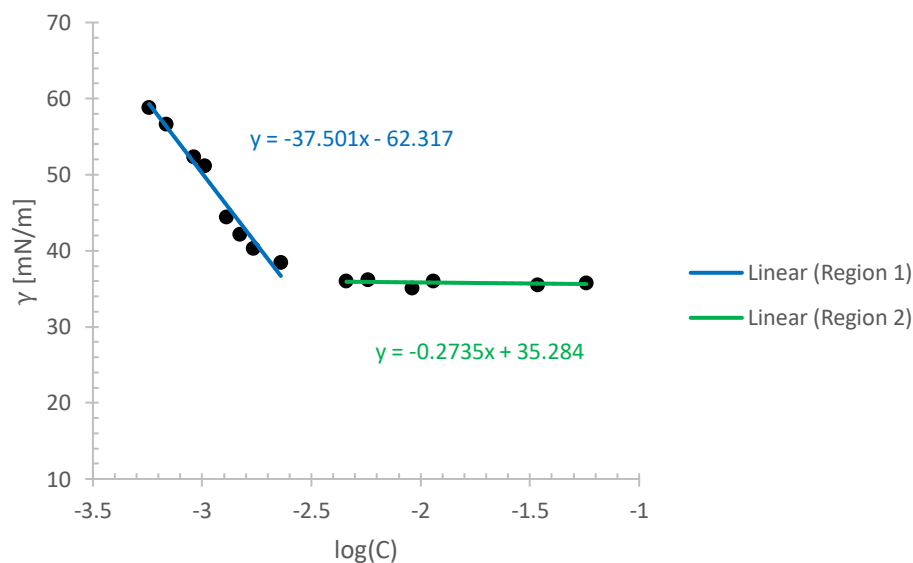


Figure 30: Surface tension measurements and linear adjustment

The resulting CMC from the calculation of the intercept is 23.89 mg L^{-1} ($\sim 0.0024 \text{ \% wt}$) for the CAPB in brine.

6.1.2 CAPB identification and quantification through HPLC

6.1.2.1 Results from determination of CAPB absorption spectrum

Figure 31 shows the CAPB spectrum obtained through the methodology of the Section 5.2.3 Quantification of CAPB by High performance liquid chromatography (HPLC):

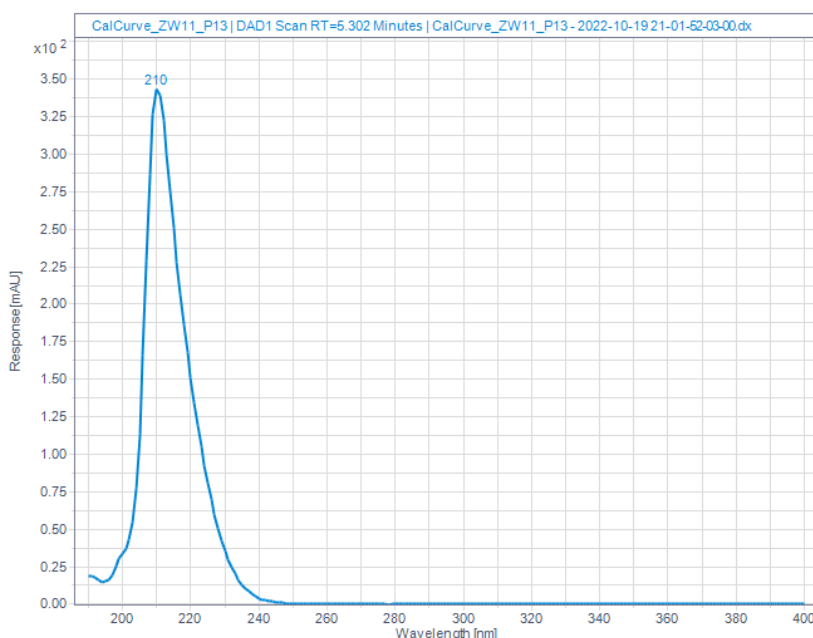


Figure 31: CAPB (tagged as ZW11) absorbance spectrum

It's observed that CAPB maximum absorbance is in the UV region, with a wavelength value closer to the minimum that could be emitted by the spectrometer (190 nm). Other impurities from the commercial mixture could also absorb light in that range of spectrum, such as free amidoamine, sodium dichloroacetate and monochloroacetate [87], however, the selectivity of the analytical method would occur at time of retardation, not at the specific wavelength of absorption, as is explained in Section 5.2.3 Quantification of CAPB by High performance liquid chromatography (HPLC)

6.1.2.2 Results from method of quantification of CAPB by HPLC

The CAPB peak appears in the 5 – 6 min of injection with a significant signal value (Figure 32).

Three calibration curves were made for static experiments in different days of sample preparation: one for the batch experiment with the carbonate, another for the sandstone, and a curve for the dynamic experiment of adsorption on the carbonate. As the section 6.3.2 Results of dynamic adsorption experiments and history-matching of experimental results shows, the sandstone did not need a calibration curve because no surfactant was detected in the effluent samples from injection.

The prepared surfactant solutions (triplicates) for calibration curves had concentrations equal to 0.050, 0.100, 0.300, 0.500, 1.000, 1.500 g L⁻¹. The adjustment was made with weighted linear fit. Adjusted R² and weighted sum of square residuals (WSS) were the metric applied to evaluate the calibration curve performance (Table 11). Figure 33 shows the calibrations curves for solutions in each test.

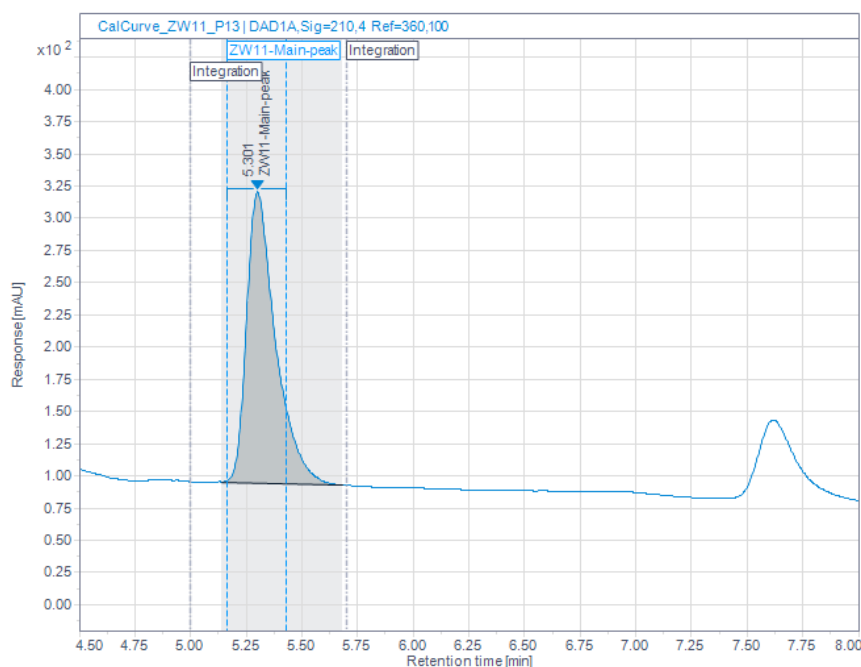


Figure 32: CAPB (tagged as ZW11) chromatogram peak

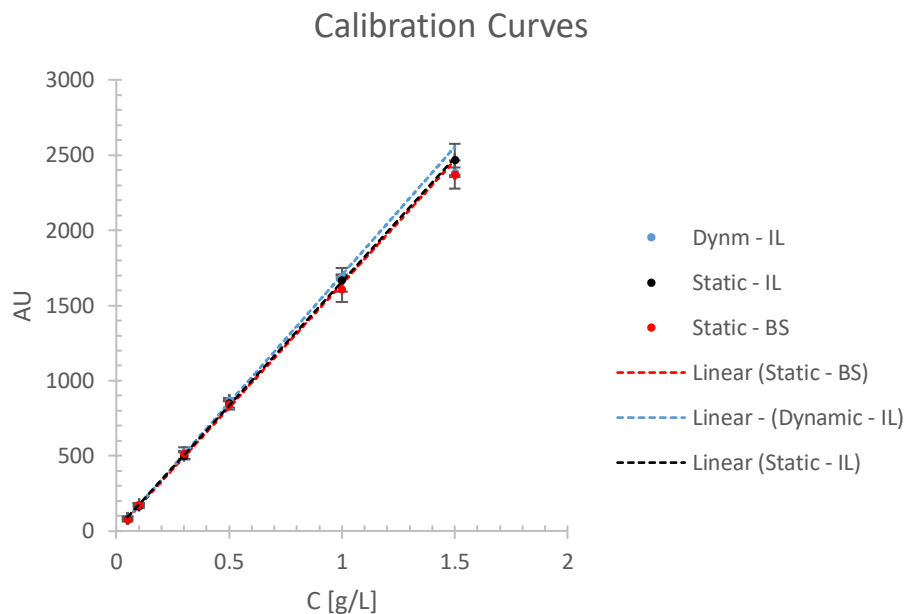


Figure 33: CAPB calibration curves in DSW for HPLC

Calibration Curve	Adj-R ²	WSS
IL - Dynamic	0,9990	45,25
IL- Static	0,9998	0,457
BS - Static	0,9983	2,778

Table 11: Calibration curves evaluation metrics

The three adjustments were satisfactory as the analyte is expected to be quantified in the 0.05-1.00 g L⁻¹ interval. Errors in quantification due to the weighted linear regression were higher for the calibration curve of the dynamic tests for the carbonate core, however, most of variations are outside the quantitative range of the analysis.

6.2 Specific Surface Area (SSA) results for static and dynamic experiments

6.2.1 Results of specific surface area from Brunauer-Emmett-Teller (BET) adsorption isotherm

As a result, from the methodology explained in Section 5.3.2 Determination of superficial area by Brunauer-Emmett-Teller (BET) adsorption

isotherm, the fitting of N₂ adsorption isotherms for both adsorbents, are shown in Figure 34 and Figure 35.

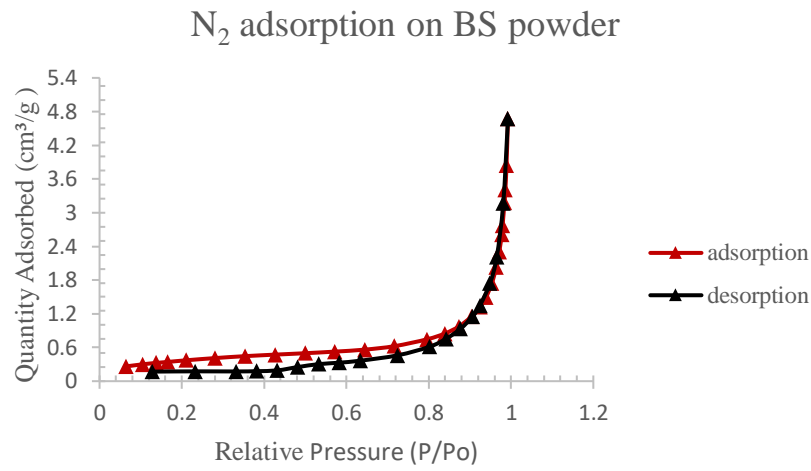


Figure 34: Isotherm plot for N₂ adsorption on Berea Buff sandstone

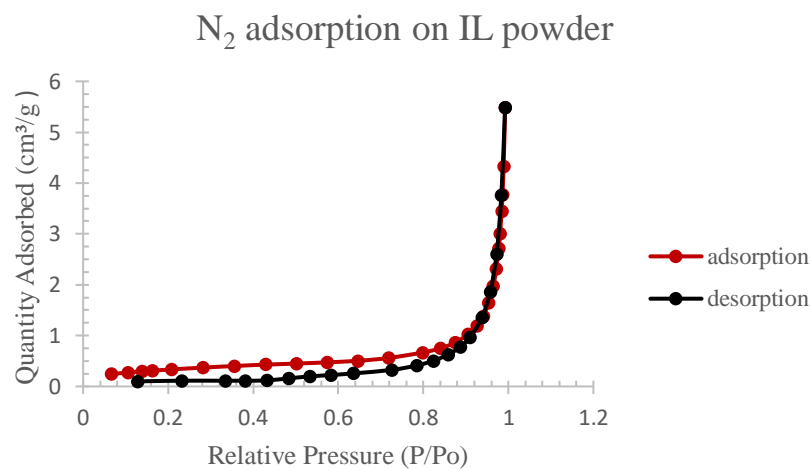


Figure 35: Isotherm plot for N₂ adsorption on Indiana limestone

The calculated BET surface area from the isotherm adjustment for each rock powder is shown in Table 12.

	Berea Buff sandstone	Indiana limestone
BET SSA (m² g⁻¹)	1.3703 ± 0.0036	1.2336 ± 0.0065

Table 12: BET Specific Surface Area of the sandstone and limestone powder

6.2.2 Results of specific surface area from μ CT-scan image analysis

As proposed in Section 5.4.2 Determination of rock cores surface area (pore space) using microtomography, the extrapolation of the specific surface area related to pore volume SSA_{vol} will be used as a mean of determine the SSA for each core sample. It can be obtained by the intercept of the adjusted line of the two data points in the plot: SSA_{vol} versus image resolution, with the vertical axis (Figure 36). A representative measure of SSA_{vol} was made for each core sample, and the properties of the REV are shown in table 13.

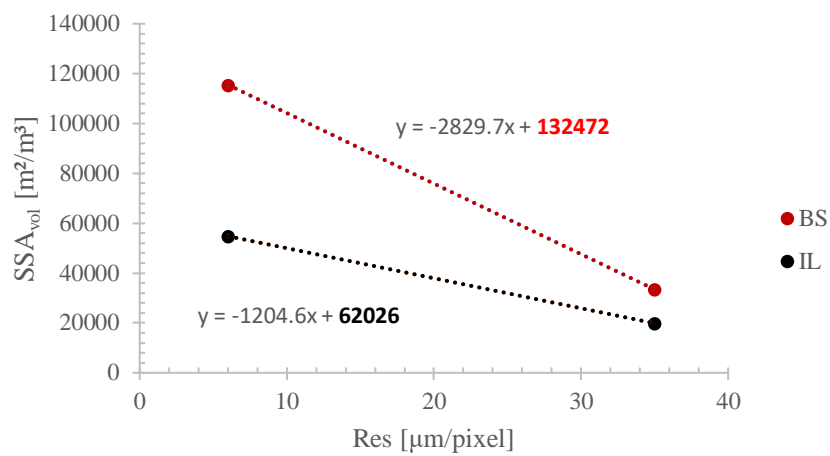


Figure 36: SSA_{vol} extrapolation with image resolution

As well as the SSA_{vol} , tortuosity (CPT) trends were extrapolated to image resolution value of zero (Figure 37):

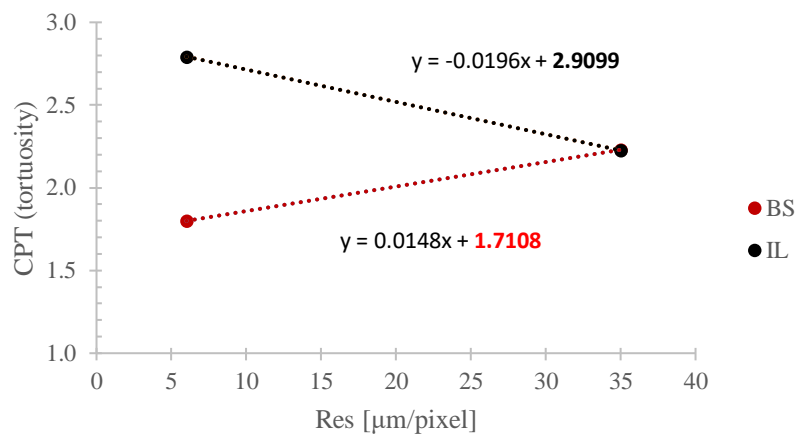


Figure 37: CPT extrapolation through μ CT-scan image resolution

Firstly, the REV data for the SSA_{vol} and CPT properties are shown in Table 13 for demonstrations of the representativity of the REV's in comparison to the measured porosity.

Core type	Resolution [$\mu\text{m}/\text{pixel}$]	ϕREV [%] for SSA_{vol}	ϕREV [%] for CPT	Measured ϕ [%]
Sandstone	35	0.184 ± 0.005	0.185 ± 0.007	19.52 ± 0.04
Sandstone	6	0.178 ± 0.001	0.179 ± 0.000	
Limestone	35	0.149 ± 0.001	0.155 ± 0.007	15.22 ± 0.14
Limestone	6	0.142 ± 0.009	0.157 ± 0.001	

Table 13: REV data for each core

Then, all core properties extracted from the μCT -scan images were compiled in Table 14:

Core type	SSA_{vol} [$\text{m}^2 \text{m}^{-3}$]	SA [m^2]	SSA [$\text{m}^2 \text{g}^{-1}$]	CPT
Sandstone	132472	1.96	1.24E-02	1.71
Limestone	62026	0.71	4.26E-03	2.91

Table 14: Calculated pore space properties for each core

6.3 Adsorption behavior and mechanisms of CAPB adsorption on sandstone and limestone

6.3.1.1 Results of CAPB static adsorption behavior

The first goal of this dissertation was to provide models that could explain adsorption behavior in both experiments static and dynamic. In order to do that experimental data needs to have some pattern and not seemly random results. In the case of this wok, adsorption isotherms were constructed with experimental data for surfactant concentration ranging from 0.05 to 0.6 g L^{-1} considering both the mass of rock powder and its specific surface area. After the batch experiments, CAPB adsorption was evaluated with the method of quantification described in section 5.3.3 Methodology for static adsorption test.

Results showed that an isotherm-like curve for CAPB on both adsorbents was obtained by the static adsorption experiments (Figure 38 (a) and (b)). That could not have been the case as seen in some works in literature involving zwitterionic surfactants [34], where adsorption seemed to increase without an isotherm-like pattern like L, S or L-S shaped curves [25]. The data showed that maximum adsorption per gram of adsorbent was higher in the sandstone at the same experimental conditions compared with Indiana limestone rock powder.

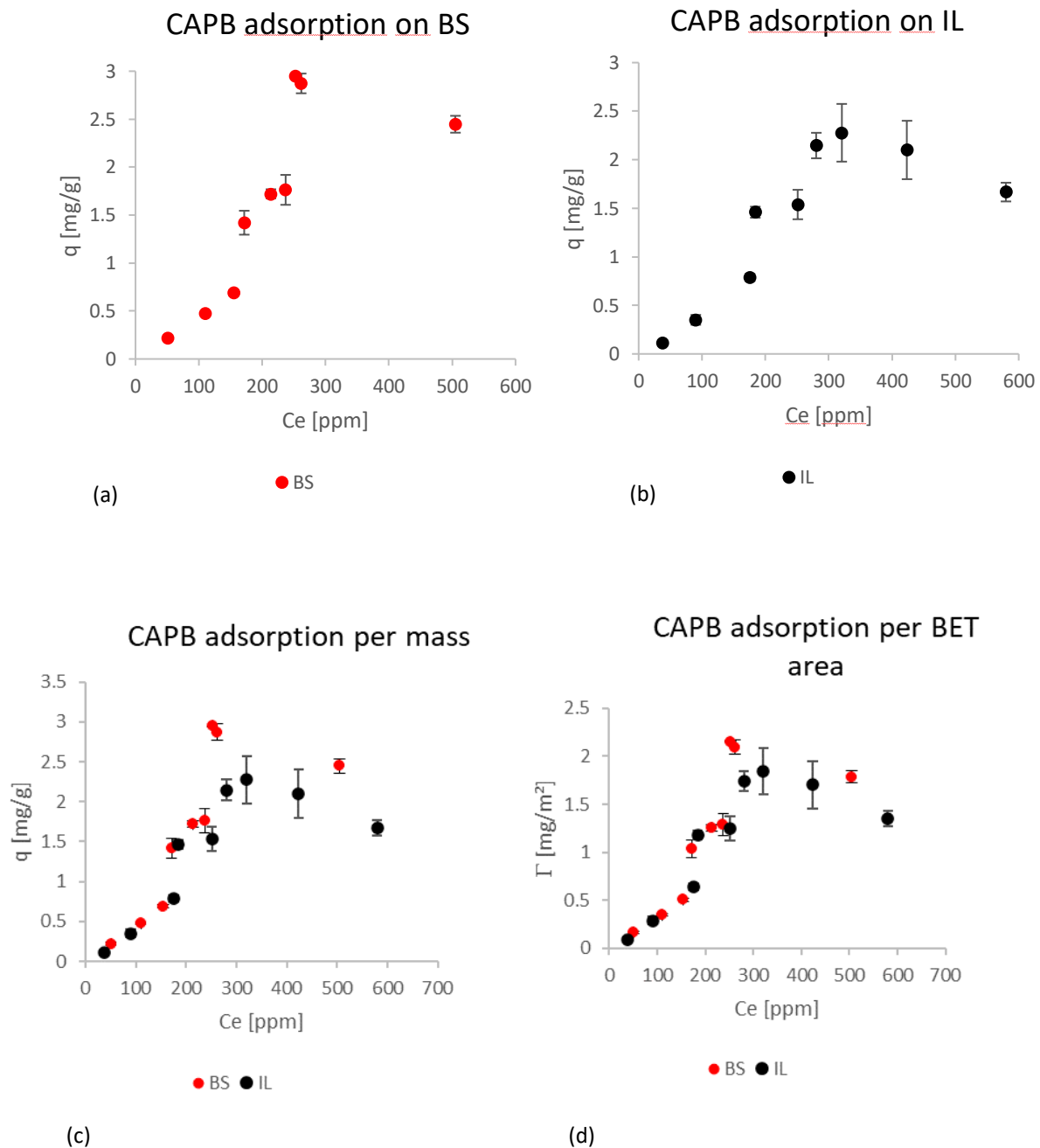


Figure 38: Static adsorption of CAPB on (a) Berea Buff Sandstone and (b) Indiana limestone, (c) both per mass of rock and (d) both per BET area

The difference between maximum adsorption of CAPB in the adsorbents is reduced when the BET specific area is used for normalization (Table 15). This happens because the sandstone powder has a slightly higher surface area per gram of material, thus reducing slightly its normalized values.

The results for maximum adsorption (normalized and not normalized) are shown in Table 15:

Max Adsorption	Berea sandstone	Indiana limestone
q [mg g ⁻¹]	2.951 ± 0.003	2.3 ± 0.3
Γ [mg m ⁻²]	2.153 ± 0.002	1.846 ± 0.241

Table 15: Maximum CAPB static adsorption on static experiments

Both adsorption curves resemble type-S isotherms (Figure 38 (a) and (b)), however adsorption tends to drop at highest concentrations. Some works in literature attribute this observation to monomer-micelle-vesicle equilibrium, with betaines capable of forming vesicles, since the aqueous solutions were prepared with high salinity brines [32], thus favoring micelle/vesicle formation at high surfactant concentrations at the expense of the monomers involved in adsorption equilibrium.

Negligible changes were observed for pH and small variations in conductivity were observed in the equilibrated solution (Table 16). The low increase in conductivity demonstrates the dissolution or exchange of rock matrix and brine ions within the surfactant solution, but not enough to significantly affect brine salinity.

Suspended powder	ΔpH	ΔC [mS cm⁻¹]
Sandstone	0	2.6
Limestone	0.4	2.5

Table 16: Change of solution properties with batch experiments

However, these changes could be responsible for more variability on the results for limestone, where the calcite-brine equilibrium could be more sensible to pH and ionic changes in composition.

6.3.1.2 Evaluation of static adsorption results by analysis of estimated rock surface potential and speciation

The CD-MUSIC model was used as a triple-layer surface complexation model for estimation of zeta potential and surface speciation. By estimating the zeta potential, one can infer the possibility of electrostatic interaction between surfactant and rock surface and by having the surface speciation, inferences about adsorption sites can be done for adsorption.

For a matter of quality verification of the data generated by the PHREEQC simulations, pH and aqueous phase conductivity of the synthetic brines and the simulated brines were checked (Table 17). Good agreement between estimated and determined values was observed. Therefore, the assumptions underlying the equilibrium between suspended rock powder and the DSW/brine were considered valid.

Powder	Data	pH	C [mS cm⁻¹]
Sandstone	estimated	7.92	51.6
	measured	7.95	48.2
Limestone	estimated	8.03	51.6
	measured	7.99	48.0

Table 17: Estimated vs measured physical-chemical properties of the equilibrated brine

The estimated zeta potential (Figure 39 (a)) for quartz and kaolinite, representing the sandstone surface, is considerably negative at the pH, temperature, and brine conditions of the test. For the calcite zeta potential, representing potential at the ion-covered limestone surface, is high and positive. As Figure 39 (b) shows, the distribution of sites in the quartz surface is mainly neutral silanol ($>SiOH$), followed by deprotonated silanol ($>SiO^-$), positive sites with adsorbed divalent cations ($>SiOMg^+$ and $>SiOCa^+$) and, for the last, the protonated silanol ($>SiOH_2^+$). The same can be observed in kaolinite aluminol ($>AlOH$) and silanol. Yet, for the calcite surface (Figure 39 (c)), the main site composition is the protonated $>CaOH$ site ($>CaOH_2^+$) and the deprotonated $>CO_3H$ one ($>CO_3^-$). In this case the positive site has a slightly higher quantity than the negative one, contributing to the positive zeta potential. The sites with divalent cations do not have significant concentration in the calcite surface, thus its quantity is negligible.

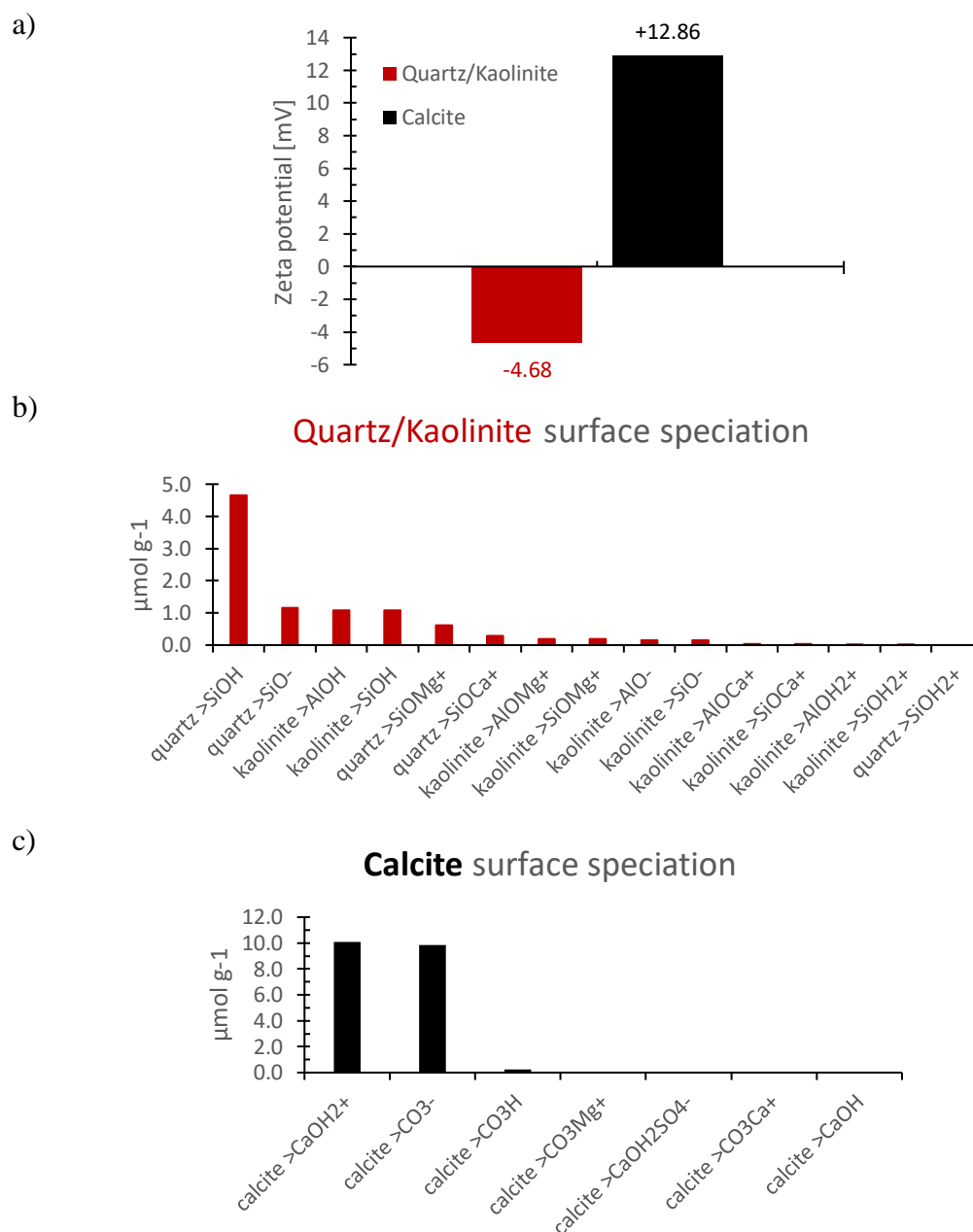


Figure 39: a) Zeta potential estimation from CD-MUSIC built-in PHREEQC for the brine and mineral equilibrium. b) Surface speciation of the quartz/kaolinite equilibrium with DSW per mass of sandstone. v) Surface speciation of the calcite equilibrium with DSW per mass of limestone.

Table 18 sums up the contributions of the electrostatic nature of each site for each type of rock, as well as the comparison between the maximum quantity of surfactant adsorbed and the estimated total number of sites:

Rock	Surface species charge	Fraction [%]	Total estimated sites per rock mass [$\mu\text{mol g}^{-1}$]	Maximum CAPB adsorption [$\mu\text{mol g}^{-1}$]
Sandstone	Neutral	70.6	9.62	8.62
	Negative	15.2		
	Positive	14.1		
Limestone	Neutral	1.3	20.21	6.71
	Negative	48.7		
	Positive	50.0		

Table 18: Estimated surface sites density and polarity

It was observed in static adsorption experiments that a larger adsorption of CAPB was found on sandstone rock (2.153 mg m^{-2}) compared to limestone rock (1.846 mg m^{-2}). Based on the surface complexation and zeta potential results, one should expect that for sandstone rocks, whose largest fraction of adsorption sites were neutral, adsorption would be dominated by ion-dipole interactions between the quaternary amine in CAPB molecules and hydroxylated surface species such as silanol ($>\text{SiOH}$). A smaller fraction of adsorption was due to electrostatic interactions between the positive CAPB charge and negatively charged silanol site ($>\text{SiO}^-$). Furthermore, the negative charge of CAPB head could also interact with positively charged sites ($>\text{SiOCa}^+$, $>\text{SiOMg}^+$) through ion binding. At least three mechanisms of adsorption could be identified for CAPB on Berea Buff sandstone, where two are ion-ion interactions and one ion-dipole interaction.

As for calcite surface, electrostatic interactions take place between CAPB's positive charge and $>\text{CO}_3^-$ sites; or between CAPB's negative charge and $>\text{CaOH}^{2+}$ sites. Lower adsorption values for limestone rock compared to sandstone rock could be attributed to electrostatic hindrance effect of the alternate $>\text{CO}_3^-$ and $>\text{CaOH}_2^+$ sites, where there is simultaneous attraction and repulsion depending on the charge of CAPB's head that is approaching the surface, causing poorer packing of the molecules (right hand-side Figure 40). For the sandstone rock surface better packing, thus higher adsorption, could be achieved (left-hand side Figure 40)

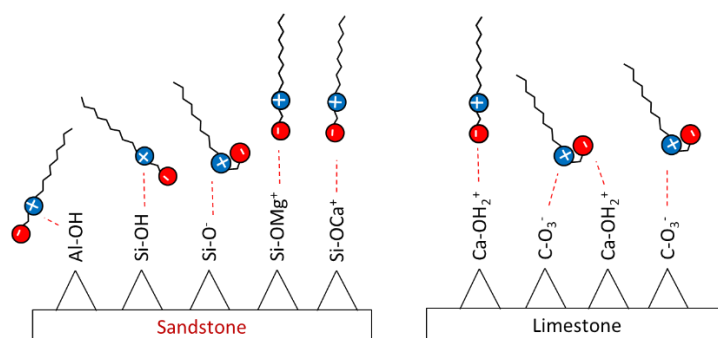


Figure 40: CAPB interactions with probable surface species by CD-MUSIC triple layer model

After understanding how surface potential and available adsorption sites affected static adsorption results, the aim was to understand what kind of adsorption models (monolayer/bilayer) would best describe the results obtained.

It is worth mentioning that monolayer approach does not mean the mechanisms are limited to a monolayer formation, as some models incorporate multilayer adsorption through Freundlich isotherm approximations, but rather to distinguish between models where the next layer of adsorbed molecules does not depend on the first layer. The bilayer approach tries to extend the available isotherm models for combinations of isotherms which are necessarily dependent on adsorption of the first layer. With that in mind, one can have a complete overview of the adsorption mechanisms for CAPB molecules.

6.3.1.3 Fitting of static adsorption results with monolayer models

The results of the data fitting utilizing the monolayer approach group are shown in Figure 41 and Table 19:

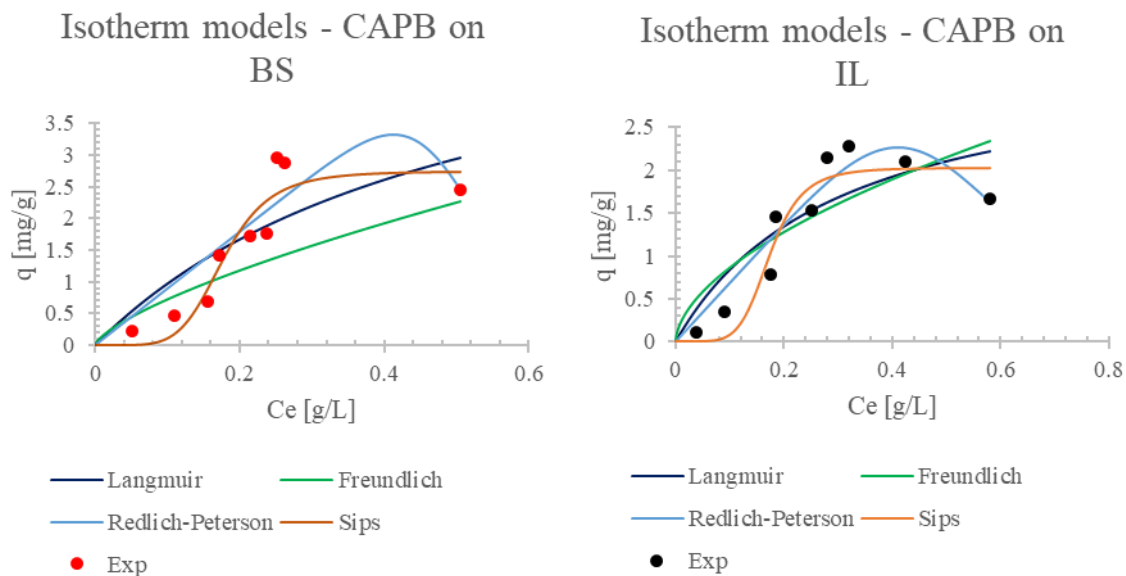


Figure 41: Adjusted isotherm models from monolayer approach

Isotherm model	BS		IL	
	Adj - R ²	RMSE	Adj - R ²	RMSE
Langmuir	0.60	0.64	0.69	0.44
Freundlich	0.54	0.50	0.60	0.50
Redlich-Peterson	0.72	0.54	0.87	0.28
Sips	0.82	0.43	0.84	0.32

Table 19: Evaluation metrics of adjusted isotherm models from monolayer approach.

Best fit models are highlighted.

In this approach Redlich-Peterson and Sips isotherms were the best isotherm fit to experimental data of CAPB adsorption on Indiana Limestone and Berea Sandstone respectively (Figure 42), accordingly to the chosen metrics (adjusted R² and RMSE).

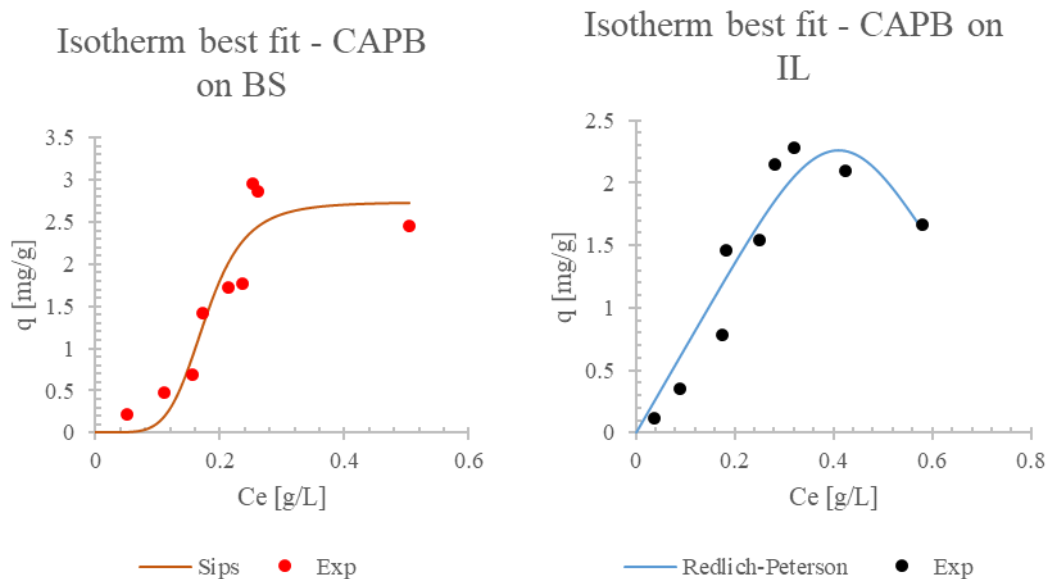


Figure 42: Best-fit isotherm models, monolayer approach.

The parameters from the best evaluated isotherm models for each dataset are shown in Table 20 for interpretation of potential adsorption mechanisms.

Sandstone			Limestone		
Sips (monolayer)			Redlich-Peterson (monolayer)		
K_s [$L g^{-1}$]	β_s	α_s [$L m^{-1}g$]	K_r [$L g^{-1}$]	β_r	α_r [$L m^{-1}g$]
3.9×10^4	5.5	1.4×10^4	6.8	5.2	24

Table 20: Sips and Redlich-Peterson isotherms parameters from best fit

This best fit result could be interpreted in a way that one of the underlying mechanisms in CAPB adsorption on Indiana Limestone is a heterogeneous distribution of the adsorbate due to adsorption sites with different adsorption energies, as seen in the speciation results that show high quantities of deprotonate carbonate sites ($>CO_3^-$) and protonated hydroxyl groups ($>CaOH_2^+$) in calcite. The same could be stated for the Berea Buff sandstone where there is a high quantity of neutral sites and a significant quantity of charged sites.

A major difference in the observed heterogeneity mechanism resides in a property of Sips isotherm that consists in reaching a plateau of amount of surfactant adsorbed at higher concentrations, as Redlich-Peterson model would not have a

finite limit. However, due to exponent values greater than 1, Redlich-Peterson will have a finite limit of zero adsorption at higher concentrations and an adsorption maximum. This could be explained by a similarity between Redlich-Peterson model and an approximation of a novel and validated isotherm model, that accounts for monomer-micelle-vesicle equilibrium in adsorption of a zwitterionic surfactant on limestone with seawater [32]:

$$\Gamma = \frac{\Gamma_{\infty} k C_e}{1 + k C_e + k_m (C_e - C_{CMC})^n H(C_e - C_{CMC})} \quad (27)$$

Where Γ_{∞} is the maximum adsorption capacity, k is the adsorption equilibrium constant, k_m is the adsorbed monomer-micelle equilibrium constant and the $H(C_e - C_{CMC})$ is a Heavside function that activates when the equilibrium concentration is greater than the critical micelle concentration. Considering a greater contribution of the monomer-micelle equilibrium ($k_m \gg k$), the model becomes:

$$\Gamma = \frac{\Gamma_{\infty} k C_e}{1 + k_m C_e^n} \quad (28)$$

This mathematical description is very similar to Redlich-Peterson isotherm model and could imply that surfactant aggregation in form of micelles is a major factor in the surfactant-surface equilibrium of a zwitterionic surfactant in DSW. In this case, the mechanism of desorption into bulk to aggregate in form of micelle/vesicle could be responsible for reducing CAPB adsorption on Indiana Limestone at higher equilibrium concentrations thus creating a maximum point in the isotherm curve. As explained in the previous section, the electrostatic hindrance effect would imply that as surfactant keeps being added to the bulk, more favorable sites are occupied and more hindrance will be encountered by other molecules diffusing to the interface, since their only interactions would be electrostatic repulsion and hydrophobic interactions with the already adsorbed ones. This could favor micelle formation on the bulk because the surfactant doesn't need to diffuse all the way to the surface to make hydrophobic interactions at higher concentrations.

In the case of CAPB adsorption on Berea Sandstone, Sips isotherm model was more adequate because of the apparent behavior observed in the experiments resembling a S-type or sigmoid curve. The underlying mechanism of the Sips adsorption isotherm is related to heterogeneous adsorption because of the unequal energy distribution through sites, low and high energy sites appear far less frequent than average energy, this stimulates competition between adsorbates molecules for higher energy sites since there are few. Despite the similarities with the Redlich-Peterson model, Sips could not be approximated to a model that involves monomer-micelle equilibrium and therefore the exponent won't be interpreted as an aggregation number. However, a Sips exponent greater than one could be a sign of cooperative adsorption and lateral interaction between adsorbates [107, 108]. This could mean that $1/\beta_s$ (~ 0.2) is the number of sites a single molecule of surfactant would interact with and adsorb. Therefore, considering lateral interactions, a minimum of 5 molecules would be involved in a single site adsorption, on average, in the case of Berea Sandstone.

New experiments need to be carried out at larger concentrations intervals to confirm if these models could predict CAPB adsorption behavior on Indiana Limestone and Berea Sandstone at higher concentrations. The proposed mechanisms for this approach are illustrated in Figure 43:

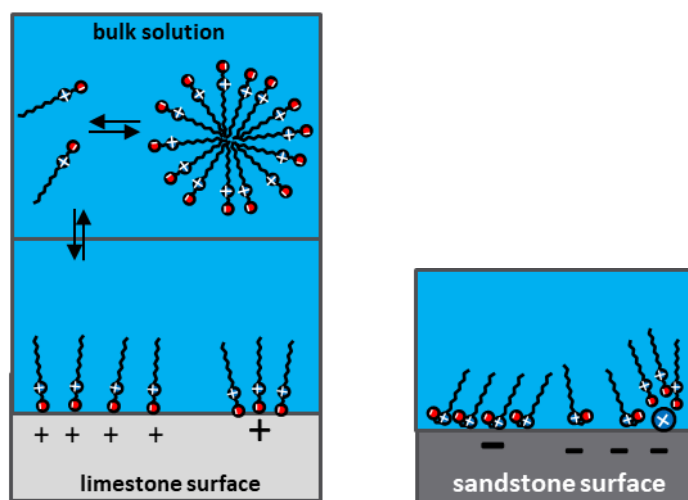


Figure 43: Monolayer approach proposed mechanisms.

6.3.1.4 Fitting of static adsorption results with bilayer models

The monolayer approach models are limited to one distribution of sites and interdependence of the layers. The bilayer approach tries to mitigate the neglected effects of bilayer formation (admicelles and hemimicelles formation), directly considering the dependence of adsorption on the first layer.

Figure 44 and Table 21 show fitting results for bilayer premise and its combinations for first and second layers:

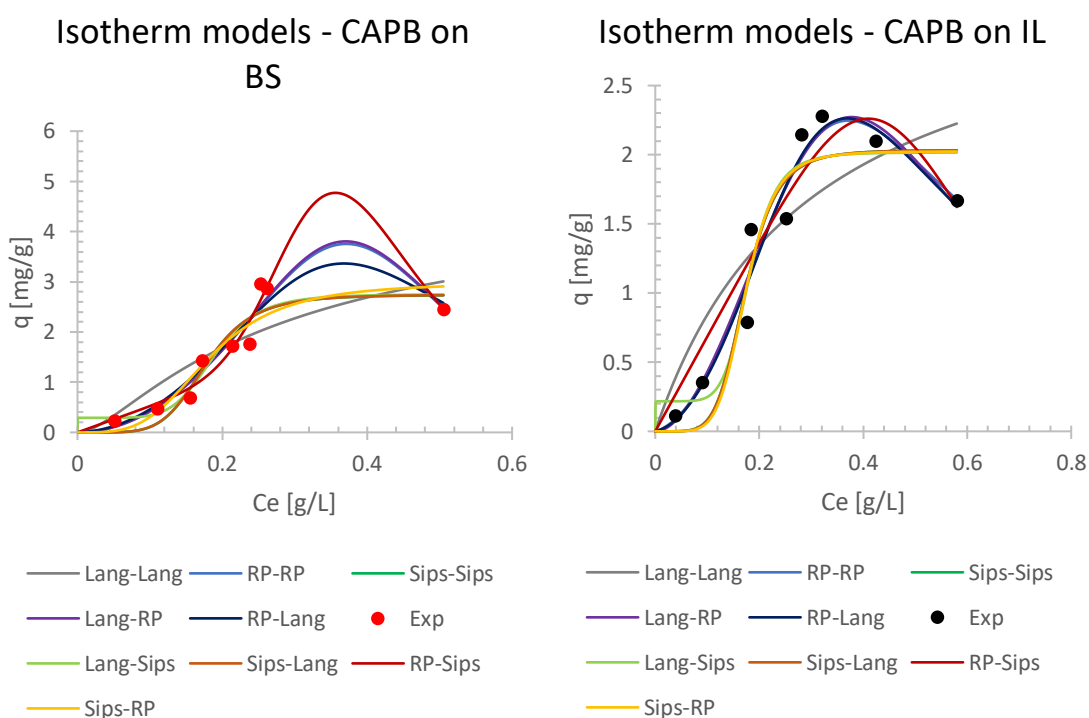


Figure 44: Adjusted isotherm models for bilayer approach

Isotherm models	BS		IL	
	adjusted R ²	RMSE	adjusted R ²	RMSE
Lang-Lang bi	0.51	0.71	0.69	0.44
RP-RP bi	0.84	0.40	0.89	0.26
Sips-Sips bi	0.82	0.43	0.84	0.32
Lang-RP bi	0.84	0.40	0.92	0.22
RP-Lang bi	0.81	0.44	0.89	0.26
Lang-Sips bi	0.76	0.50	0.79	0.36
Sips-Lang bi	0.82	0.43	0.84	0.32

RP-Sips bi	0.88	0.35	0.81	0.35
Sips-RP bi	0.79	0.47	0.84	0.32

Table 21: Evaluation metrics of adjusted isotherm models from bilayer approach. Best fit models are highlighted.

In this approach Langmuir-Redlich-Peterson and Redlich-Peterson-Sips isotherms were the best fit to experimental data of CAPB adsorption on Indiana Limestone and Berea Sandstone respectively (Figures 45), according to the chosen metrics.

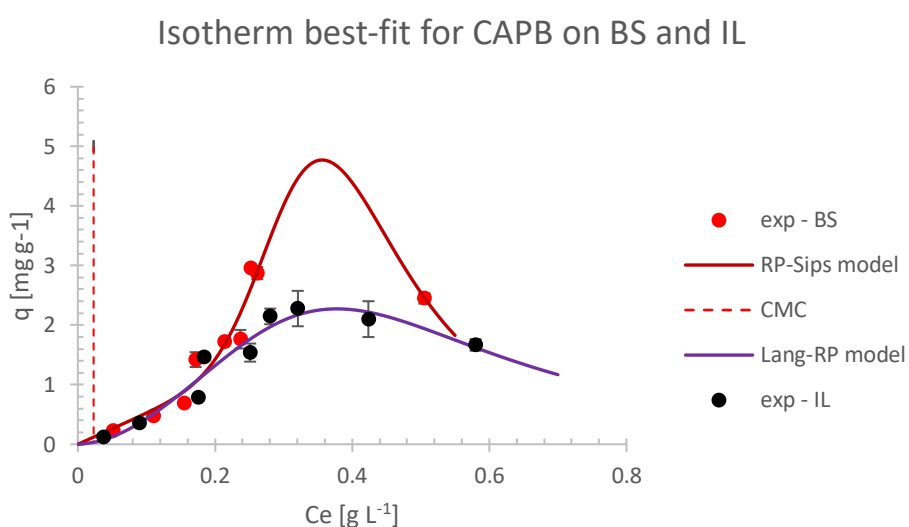


Figure 45: Best-fit isotherm models, bilayer approach

The parameters of the adjusted models are demonstrated in Table 22:

Berea Sandstone			Indiana Limestone		
Redlich-Peterson (first layer)			Langmuir (first layer)		
K_r [L g ⁻¹]	β_r	α_r [L m ⁻¹ g]	q_∞ [mg g ⁻¹]	K [L g ⁻¹]	
5.2	5.4	3.3×10^2	2×10^{-4}	3.10	
Sips (second layer)			Redlich-Peterson (second layer)		
$\alpha = 8.40$			$\alpha = 3.49 \times 10^3$		
K_s^*	β_s	α_s^*	K_r^*	β_r	α_r^*
3.4×10^2	5.4	3.4×10^2	2.5×10^1	3.8	2.5×10^1

Table 22: R-P-Sips and Langmuir-R-P isotherms parameters from best fit

In this approach, the combination of Langmuir (first layer) and Redlich-Peterson (second layer) isotherms had the best fit for adsorption, according to the previous metrics, on Indiana Limestone. Redlich-Peterson (first layer) and Sips (second layer) combined were the best fit to experimental data of CAPB adsorption on Berea Sandstone.

Both fits surpassed in evaluation metrics (adjusted R^2 and RMSE) the previous approach of monolayer adsorption and maintained the potential mechanisms described but, in this case, only for the second layer. New potential mechanisms arise from this data for the first layer adsorption of CAPB in both rocks.

Given the bilayer approach results, adsorption takes place homogeneously and with much less intensity for CAPB on the Limestone surface due to the Langmuir premise of uniform energy distribution across the adsorbent surface.

Contradicting the previous interpretation, the uniform adsorption of the CAPB for limestone paves the way for adsorption on the second layer which occurs in a heterogenous manner. The second layer is formed due to hydrophobic interactions between CAPB hydrocarbon chains. Which makes surfactant aggregate on the already adsorbed monomers. The complete potential arrangement related to this approach is illustrated in Figure 46.

So, a closer look at the fitted parameters reveals that maximum capacity for Langmuir type behavior is very low and second layer capacity is very high (α), therefore a major contribution of the hydrophobic interactions exists for surfactant adsorption on the limestone. The same could not be said for sandstone, which has a low α , indicating less effect of the bilayer formation.

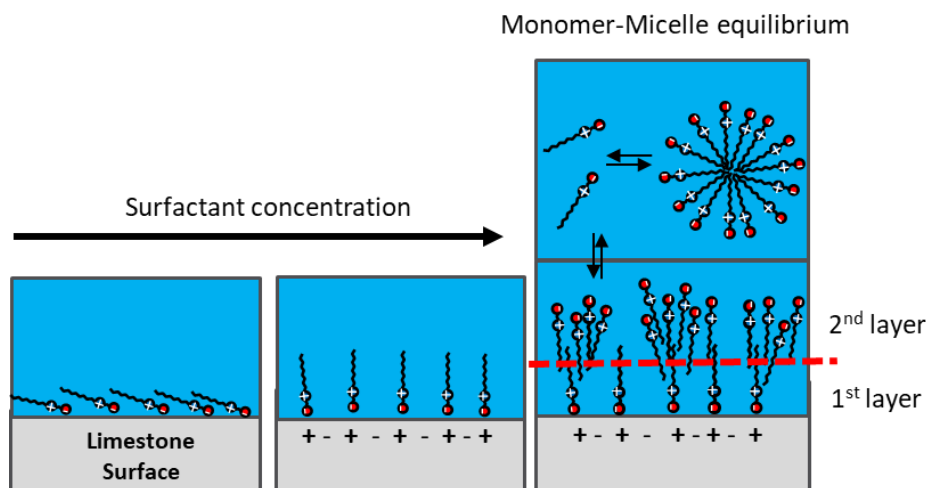


Figure 46: Potential mechanisms of CAPB adsorption on Indiana Limestone

In the first layer of the Sandstone, two aspects of CAPB adsorption can be proposed: a mechanism of heterogeneous adsorption due to unequal site energy, and a monomer micelle equilibrium that promotes a maximum point in the isotherm curve because of the Redlich-Peterson model adjustment for first layer. Differently from adsorption on limestone where the monomer micelle-equilibrium impacted the second layer, in the sandstone the first layer is involved in monomer-micelle equilibrium with the bulk of the solution. As explained earlier, because of a low α does not contribute much to the adsorption on sandstone compared with limestone.

For the second layer, the Sips adequacy implies a heterogeneous distribution of monomers adsorbing and a possible lateral interaction that could make the exponent β_S mean that roughly 5 monomers aggregate per site.

Adsorption capacity is considerable higher for the second layer as created sites on the first layer adsorption permits more adsorption. This could be intermediate by ion binding (Mg^{+2} and Ca^{+2}) since the zeta potential is negative. Surfactants could also aggregate closer to these ions and interact with each other chains laterally.

Because of low Ca^{+2} and Mg^{+2} concentrations in DSW, this type of facilitated adsorption is not so common but the lateral interactions could increase adsorption significantly per ion, implicating in a higher adsorption capacity for the second layer as we increase divalent ions concentrations in solution. As seen in the estimated surface species, neutral sites such as silanol promotes ion-dipole interactions of the quaternary amine group of CAPB molecule, and this could

promote lateral interactions as the CAPB molecules interact with the distorted orbitals of the hydroxylated groups of the surface.

Figure 47 illustrates the potential mechanism for CAPB adsorption on Berea Sandstone surface.

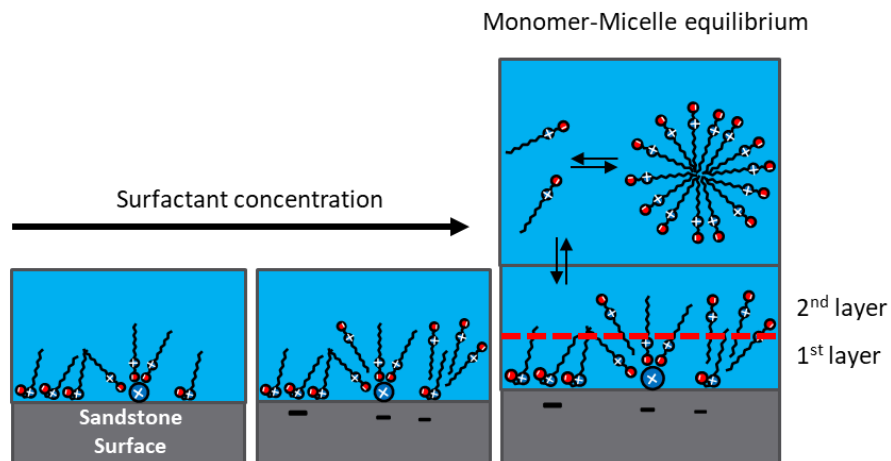


Figure 47: Potential mechanisms of CAPB adsorption on Berea Sandstone

6.3.2 Results of dynamic adsorption experiments and history-matching of experimental results

6.3.2.1 Evaluation of brine-rock interactions through dispersion and ion concentration profile

For the tracer model adjustment, the parameters D (dispersion coefficient) and V (interstitial velocity) are shown in Table 23.

Core	D [cm ² min ⁻¹]	V [cm min ⁻¹]	Tortuosity (CPT)
sandstone	0.33	0.60	1.71
limestone	1.25	0.63	2.91

Table 23: Transport properties in the pore space for both cores

It was observed that the limestone core promotes much more dispersion throughout the transport of the non-adsorbent species and the interstitial velocity is slightly higher for the limestone due to its lower porosity.

The higher dispersion in limestone core is noticeable in the tracer breakthrough because of the less pronounced curves, and it is explained by the considerably higher tortuosity, almost 2 times higher than the sandstone. This feature could lead to higher variations in the elements involved in brine/rock equilibrium, which will be analyzed next.

6.3.2.2 Ion profiles on sandstone

Element profiles were determined by ICP-OES from effluent samples to observe cation exchange or adsorption throughout surfactant injection, as the DSW equilibrated with the core is displaced by the surfactant solution in a non-equilibrated DSW. Results were analyzed for Ca, Mg, Na and K and it is considered that these species are in the form of cations. Divalent and monovalent cations profiles were compared separated for both injections (Figure 48 and 49):

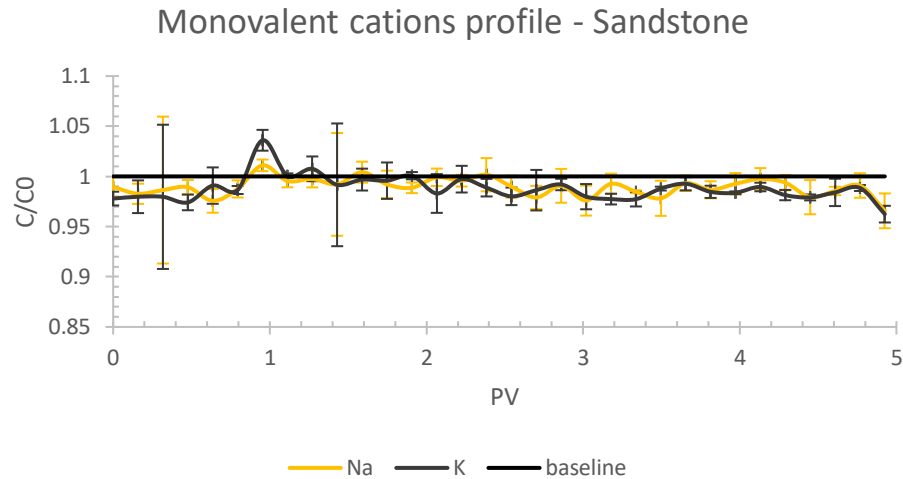


Figure 48: Monovalent cations profile during adsorption on sandstone

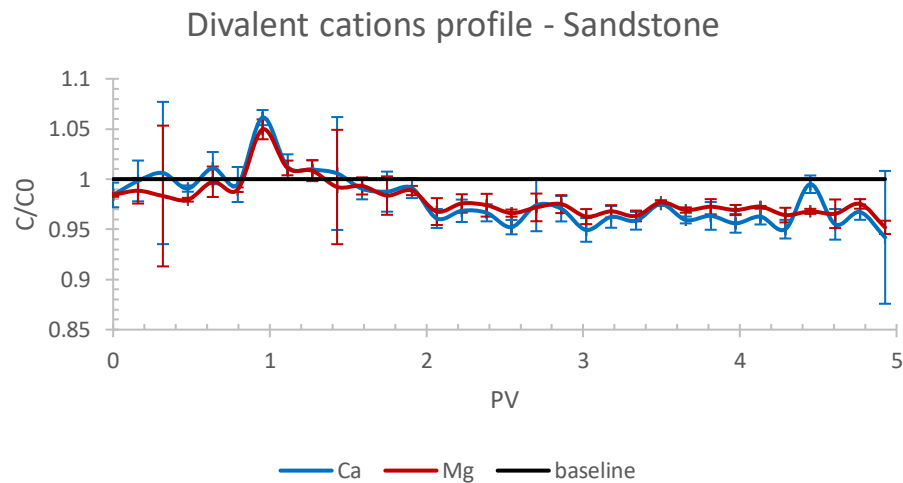


Figure 49: Divalent cations profile during adsorption on sandstone

Sodium and potassium concentrations seem to oscillate inside reproducibility uncertainty and below the initial concentration baseline for the sandstone; however, calcium and magnesium concentrations oscillate in lower levels and tends to increase its distance to the baseline. This could imply divalent cation retention through adsorption, as considered in the surface complexation model, or exchange with monovalent cations on the pore surface of sandstone. Cation exchange pattern is not so obvious but could happen in a subtle manner, as sometimes the profiles do not follow the same trends.

Both types of cations presented a peak on samples close to 1 PV on the sandstone. Dispersion has an important role in this behavior since the cations

followed similar paths independently of their valence. This pattern breaks throughout the injection past 1 PV, when divalent cations lowered its overall concentration.

As the CAPB molecule has two ionic charges which allow electrostatic interactions with charged sites of the mineral surface and solvated ions in brine, CAPB could adsorb via divalent cation bridging [109]. Where the CAPB molecule interacts with Ca^{+2} and Mg^{+2} , which are binding with negative sites or other surfactant molecules. The occurrence of these phenomena could be evidenced by the lowered concentrations of divalent throughout the injection of surfactant solution.

6.3.2.3 Ion profiles on limestone

In the case of the limestone (Figures 50 and 51), the equilibrated brine with the limestone core presented a stable concentration of divalent and monovalent cations before the non-equilibrated brine reached 1 PV. Sodium, calcium, and magnesium concentrations in equilibrated brine are lower than the initial. Only potassium remains entirely on solution until 1 PV. This means that Na^+ , Ca^{+2} and Mg^{+2} could be initially adsorbed in the limestone surface.

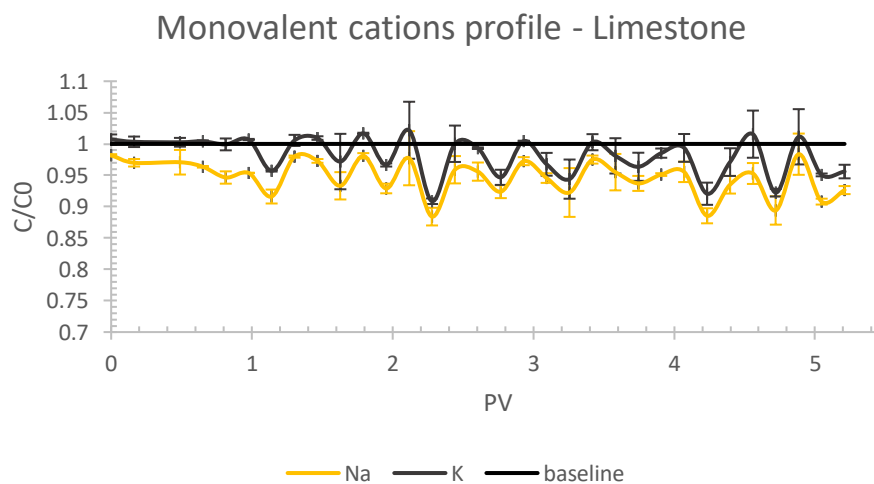


Figure 50: Monovalent cations profile during adsorption on limestone

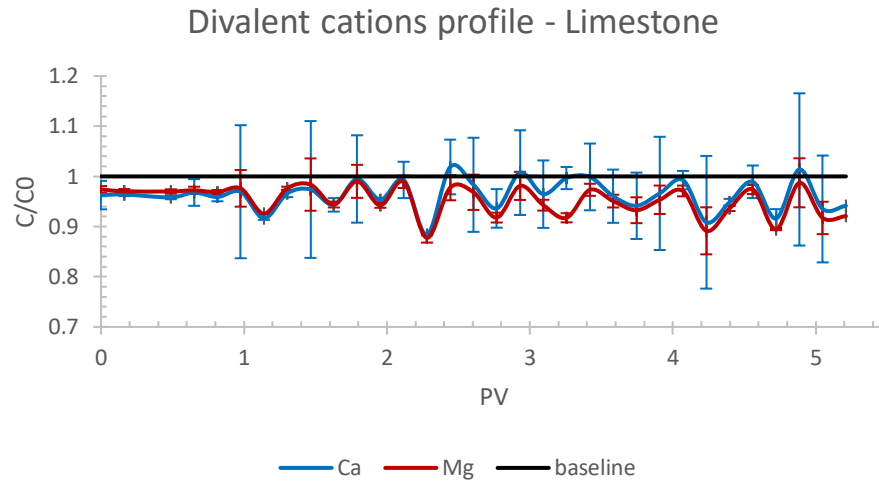


Figure 51: Divalent cations profile during adsorption on limestone

After 1 PV of surfactant solution in brine all the analyzed cations concentrations oscillated most of the time with the same pattern due to dispersion effects. Differently from the sandstone, there is no evidence of significant cation exchange of divalent cations because of the similar profile between the divalent and monovalent cations throughout the injection and the high uncertainty values.

In general aspects, there is no significant rock matrix dissolution of both cores tested because of the close distance to the initial concentration baseline. The divalent cations seemed sorbed in the sandstone throughout the tests, but it is not clear if that happens significantly in the limestone case.

6.3.3 Determination of dynamic adsorption by comparison of breakthrough curves for CAPB and tracer

The main results of dynamic adsorption experiments are breakthrough curves, as shown in Figures 52 e 53. These curves are obtained from surfactant and tracer quantification in the effluent samples during core flood, and then normalized by initial solution concentration. Surfactant breakthrough curves need to be accompanied by tracer breakthrough curves to quantify retention of surfactant due only by adsorption phenomena, excluding dispersion phenomena. In the case of the dynamic adsorption of CAPB, the adsorption was calculated from difference of the area under the tracer (Li^+) and surfactant breakthrough curves. Both curves for the sandstone and limestone were constructed at 5 pore volumes (PV, given by $PV = \frac{\text{flow rate} * \text{time}}{\text{core pore volume}}$) of surfactant and tracer injection.

Neither CAPB breakthrough curves recorded for Indiana limestone and Berea sandstone reached initial concentration ($C/C_0 = 1$) in effluent samples, indicating that there was no dynamic equilibrium. That is, adsorption for the surfactant was not satisfied after 5PV of CAPB injection. For the sandstone core, no surfactant was detected in the effluent during 5PV of injection, hence all the surfactant injected remained adsorbed on the rock surface.

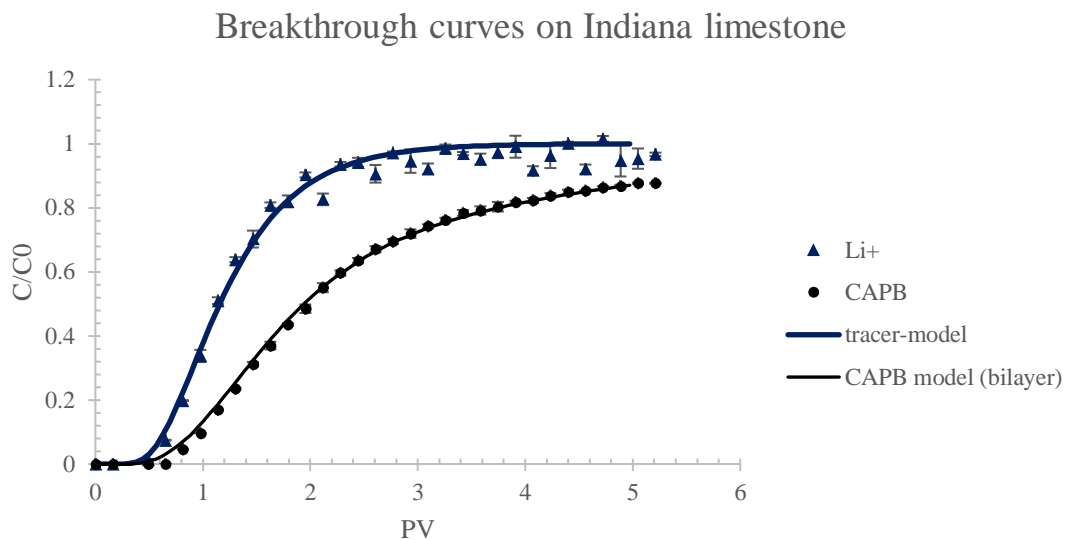


Figure 52: Breakthrough curves of CAPB and tracer for limestone

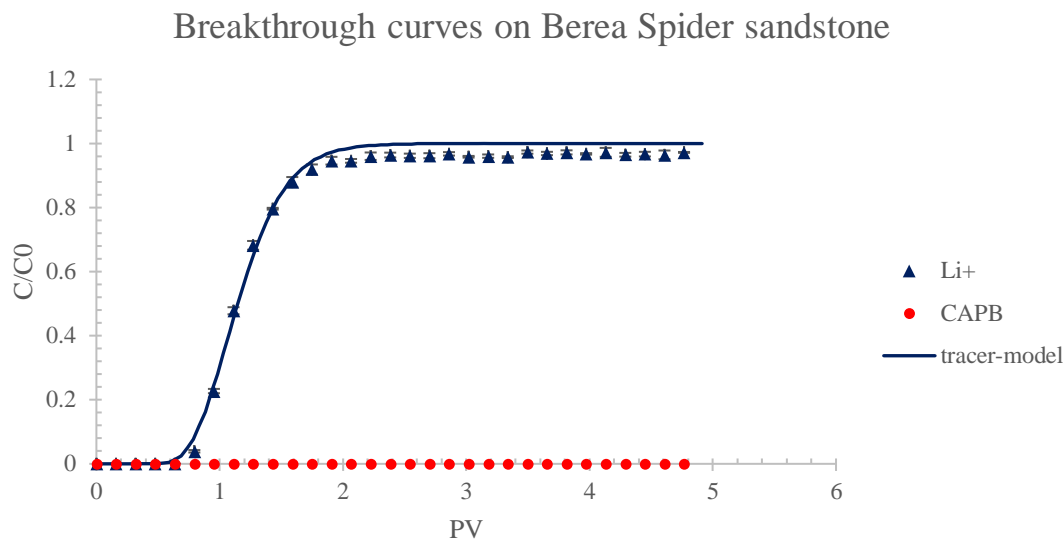


Figure 53: Breakthrough curves of CAPB and tracer for sandstone

The calculated adsorption through difference of area under the curve between tracer and surfactant on both rocks at dynamic conditions is shown in Table 24:

Type of rock	Adsorption [mg g^{-1}]	SSA [$\text{m}^2 \text{g}^{-1}$]	Adsorption at 5 PV [mg m^{-2}]
Berea Spider sandstone	0.339 ± 0.002	1.24×10^{-2}	27.34
Indiana limestone	0.072 ± 0.002	4.26×10^{-3}	16.90

Table 24: Dynamic adsorption from breakthrough curves

CAPB adsorption was nearly five times higher for Berea Spider Sandstone core than for Indiana Limestone. This could be explained by two factors: a much higher surface area of the sandstone compared with the limestone and the number of interactions related to CAPB molecules on each active site. As seen in the Table 24, the specific surface area of the sandstone ($1.24 \times 10^{-2} \text{ m}^2 \text{g}^{-1}$) core is almost 3-fold the one the limestone core ($4.26 \times 10^{-3} \text{ m}^2 \text{g}^{-1}$), and the difference tends to increase with higher μCT image resolution.

Differently from the statics tests, where particle size is considered controlled (slightly difference in BET area), the dynamic tests do not have particle

distribution, or in this case, a controlled pore distribution. This means that static experiments could be more representative of the mechanisms of CAPB adsorption.

And for the dynamic experiments, the different pore size distributions could imply major differences in specific surface area. Just like determined by μ CT-scan images, it is the main factor of adsorption differences between dynamic adsorptions. This surface area effect is evidenced in the almost 300% difference in normalized dynamic adsorption, compared with nearly 16% difference in normalized adsorption in static experiments.

6.3.4 Evaluation of history-match models for Li⁺ and CAPB on limestone core

The results of history-match model performance for CAPB and Li⁺ breakthrough curves during surfactant injection are shown in Table 25:

Specie	Model	Metrics	
		adjusted R ²	RMSE
CAPB (In limestone core)	Langmuir	0.9513	0.0706
	Freundlich	0.9917	0.0292
	Redlich-Peterson	0.9500	0.0716
	Sips	0.9914	0.0296
	Langmuir - kinetic	0.9888	0.0338
	Sips - kinetic	0.9884	0.0345
	Two-Site - kinetic	0.9997	0.0060
	Bilayer - kinetic	0.9997	0.0058
Li ⁺ (tracer)	Limestone	0.9873	0.0380
	Sandstone	0.9934	0.0310

Table 25: History-match model performance for core effluent data

The breakthrough curves of CAPB on limestone, and Li⁺ (tracer) on the sandstone and limestone at dynamic condition seemed to be in accordance with the proposed models for each species.

Surfactant adsorption behavior is better explained by kinetic models, which assumes adsorption occurs gradually as injection continues. Some equilibrium models performed well, but the predictability observed in RMSE reduces an order of magnitude if equilibrium is not a premise.

Both two-site Langmuir and bilayer kinetic Langmuir assumptions performed surprisingly well, with $R^2 > 0.9995$. Considering the lowest RMSE for its predictability, bilayer Langmuir approach was the chosen model to represent CAPB breakthrough data. Figure 54 shows the history-match of the model implemented for CAPB breakthrough curve and its continuity through brine injection.

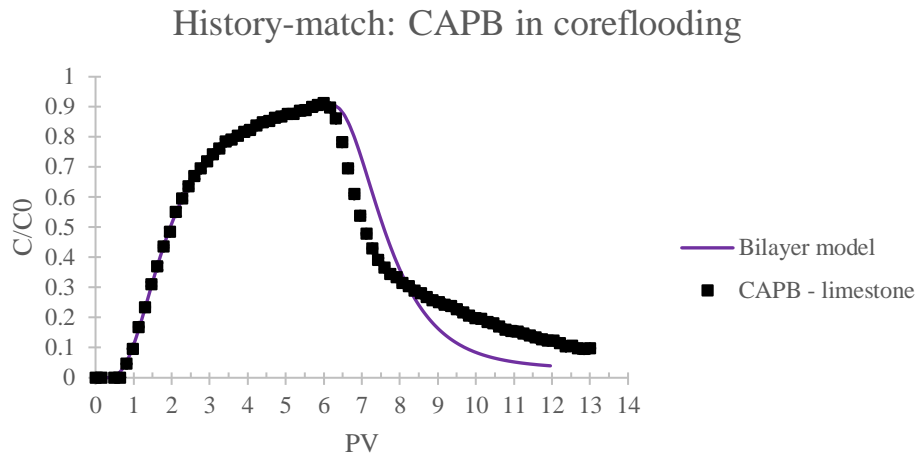


Figure 54: History-match of CAPB adsorption and desorption data in limestone core

As seen in the previous plot, the model was outstandingly good at adjusting data through surfactant injection but performed poorly after brine injection past 5 PV, when DSW was injected and eluted the surfactant in the pore space. This could indicate that this model was not suitable for describing desorption behavior of CAPB in the limestone in coreflood tests, since it would overestimate desorption velocity until approximately 8 PV and underestimate past that value.

The resulting parameters for bilayer kinetic model are shown in Table 26:

Bilayer model adjusted parameters		
Γ_{∞_1}	0.694	mg g ⁻¹
k_{ad_1}	0.060	L g ⁻¹ .s
k_{d_1}	1.001	s ⁻¹
Γ_{∞_2}	0.873	mg g ⁻¹
k_{ad_2}	0.020	L g ⁻¹ .s
k_{d_2}	0.005	s ⁻¹
Calculated Equilibrium Values		
K_1	0.06	L g ⁻¹

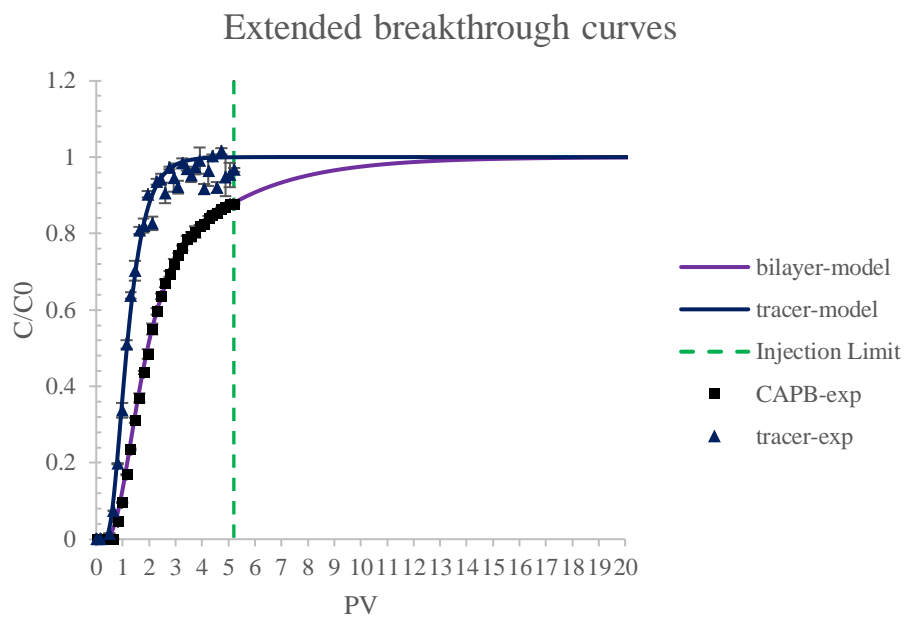
K_2	3.89	$L g^{-1}$
Γ_{∞}	1.567	$mg g^{-1}$

Table 26: Bilayer (kinetic) parameters from best history-match

Like the static experiment, the best adjusted model for CAPB adsorption demonstrated a higher equilibrium constant and larger adsorption capacity in the second layer of adsorption ($\Gamma_{\infty_2} > \Gamma_{\infty_1}$) meaning that adsorption could extend more into the second layer created by already adsorbed surfactants.

6.4 Adsorption estimation in dynamic conditions with the best history-match model

Having described CAPB adsorption behavior sufficiently well during coreflood experiments, bilayer model was used to estimate adsorption at dynamic equilibrium conditions, that is, when effluent surfactant concentration reaches the initial surfactant concentration ($C = C_0$). The tracer model was also used to extend the breakthrough curve of Li^+ until dynamic equilibrium of CAPB, then the difference of area under the curve of both extended breakthrough curves was used to calculate adsorption at this infinite time of injection. The value obtained in this study was $0.102 mg g^{-1}$ (Figure 55).

Figure 55: Extended breakthrough curves of CAPB and Li^+ (tracer)

The extended breakthrough curves (Figure 55) of both tracer and surfactant appeared to intercept at 15 PV, meaning the dynamic equilibrium of the CAPB adsorption was reached near that time.

Note that the equilibrium value was approximately 40% larger than the one found considering solely injection of 5 PV of surfactant solution. Interestingly, by comparing adsorption value for specific area at equilibrium for Indiana Limestone (23.94 g m^{-2}) with that of Berea Spider (27.34 g m^{-2}), the value for the latter is still greater than for the former which is at dynamic equilibrium. However, this difference (14%) is significantly lower for the equilibrium value compared with the difference in adsorption value taken at 5 PV of injection (62%, BS = 27.34 g m^{-2} and IL = 16.90 g m^{-2}). This means that CAPB alone is very much eligible to EOR projects in limestones/carbonates reservoir than sandstone ones, because it reaches dynamic equilibrium at much shorter injection time than in sandstone which keeps adsorbing.

7. Conclusions

Static and dynamic adsorption experiments for a zwitterionic surfactant (CAPB) were performed on limestone and sandstone cores at ambient temperature with desulfated sea water (DSW). The surfactant adsorption behavior was evaluated experimentally and theoretically, thus determining characteristics of the adsorption process on each rock.

It was found that CAPB adsorption increased in both Berea Buff sandstone and Indiana limestone until reaching 0.3 g L^{-1} in equilibrium concentration. After that, adsorption starts to drop on both adsorbents. This behavior is attributed to vesicle-micelle-monomer equilibrium in the bulk solution which could be more energetically favored than the adsorption itself past 0.3 g L^{-1} .

It was concluded that the sandstone active sites could provide more different interactions with the CAPB molecules, in comparison to limestone sites. This explains the higher adsorption on sandstone compared to limestone. Ion-dipole interactions between silanol groups and quaternary amine could be evidenced by the large quantity of neutral sites revealed on the site speciation through surface complexation modelling for sandstone. Ion-ion interactions, including ion binding, were evidenced by divalent adsorption shown in ICP-OES results, even though it was under dynamic conditions.

The adsorption on limestone sites is limited to directly electrostatic interactions, also evidenced in the surface complexation modelling. Furthermore, an electrostatic hindrance effect in adsorption of CAPB on limestone is considered since there is a high quantity of negative sites on the limestone surface at the tested conditions, despite the high quantity of positive ones, the negatives might be alternated with the positive sites, repelling the CAPB deprotonated carboxyl group and making it hard for other molecules to adsorb in the same site. Another aspect of zwitterionic adsorption, which was correlated with this work, and only previously demonstrated by Kumar et. al [53], was the heterogeneous way of a zwitterionic surfactant adsorbing on carbonate and sandstone. It was concluded that heterogeneous adsorption was the main aspect of CAPB adsorption on these rocks, despite the first layer of CAPB adsorption on limestone surface, which a homogeneous behavior was observed through the model fitted parameters. The explanation for this is the same presented in the previous paragraph.

The bilayer isotherm approach was found to perform better than the monolayer approach on static experimental data, and the bilayer kinetic model on the history-match results was found to perform better than equilibrium models on dynamic data, because of the better values of the fitting metrics (adjusted R^2 and RMSE). It is concluded that hydrophobic interactions played a significant role in CAPB adsorption on both rocks, as evidenced by good fitting of bilayer models. The literature demonstrated that admicelles, or bilayers, could form for cationic, anionic, and non-ionic surfactants, where at concentrations past the CMC, the bilayer would be saturated and no more adsorptions would occur [20, 25], but these phenomena were never demonstrated for zwitterionic surfactants. The major difference spotted in this work is that these hydrophobic interactions which form bilayers take place way past the CMC value for CAPB.

CAPB adsorbed more on sandstone, compared to limestone, in both static and dynamic experiments. In the static tests, because surface area values were very close to each other for both adsorbents, adsorption data could be interpreted as more representative of an adsorption behavior lead by interactions rather than site availability. It was also found that dynamic conditions imply more pronounced differences in adsorption between rock types than static tests. This could be attributed to the fact that in the static test methodology, each rock powder is sieved thus forcing very similar particle size distributions for both rocks. Since the distribution of adsorbent particles, or pores, is not controlled on the cores, adsorption becomes more area dependent on the dynamic case. Which means this is a great factor that influences its retention on EOR applications.

CAPB proved to be a good choice for EOR projects in carbonate /limestones reservoirs than sandstone ones, because even at 15 PV of injection on limestone (simulated dynamic equilibrium) the amount of CAPB adsorbed did not surpass the one on sandstone for only 5 PV.

Finally, the adsorption behavior proved to be dependent on the hydrophobic and ion-dipole interactions, which were never demonstrated in the literature for zwitterionic surfactants on such conditions, as bilayer models could explain the experimental data better than the classical isotherms. In the end, adsorption at dynamic equilibrium could be estimated with a provided bilayer kinetic model which can be used to generate reliable adsorption estimates for zwitterionic surfactant adsorption in porous media.

8. Bibliography

- [1] U.S. ENERGY INFORMATION ADMINISTRATION. **Short-Term Energy Outlook**. Available in: <<https://www.eia.gov/outlooks/steo/archives/aug22.pdf>>.
- [2] HACQUARD, P. SIMÖEN, M. HACHE, E. Is the oil industry able to support a world that consumes 105 million barrels of oil per day in 2025? **Oil & Gas Science and Technology – Rev. IFP Energies Nouvelles** 74, 88, 2019.
- [3] LAKE, L.W. **Enhanced Oil Recovery**. Prentice-Hall. 1989.
- [4] SHENG J. J. **Modern chemical enhanced oil recovery: theory and practice**. Gulf Professional Publishing, 2010.
- [5] MANDAL, A. Chemical flood enhanced oil recovery: A review. **International Journal of Oil, Gas and Coal Technology**. 9. 241. 2015.
- [6] KOVSCEK, A. R.; BERTIN, H. Foam Mobility in Heterogeneous Porous Media. **Transport in Porous Media**, v. 52, n. 1, p. 17–35, 1 jan. 2003.
- [7] SKAUGE, A. et al. Foam Generation, Propagation and Stability in Porous Medium. **Transport in Porous Media**, v. 131, n. 1, p. 5–21, 11 mar. 2019.
- [8] KALAM, S. et al. A review on surfactant retention on rocks: mechanisms, measurements, and influencing factors. **Fuel**, v. 293, p. 120459–120459, 1 jun. 2021.
- [9] DONALDSON, E. C.; G.V. CHILINGARIAN; YEN, T. F. **Enhanced Oil Recovery, II**. [s.l.] Elsevier, 1989.
- [10] KAMAL, M. S.; HUSSEIN, I. A.; SULTAN, A. S. Review on Surfactant Flooding: Phase Behavior, Retention, IFT, and Field Applications. **Energy & Fuels**, v. 31, n. 8, p. 7701–7720, 9 ago. 2017.
- [11] MANNHARDT, K.; NOVOSAD, J. J.; JHA, K. N. Adsorption of Foam-forming Surfactants in Berea Sandstone. **Journal of Canadian Petroleum Technology**, v. 33, n. 02, 1 fev. 1994.

- [12] DAI, C. et al. Adsorption behavior of cocamidopropyl betaine under conditions of high temperature and high salinity. **Journal of Applied Polymer Science**, v. 131, n. 12, p. n/a-n/a, 27 jan. 2014.
- [13] KOPARAL, G. **Surfactant retention analysis in Berea sandstones**. Thesis—The University of Texas at Austin: [s.n.].
- [14] ALCONOX. **types of surfactants**. Available in: <<https://technotes.alconox.com/detergents/types-of-surfactants/>>.
- [15] ROSEN, M. J. **Surfactants and Interfacial Phenomena**. New York: Wiley, 2004.
- [16] BUTT, H.-J.; GRAF, K.; KAPPL, M. **Physics and Chemistry of Interfaces**. [s.l.] John Wiley & Sons, 2006.
- [17] HOLMBERG, K.; DINESH OCHHAVLAL SHAH; SCHWUGER, M. J. **Handbook of Applied Surface and Colloid Chemistry**. [s.l.] JOHN WILEY & SONS, LTD, 2002.
- [18] BELHAJ, A. F. et al. The effect of surfactant concentration, salinity, temperature, and pH on surfactant adsorption for chemical enhanced oil recovery: a review. **Journal of Petroleum Exploration and Production Technology**, v. 10, n. 1, p. 125–137, 16 maio 2019.
- [19] QUY, T. et al. Development of Isotherm Polymer/Surfactant Adsorption Models in Chemical Flooding. **SPE Asia Pacific Oil Gas Conf. Exhib**, 20 set. 2011.
- [20] PARIA, S.; KHILAR, K. C. A review on experimental studies of surfactant adsorption at the hydrophilic solid–water interface. **Advances in Colloid and Interface Science**, v. 110, n. 3, p. 75–95, ago. 2004.
- [21] SOMASUNDARAN, P.; HUANG, L. Q. Adsorption/aggregation of surfactants and their mixtures at solid–liquid interfaces. **Advances in Colloid and Interface Science**, v. 88, n. 1-2, p. 179–208, 11 dez. 2000.

[22] SOMASUNDARAN, P.; ZHANG, L. Adsorption of surfactants on minerals for wettability control in improved oil recovery processes. **Journal of Petroleum Science and Engineering**, v. 52, n. 1-4, p. 198–212, jun. 2006.

[23] AZAM, M. R. et al. Static adsorption of anionic surfactant onto crushed Berea sandstone. **Journal of Petroleum Exploration and Production Technology**, v. 3, n. 3, p. 195–201, 18 abr. 2013.

[24] LIU, Z. et al. Comprehensive review on surfactant adsorption on mineral surfaces in chemical enhanced oil recovery. **Advances in Colloid and Interface Science**, v. 294, p. 102467, ago. 2021.

[25] KALAM, S. et al. Surfactant Adsorption Isotherms: A Review. **ACS Omega**, v. 6, n. 48, p. 32342–32348, 24 nov. 2021b.

[26] SOMASUNDARAN, P.; HEALY, T. W.; FUERSTENAU, D. W. The aggregation of colloidal alumina dispersions by adsorbed surfactant ions. **Journal of Colloid and Interface Science**, v. 22, n. 6, p. 599–605, 1 dez. 1966.

[27] PARIA, S.; MANOHAR, C.; KHILAR, K. C. Adsorption of anionic and non-ionic surfactants on a cellulosic surface. **Colloids and Surfaces A: Physicochemical and Engineering Aspects**, v. 252, n. 2-3, p. 221–229, 1 jan. 2005.

[28] PAGAC, E. S.; PRIEVE, D. C.; TILTON, R. D. Kinetics and Mechanism of Cationic Surfactant Adsorption and Coadsorption with Cationic Polyelectrolytes at the Silica–Water Interface. **Langmuir**, v. 14, n. 9, p. 2333–2342, 1 abr. 1998.

[29] TROGUS, F. J.; SCHECHTER, R. S.; WADE, W. H. A new interpretation of adsorption maxima and minima. **Journal of Colloid and Interface Science**, v. 70, n. 2, p. 293–305, 1 jun. 1979.

[30] ARNEBRANT, T. et al. An ellipsometry study of ionic surfactant adsorption on chromium surfaces. **Journal of Colloid and Interface Science**, v. 128, n. 2, p. 303–312, 1 mar. 1989.

- [31] CURBELO, F. D. S. et al. Adsorption of non-ionic surfactants in sandstones. **Colloids and Surfaces A: Physicochemical and Engineering Aspects**, v. 293, n. 1-3, p. 1–4, fev. 2007.
- [32] NIETO-ALVAREZ, D. A. et al. Adsorption of Zwitterionic Surfactant on Limestone Measured with High-Performance Liquid Chromatography: Micelle–Vesicle Influence. **Langmuir**, v. 30, n. 41, p. 12243–12249, 6 out. 2014.
- [33] LV, W. et al. Static and dynamic adsorption of anionic and zwitterionic surfactants with and without the presence of alkali. **Journal of Petroleum Science and Engineering**, v. 77, n. 2, p. 209–218, 1 maio 2011.
- [34] LI, N. et al. Adsorption Behavior of Betaine-Type Surfactant on Quartz Sand. **Energy & Fuels**, v. 25, n. 10, p. 4430–4437, 3 out. 2011.
- [35] ZHONG, X. et al. Comparative Study on the Static Adsorption Behavior of Zwitterionic Surfactants on Minerals in Middle Bakken Formation. **Energy & Fuels**, v. 33, n. 2, p. 1007–1015, 11 jan. 2019.
- [36] LEE, E. M.; KOOPAL, L. K. Adsorption of Cationic and Anionic Surfactants on Metal Oxide Surfaces: Surface Charge Adjustment and Competition Effects. **Journal of Colloid and Interface Science**, v. 177, n. 2, p. 478–489, 1 fev. 1996.
- [37] DENOYEL, R.; ROUQUEROL, J. Thermodynamic (including microcalorimetry) study of the adsorption of non-ionic and anionic surfactants onto silica, kaolin, and alumina. **Journal of Colloid and Interface Science**, v. 143, n. 2, p. 555–572, 1 maio 1991.
- [38] NEVSKAIA, D. M.; GUERRERO-RUIZ, A.; DE D. LÓPEZ-GONZÁLEZ, J. Adsorption of Polyoxyethylenic Non-ionic and Anionic Surfactants from Aqueous Solution: Effects Induced by the Addition of NaCl and CaCl₂. **Journal of Colloid and Interface Science**, v. 205, n. 1, p. 97–105, 1 set. 1998.
- [39] MANNHARDT, K.; SCHRAMM, L. L.; NOVOSAD, J. J. Effect of Rock type and Brine Composition on Adsorption of Two Foam-Forming Surfactants. **SPE Advanced Technology Series**, v. 1, n. 01, p. 212–218, 1 abr. 1993.

- [40] HIRASAKI, G. J.; DANHUA LESLIE ZHANG. Surface Chemistry of Oil Recovery From Fractured, Oil-Wet, Carbonate Formation. **SPE International Symposium on Oilfield Chemistry**, 5 fev. 2003.
- [41] HIRASAKI, G.; ZHANG, D. L. Surface Chemistry of Oil Recovery From Fractured, Oil-Wet, Carbonate Formations. **SPE Journal**, v. 9, n. 02, p. 151–162, 1 jun. 2004.
- [42] TACKIE-OTOO, B. N. et al. Alternative chemical agents for alkalis, surfactants and polymers for enhanced oil recovery: Research trend and prospects. **Journal of Petroleum Science and Engineering**, v. 187, p. 106828, 1 abr. 2020.
- [43] CORKILL, J. M.; GOODMAN, J. F.; TATE, J. R. Adsorption of non-ionic surface-active agents at the Graphon/solution interface. **Transactions of the Faraday Society**, v. 62, p. 979–979, 1 jan. 1966.
- [44] ZIEGLER, V. M.; HANDY, L. L. Effect of Temperature on Surfactant Adsorption in Porous Media. **Society of Petroleum Engineers Journal**, v. 21, n. 02, p. 218–228, 1 abr. 1981.
- [45] JIAN, G. et al. Characterizing adsorption of associating surfactants on carbonates surfaces. **Journal of Colloid and Interface Science**, v. 513, p. 684–692, mar. 2018.
- [46] SOMASUNDARAN, P.; HANNA, H. S. Adsorption of Sulfonates on Reservoir Rocks. **Society of Petroleum Engineers Journal**, v. 19, n. 04, p. 221–232, 1 ago. 1979.
- [47] SOMASUNDARAN, P.; HANNA, H. S. Adsorption/Desorption of Sulfonates by Reservoir Rock Minerals in Solutions of Varying Sulfonate Concentrations. **Society of Petroleum Engineers Journal**, v. 25, n. 03, p. 343–350, 1 jun. 1985.
- [48] BERA, A. et al. Adsorption of surfactants on sand surface in enhanced oil recovery: Isotherms, kinetics and thermodynamic studies. **Applied Surface Science**, v. 284, p. 87–99, nov. 2013.

- [49] MANNHARDT, K.; SCHRAMM, L. L.; NOVOSAD, J. J. Adsorption of anionic and zwitterionic foam-forming surfactants on different rock types. **Colloids and Surfaces**, v. 68, n. 1-2, p. 37–53, nov. 1992.
- [50] SATTER, A. et al. Chemical Transport in Porous Media With Dispersion and Rate-Controlled Adsorption. **Society of Petroleum Engineers Journal**, v. 20, n. 03, p. 129–138, 1 jun. 1980.
- [51] NOVOSAD, J. J.; MAINI, B. B.; HUANG, A. Retention Of Foam-Forming Surfactants At Elevated Temperatures. **The Journal of Canadian Petroleum Technology**, 1 maio 1986.
- [52] ZHAO, J. et al. Surface properties and adsorption behavior of cocamidopropyl dimethyl amine oxide under high temperature and high salinity conditions. **Colloids and Surfaces A: Physicochemical and Engineering Aspects**, v. 450, p. 93–98, maio 2014.
- [53] KUMAR, A.; MANDAL, A. Critical investigation of zwitterionic surfactant for enhanced oil recovery from both sandstone and carbonate reservoirs: Adsorption, wettability alteration and imbibition studies. **Chemical Engineering Science**, v. 209, p. 115222, dez. 2019.
- [54] FOO, K. Y.; HAMEED, B. H. Insights into the modeling of adsorption isotherm systems. **Chemical Engineering Journal**, v. 156, n. 1, p. 2–10, 1 jan. 2010.
- [55] WANG, J.; GUO, X. Adsorption isotherm models: Classification, physical meaning, application and solving method. **Chemosphere**, v. 258, p. 127279, nov. 2020.
- [56] LANGMUIR, I. THE ADSORPTION OF GASES ON PLANE SURFACES OF GLASS, MICA AND PLATINUM. **Journal of the American Chemical Society**, v. 40, n. 9, p. 1361–1403, set. 1918.
- [57] FREUNDLICH, H. Über die Adsorption in Lösungen. **Zeitschrift für Physikalische Chemie**, v. 57U, n. 1, 1 jan. 1907.

- [58] REDLICH, O.; PETERSON, D. L. A useful adsorption isotherm. **The Journal of Physical Chemistry**, v. 63, n. 6, p. 1024, jun. 1959.
- [59] SIPS, R. On the Structure of a Catalyst Surface. **The Journal of Chemical Physics**, v. 16, n. 5, p. 490–495, maio 1948.
- [60] AYAWEI, N.; EBELEGI, A. N.; WANKASI, D. Modelling and Interpretation of Adsorption Isotherms. **Journal of Chemistry**, v. 2017, p. 1–11, 2017.
- [61] SHARMA, S. et al. RUPTURA: simulation code for breakthrough, ideal adsorption solution theory computations, and fitting of isotherm models. **Molecular Simulation**, v. 49, n. 9, p. 893–953, 12 maio 2023.
- [62] GANGULA, S.; SUEN, S.-Y.; CONTE, E. D. Analytical applications of admicelle and hemimicelle solid phase extraction of organic analytes. **Microchemical Journal**, v. 95, n. 1, p. 2–4, 1 maio 2010.
- [63] WANG, Z.; XU, S.; ACOSTA, E. Heat of adsorption of surfactants and its role on nanoparticle stabilization. **The Journal of Chemical Thermodynamics**, v. 91, p. 256–266, dez. 2015.
- [64] KWOK, W.; HAYES, R. E.; NASR-EL-DIN, H. A. Modelling dynamic adsorption of an anionic surfactant on Berea sandstone with radial flow. **Chemical Engineering Science**, v. 50, n. 5, p. 769–783, mar. 1995.
- [65] KORESH, J.; SOFFER, A. Application of the two-site Langmuir isotherm to microporous adsorbents. **Journal of Colloid and Interface Science**, v. 92, n. 2, p. 517–524, abr. 1983.
- [66] GUPTA, S. P.; GREENKORN, R. A. Determination of dispersion and nonlinear adsorption parameters for flow in porous media. **Water Resources Research**, v. 10, n. 4, p. 839–846, ago. 1974.
- [67] LAKE, L. W.; HELFFERICH, F. Cation Exchange in Chemical Flooding: Part 2--The Effect of Dispersion, Cation Exchange, and Polymer/Surfactant Adsorption

on Chemical Flood Environment. **Society of Petroleum Engineers Journal**, v. 18, n. 06, p. 435–444, 1 dez. 1978.

[68] RAMIREZ, W. F.; SHULER, P.; FRIEDMAN, F. Convection, Dispersion, and Adsorption of Surfactants in Porous Media. **Society of Petroleum Engineers Journal**, v. 20, n. 06, p. 430–438, 1 dez. 1980.

[69] CHUNG, F. T. H. Modeling of surfactant transport and adsorption in porous media. **U.S. Department of Energy Assistant Secretary for Fossil Energy**, 1 abr. 1991.

[70] AUSTAD, T. et al. Chemical flooding of oil reservoirs Part 9. Dynamic adsorption of surfactant onto sandstone cores from injection water with and without polymer present. **Colloids Surfaces A: Physicochem. Eng. Aspects**, v. 127, n. 1–3, p. 69–82, 1 jul. 1997.

[71] AMIRMOSHIRI, M. et al. Role of Wettability on the Adsorption of an Anionic Surfactant on Sandstone Cores. **Langmuir**, v. 36, n. 36, p. 10725–10738, 15 set. 2020.

[72] BEAR, J. **Dynamics of fluids in porous media**. New York: Dover, 1988.

[73] TROGUS, F. J. et al. Static and Dynamic Adsorption of Anionic and Non-ionic Surfactants. **Society of Petroleum Engineers Journal**, v. 17, n. 05, p. 337–344, 1 out. 1977.

[74] SHAW, D. J. **Introduction to Colloid and Surface Chemistry**. [s.l.] Butterworth-Heinemann, 1970.

[75] HIEMSTRA, T.; VAN RIEMSDIJK, W. H. A Surface Structural Approach to Ion Adsorption: The Charge Distribution (CD) Model. **Journal of Colloid and Interface Science**, v. 179, n. 2, p. 488–508, 1 maio 1996.

[76] LEROY, P.; REVIL, A. A triple-layer model of the surface electrochemical properties of clay minerals. **Journal of Colloid and Interface Science**, v. 270, n. 2, p. 371–380, 1 fev. 2004.

[77] RAHNEMAIE, R.; HIEMSTRA, T.; W.H. VAN RIEMSDIJK. A new surface structural approach to ion adsorption: Tracing the location of electrolyte ions. **Journal of Colloid and Interface Science**, v. 293, n. 2, p. 312–321, 1 jan. 2006.

[78] TAKEYA, M. et al. Predicting the electrokinetic properties of the crude oil/brine interface for enhanced oil recovery in low salinity water flooding. **Fuel**, v. 235, p. 822–831, jan. 2019.

[79] HIEMSTRA, T.; VAN RIEMSDIJK, W. H.; BOLT, G. H. Multisite proton adsorption modeling at the solid/solution interface of (hydr)oxides: A new approach. **Journal of Colloid and Interface Science**, v. 133, n. 1, p. 91–104, 1 nov. 1989.

[80] TAKEYA, M. et al. Crude oil/brine/rock interface in low salinity waterflooding: Experiments, triple-layer surface complexation model, and DLVO theory. **Journal of Petroleum Science and Engineering**, v. 188, p. 106913–106913, 1 maio 2020.

[81] ELAKNESWARAN, Y. et al. Effect of Electrokinetics and Thermodynamic Equilibrium on Low-Salinity Water Flooding for Enhanced Oil Recovery in Sandstone Reservoirs. **ACS Omega**, v. 6, n. 5, p. 3727–3735, 1 fev. 2021.

[82] BONTO, M.; EFTEKHARI, A. A.; NICK, H. M. Electrokinetic behavior of artificial and natural calcites: A review of experimental measurements and surface complexation models. **Advances in Colloid and Interface Science**, v. 301, p. 102600–102600, 1 mar. 2022.

[83] LEROY, P. et al. The zeta potential of quartz. Surface complexation modelling to elucidate high salinity measurements. **Colloids and Surfaces A: Physicochemical and Engineering Aspects**, v. 650, p. 129507–129507, 1 out. 2022.

[84] SONG, J. et al. Surface complexation modeling of calcite zeta potential measurements in brines with mixed potential determining ions (Ca^{2+} , CO_3^{2-} , Mg^{2+} , SO_4^{2-}) for characterizing carbonate wettability. **Journal of Colloid and Interface Science**, v. 506, p. 169–179, nov. 2017.

[85] MASSARWEH, O.; ABUSHAIKHA, A. S. The use of surfactants in enhanced oil recovery: A review of recent advances. **Energy Reports**, v. 6, p. 3150–3178, nov. 2020.

[86] REZAEI, A. et al. Integrating surfactant, alkali and nano-fluid flooding for enhanced oil recovery: A mechanistic experimental study of novel chemical combinations. **Journal of Molecular Liquids**, v. 308, p. 113106, jun. 2020.

[87] GHOLAMI, A.; GOLESTANEH, M.; ANDALIB, Z. A new method for determination of cocamidopropyl betaine synthesized from coconut oil through spectral shift of Eriochrome Black T. **Spectrochimica Acta Part A: Molecular and Biomolecular Spectroscopy**, v. 192, p. 122–127, mar. 2018.

[88] PUBCHEM. **Cocamidopropyl betaine**. Disponível em: <<https://pubchem.ncbi.nlm.nih.gov/compound/Cocamidopropyl-betaine>>.

[89] RÓŹAŃSKA, S. Rheology of wormlike micelles in mixed solutions of cocoamidopropyl betaine and sodium dodecylbenzenesulfonate. **Colloids and Surfaces A: Physicochemical and Engineering Aspects**, v. 482, p. 394–402, out. 2015.

[90] DANOV, K. D. et al. Mixed Solutions of Anionic and Zwitterionic Surfactant (Betaine): Surface-Tension Isotherms, Adsorption, and Relaxation Kinetics. **Langmuir**, v. 20, n. 13, p. 5445–5453, 19 maio 2004.

[91] MERKOVA, M. et al. Degradation of the surfactant Cocamidopropyl betaine by two bacterial strains isolated from activated sludge. **International Biodeterioration & Biodegradation**, v. 127, p. 236–240, fev. 2018.

[92] PADDAY, J. F.; PITT, A. R.; PASHLEY, R. M. Menisci at a free liquid surface: surface tension from the maximum pull on a rod. **Journal of the Chemical Society, Faraday Transactions 1: Physical Chemistry in Condensed Phases**, v. 71, n. 0, p. 1919, 1975.

[93] JORDAN, M. M.; COLLINS, I. R.; MACKAY, E. J. Low Sulfate Seawater Injection for Barium Sulfate Scale Control: A Life-of-Field Solution to a Complex Challenge. **SPE Production & Operations**, v. 23, n. 02, p. 192–209, 19 maio 2008.

- [94] PEDENAUD, P.; HURTEVENT, C.; SALIMA BARAKA-LOKMANE. Industrial Experience in Sea Water Desulfation. **SPE International Conference and Exhibition on Oilfield Scale**, 30 maio 2012.
- [95] **Cores & Core Samples for Research in Texas at Kocurek Industries, Core Samples Expert**. Disponível em: <<https://kocurekindustries.com/>>. Acesso em: 25 jul. 2023.
- [96] BUCKLEY, J. S.; TAKAMURA, K.; MORROW, N. R. Influence of Electrical Surface Charges on the Wetting Properties of Crude Oils. **SPE Reservoir Engineering**, v. 4, n. 03, p. 332–340, 1 ago. 1989.
- [97] GAMAL, H.; ELKATATNY, S.; ADEBAYO, A. Influence of mud filtrate on the pore system of different sandstone rocks. **Journal of Petroleum Science and Engineering**, v. 202, p. 108595, jul. 2021.
- [98] AWAN, F. U. R. et al. Influence of mineralogy and surfactant concentration on zeta potential in intact sandstone at high pressure. **Journal of Colloid and Interface Science**, v. 607, p. 401–411, 1 fev. 2022.
- [99] FREIRE-GORMALY, M. et al. Pore Structure Characterization of Indiana Limestone and Pink Dolomite from Pore Network Reconstructions. **Oil & Gas Science and Technology – Revue d’IFP Energies nouvelles**, v. 71, n. 3, p. 33, 7 ago. 2015.
- [100] LUCAS, C. R. DOS S. et al. Investigating the Fluid–Solid Interaction of Acid Non-ionic Nanoemulsion with Carbonate Porous Media. **Molecules**, v. 25, n. 6, p. 1475, 24 mar. 2020.
- [101] ELIEBID, M. et al. Surfactants Impact on CO₂ Sequestration for Enhanced Gas Recovery and in Depleted Carbonate Reservoirs. **Abu Dhabi International Exhibition & Conference**, 13 nov. 2017.
- [102] DO, D. D. **Adsorption Analysis: Equilibria And Kinetics (With Cd Containing Computer Matlab Programs)**. [s.l.] World Scientific, 1998.

- [103] SATTER, A.; IQBAL, G. M. **Reservoir Engineering**. [s.l.] Gulf Professional Publishing, 2015.
- [104] KUMAR, A.; TIWARI, A. A Comparative Study of Otsu Thresholding and K-means Algorithm of Image Segmentation. **International Journal of Engineering and Technical Research (IJETR)**, v. 9, n. 5, 30 maio 2019.
- [105] Avizo module description. AVIZO SOFTWARE.
- [106] STRUTZ, T. **Data fitting and uncertainty a practical introduction to weighted least squares and beyond**. [s.l.] Wiesbaden Springer Vieweg, 2016.
- [107] KEREN, Y.; BORISOVER, M.; BUKHANOVSKY, N. Sorption interactions of organic compounds with soils affected by agricultural olive mill wastewater. **Chemosphere**, v. 138, p. 462–468, nov. 2015.
- [108] ADAMSON, A. W.; GAST, A. P. **Physical chemistry of surfaces**. New York: Wiley, 1997.
- [109] GEROLD, C. T.; HENRY, C. S. Observation of Dynamic Surfactant Adsorption Facilitated by Divalent Cation Bridging. **Langmuir**, v. 34, n. 4, p. 1550–1556, 17 jan. 2018.
- [110] SVORSTOEL, I. et al. Foam Pilot Evaluations for the Snorre Field, Part 1: Project and Laboratory Results. **8th European IOR - Symposium in Vienna**, 1 jan. 1995.

9. Appendix

9.1 Results of selected liquid to solid ratio for static experiments

Figures 56 and 57 show the liquid to solid ratio tests to select and ensure the quantity of rock powder and solution utilized on the static adsorption tests.

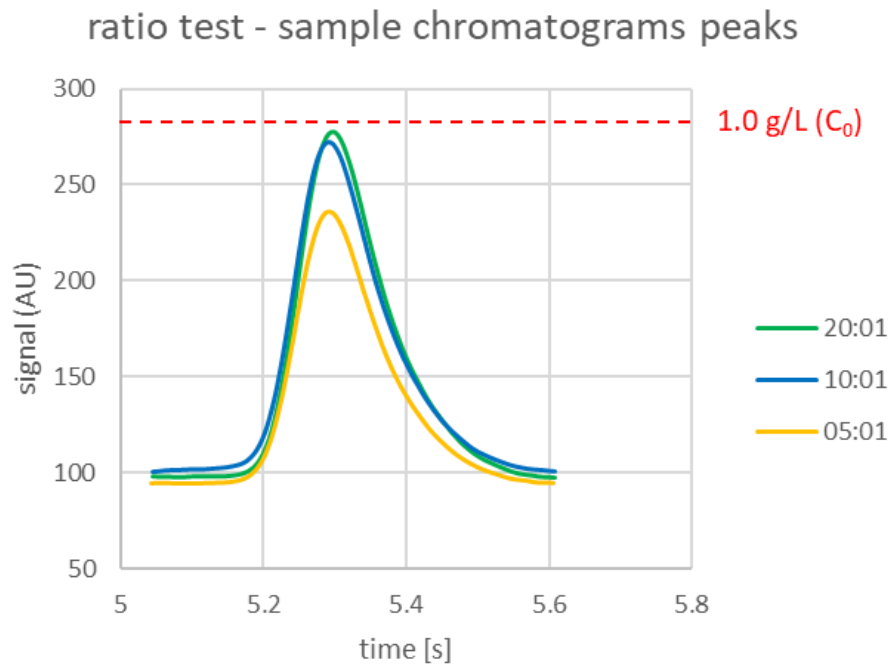


Figure 56: CAPB chromatograms peaks with different liquid to solid ratios

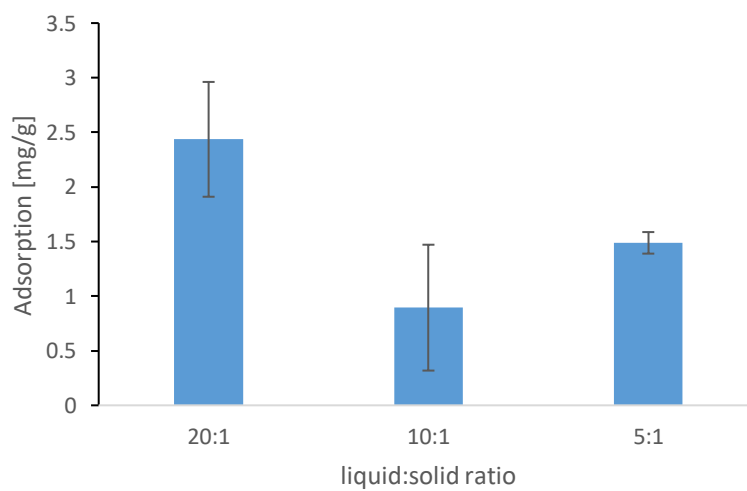


Figure 57: Variability of liquid to solid ratios in CAPB adsorption on Indiana Limestone

Despite the conclusion of the chromatograms in relation to the greater difference in peak area using the 5 to 1 liquid to solid ratio, the comparison made in Figure 57 attests the low variability of the 5 to 1 ratio adsorption results. Therefore, this ratio was the chosen one to be applied in the static studies.

9.2 Results of surface potential at literature conditions for validation of the SCM

Figure 58 and 59 show the comparison between the experimental and estimated values by their implementation and the one related to this work.

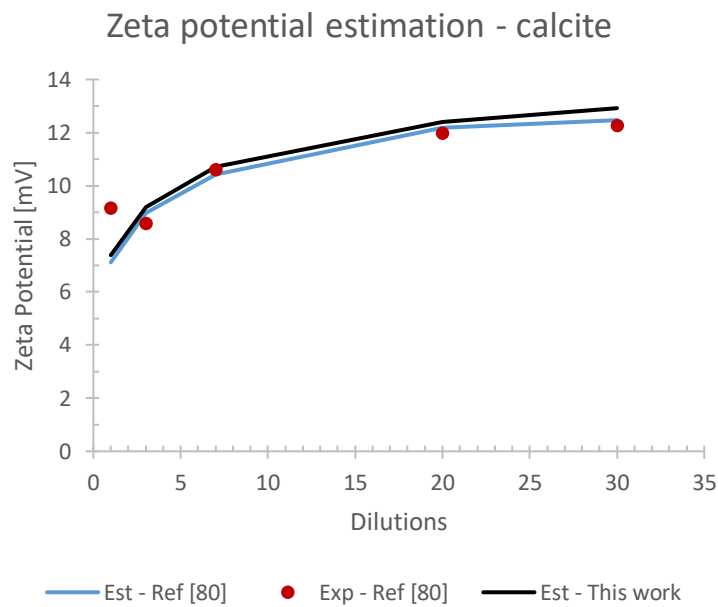


Figure 58: Zeta potential experimental data vs TL model for calcite [80]

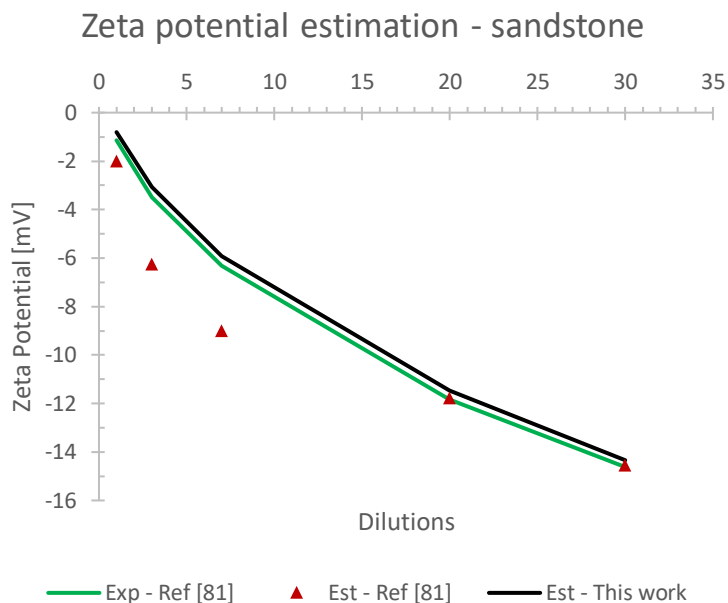


Figure 59: Zeta potential experimental data vs TL model for sandstone [81]

After validating the implementation, the parameters were changed to make the estimated conditions more like the experimental of the static adsorption experiments. In this case, the input concentration of the brine (DSW) is the one presented in Section 5.1.2 Brine (DSW) composition and properties. The pH is set to the measured value before the experiment. Then, equilibrium quantities, solution pH and conductivity were calculated utilizing the default database of PHREEQC and each amount of solid and liquid phase related to the static tests: 1 g of rock and 5 ml of aqueous phase. For the limestone case, the equilibrium is set to calcite and for the sandstone the equilibrium is set with quartz and kaolinite.

The resulting solution is then equilibrated with the surface species through CD-MUSIC routine, as the parameters were shown in Section 4.3 Surface complexation model. PHREEQC outputs the zeta potential and the molar quantities of every surface species, as well as the physical-chemical properties of the resulting solution. The results were shown at the Section 6.3.1.2 Evaluation of static adsorption results by analysis of estimated rock surface potential and speciation.

9.3 PHREEQC script for surface potential and speciation estimates

9.3.1 DSW/Calcite

```
SOLUTION 1
  temp      30
  pH        7.93
  pe        4
  redox     pe
  units     mmol/kgw
  density   1
  Na       478.73
  Ca       3.32
  Mg       6.30
  Cl       506.32
  S(6)     0.26
  K        10.05
  Alkalinity 1.18 as HCO3
  -water   0.005 # kg
```

```
EQUILIBRIUM_PHASES 1
```

```
Calcite    0      0.009891098
```

```
SURFACE_MASTER_SPECIES
```

```
Surf_cal      Surf_calOH
```

```
Surf_cal_prot Surf_cal_proth
```

```
SURFACE_SPECIES
```

```
Surf_calOH      =      Surf_calOH
```

```
-cd_music      0      0      0
```

```
log_k      0
```

```
Surf_cal_proth =      Surf_cal_proth
```

```
-cd_music      0      0      0
```

```
log_k      0
```

```
Surf_cal_proth =      Surf_cal_prot-      +      H+
```

```
-cd_music      -1      0      0
```

log_k -7.3

Surf_calOH + H+ = Surf_calOH2+

-cd_music 1 0 0

log_k 15.0

Surf_cal_protH + Ca++ =
Surf_cal_protCa+ + H+

-cd_music -1 2 0

log_k -6.45

Surf_cal_protH + Mg++ =
Surf_cal_protMg+ + H+

-cd_music -1 2 0

log_k -6.15

Surf_calOH + H+ + SO4-- = Surf_calOH2SO4-

-cd_music 1 -2 0

log_k 14.75

SURFACE 1

-equilibrate with solution 1

-sites DENSITY

Surf_calOH 4.95

Surf_cal_protH 4.95 1.23 1

-capacitance 3.098 0.65

-cd_music

END

9.3.2 DSW/Quartz/Kaolinite

SOLUTION 1

temp 30

pH 7.93

pe 4

redox pe

units mmol/kgw

density 1

Na 478.73

Ca 3.32

Mg 6.30
 Cl 506.32
 S(6) 0.26
 K 10.05
 Alkalinity 1.18 as HCO3
 -water 0.005 # kg

EQUILIBRIUM_PHASES 1
 Kaolinite 0 5.42E-05
 Quartz 0 1.52E-02

SURFACE_MASTER_SPECIES

Surf_al Surf_alOH
 Surf_si Surf_siOH
 Surf_qs Surf_qsOH

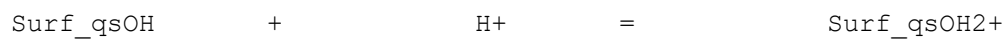
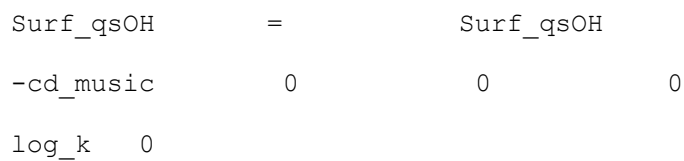
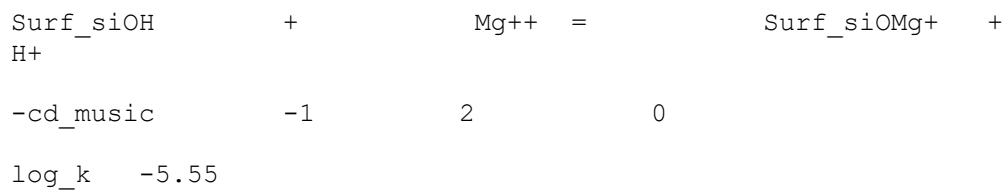
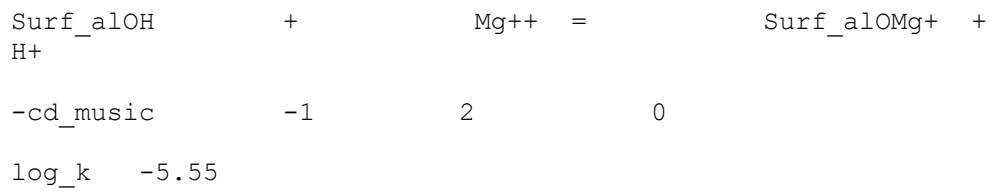
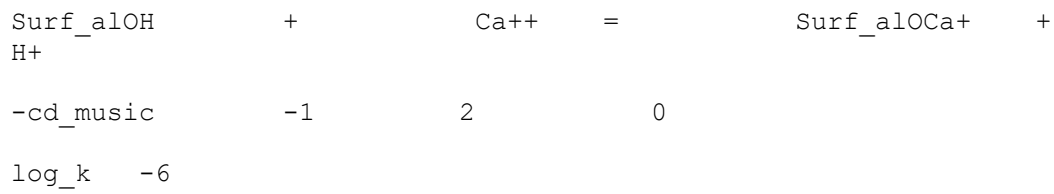
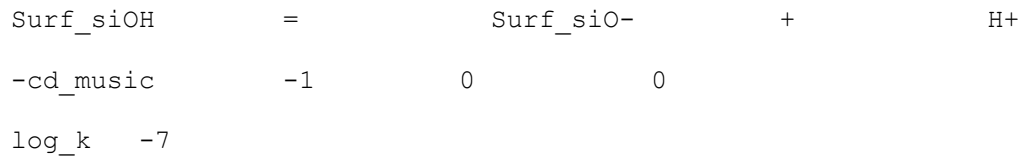
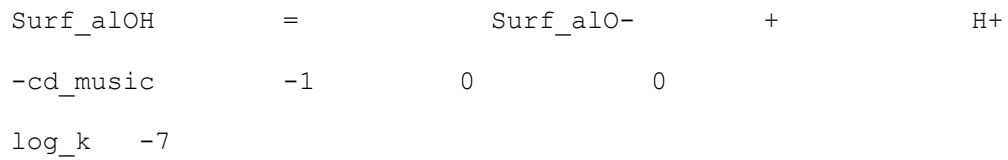
SURFACE_SPECIES

Surf_alOH = Surf_alOH
 -cd_music 0 0 0
 log_k 0

Surf_siOH = Surf_siOH
 -cd_music 0 0 0
 log_k 0

Surf_alOH + H+ = Surf_alOH2+
 -cd_music 1 0 0
 log_k 0.8

Surf_siOH + H+ = Surf_siOH2+
 -cd_music 1 0 0
 log_k 0.8



-cd_music 1 0 0

log_k -1.75

Surf_qsOH = Surf_qsO- + H+

-cd_music -1 0 0

log_k -6.75

Surf_qsOH + Ca++ = Surf_qsOCa+ +
H+

-cd_music -1 2 0

log_k -5.7

Surf_qsOH + Mg++ = Surf_qsOMg+ +
H+

-cd_music -1 2 0

log_k -5.70

SURFACE 1

-sites_units Density

-cd_music

-equilibrate 1

Surf_alOH 0.64

Surf_siOH 0.64

Surf_qsOH 2.95 1.37 1

-capacitance 3.098 0.2

END

9.4 Rights and permissions of images utilized

Figure 2 from Ref [9]:

CCC | RightsLink

My Orders My Library My Profile Welcome pabloqui@aluno.puc-rio.br Log out | Help | FAQ

My Orders > Orders > All Orders

License Details

This Agreement between Mr. Pablo Godoy ("You") and Elsevier ("Elsevier") consists of your license details and the terms and conditions provided by Elsevier and Copyright Clearance Center.

[Print](#) [Copy](#)

License Number	5613940522825
License date	Aug 21, 2023
Licensed Content Publisher	Elsevier
Licensed Content Publication	Elsevier Books
Licensed Content Title	Developments in Petroleum Science
Licensed Content Author	E. C. Donaldson, G.V. Chilingarian, T.F. Yen, M.K. Sharma
Licensed Content Date	Jan 1, 1989
Licensed Content Pages	11
Type of Use	reuse in a thesis/dissertation
Portion	figures/tables/illustrations
Number of figures/tables/illustrations	1
Format	electronic
Are you the author of this Elsevier chapter?	No
Will you be translating?	No
Title	Adsorption of cocamidopropyl betaine on analogue reservoir rocks under static and dynamic conditions
Institution name	PUC-Rio
Expected presentation date	Aug 2023
Order reference number	11082023
Portions	Figure 1-2. on page 6
Requestor Location	Mr. Pablo Godoy Av. Prefeito Dulcídio Cardoso Rio de Janeiro, RJ 22620-310 Brazil Attn: Mr. Pablo Godoy GB 494 6272 12
Publisher Tax ID	
Total	0.00 USD

[BACK](#)

Copyright © 2023 Copyright Clearance Center, Inc. All Rights Reserved. [Privacy statement](#). [Data Security and Privacy](#). For California Residents. [Terms and Conditions](#).
Comments? We would like to hear from you. E-mail us at customer-care@copyright.com

Figures 5 and 7 from Ref [16]:



Order Number: 1391411			
Order Date: 29 Aug 2023			
Payment Information			
Pablo Godoy pabloalbgodoy@gmail.com Payment method: Invoice		Billing Address: Mr. Pablo Godoy Av. Prefeito Dulcídio Cardoso Rio De Janeiro, RJ 22620-310 Brazil +55 (21)996572727 pabloalbgodoy@gmail.com	
		Customer Location: Mr. Pablo Godoy Av. Prefeito Dulcídio Cardoso Rio De Janeiro, RJ 22620-310 Brazil	
Order Details			
1. Physics and chemistry of interfaces			Billing Status: Open
Order License ID	1391411-1	Type of Use	Republish in a thesis/dissertation
Order detail status	Completed	Publisher	Wiley-VCH
ISBN-13	9783527406296	Portion	Image/photo/illustration
			0.00 USD Republication Permission
LICENSED CONTENT			
Publication Title	Physics and chemistry of interfaces	Country	Germany
Author/Editor	Butt, Hans-Jürgen., Graf, Kh., Kappl, Michael	Rightholder	John Wiley & Sons - Books
Date	01/01/2006	Publication Type	Book
Language	English		
REQUEST DETAILS			
Portion Type	Image/photo/illustration	Distribution	Worldwide
Number of Images / Photos / Illustrations	2	Translation	Original language of publication
Format (select all that apply)	Electronic	Copies for the Disabled?	No
Who Will Republish the Content?	Academic institution	Minor Editing Privileges?	No
Duration of Use	Life of current edition	Incidental Promotional Use?	No
Lifetime Unit Quantity	Up to 499	Currency	USD
Rights Requested	Main product		
NEW WORK DETAILS			
Title	Adsorption of cocamidopropyl betaine on analogue reservoir rocks at static and dynamic conditions	Institution Name	PUC-Rio
		Expected Presentation Date	2023-09-09
Instructor Name	Prof. Aurora Perez Gramatges		
ADDITIONAL DETAILS			
The Requesting Person/Organization to Appear on the License	Pablo Godoy		
REQUESTED CONTENT DETAILS			
Title, Description or Numeric Reference of the Portion(s)	Figures 9.1 and 12.7	Title of the Article/Chapter the Portion Is From	Chapter 9 and 12
Editor of Portion(s)	Hans-Jürgen Butt, Karlheinz Graf, Michael Kappl	Author of Portion(s)	Butt, Hans-Jürgen.; Graf, Kh.; Kappl, Michael
Volume / Edition	2nd., rev. and enl. ed.	Publication Date of Portion	2006-01-01
Page or Page Range of Portion	Page 177 and 257		
John Wiley & Sons - Books Terms and Conditions			
<p>No right, license or interest to any trademark, trade name, service mark or other branding ("Marks") of WILEY or its licensors is granted hereunder, and you agree that you shall not assert any such right, license or interest with respect thereto. You may not alter, remove or suppress in any manner any copyright, trademark or other notices displayed by the Wiley material. This Agreement will be void if the Type of Use, Format, Circulation, or Requestor Type was misrepresented during the licensing process. In no instance may the total amount of Wiley Materials used in any Main Product, Compilation or Collective work comprise more than 5% (if figures/tables) or 15% (if full articles/chapters) of the (entirety of the) Main Product, Compilation or Collective Work. Some titles may be available under an Open Access license. It is the Licensor's responsibility to identify the type of Open Access license on which the requested material was published, and comply fully with the terms of that license for the type of use specified. Further details can be found on Wiley Online Library http://olabout.wiley.com/WileyCDA/Section/id-217804.html</p>			

Figure 8 from Ref [15]:



Order Number: 1391429
Order Date: 29 Aug 2023

Payment Information

Pablo Godoy pabloalbgodoy@gmail.com Payment method: Invoice	Billing Address: Mr. Pablo Godoy Av. Prefeito Dulcídio Cardoso Rio De Janeiro, RJ 22620-310 Brazil +55 (21)996572727 pabloalbgodoy@gmail.com	Customer Location: Mr. Pablo Godoy Av. Prefeito Dulcídio Cardoso Rio De Janeiro, RJ 22620-310 Brazil
--	---	---

Order Details

1. Surfactants and Interfacial Phenomena **Billing Status:**
Open

Order License ID	1391429-1	Type of Use	Republish in a thesis/dissertation
Order detail status	Completed	Publisher	John Wiley & Sons
ISBN-13	9781118228920	Portion	Image/photo/illustration
			0.00 USD Republication Permission

LICENSED CONTENT

Publication Title	Surfactants and Interfacial Phenomena	Country	United States of America
Author/Editor	Rosen, Milton J., Kunjappu, Joy T.	Rightholder	John Wiley & Sons - Books
Date	04/03/2012	Publication Type	Book
Language	English		

REQUEST DETAILS

Portion Type	Image/photo/illustration	Distribution	Worldwide
Number of Images / Photos / Illustrations	5	Translation	Original language of publication
Format (select all that apply)	Electronic	Copies for the Disabled?	No
Who Will Republish the Content?	Academic institution	Minor Editing Privileges?	No
Duration of Use	Life of current edition	Incidental Promotional Use?	No
Lifetime Unit Quantity	Up to 499	Currency	USD
Rights Requested	Main product		

NEW WORK DETAILS

Title	Adsorption of cocamidopropyl betaine on analogue reservoir rocks at static and dynamic conditions	Institution Name	PUC-Rio
		Expected Presentation Date	2023-09-09
Instructor Name	Prof Aurora Perez Gramatges		

ADDITIONAL DETAILS

The Requesting Person/Organization to Appear on the License
Pablo Godoy

REQUESTED CONTENT DETAILS

Title, Description or Numeric Reference of the Portion(s)	Figures 2-5,2-6,2-7,2-9,2-10	Title of the Article/Chapter the Portion Is From	Chapter 2
Editor of Portion(s)	Milton J. Rosen	Author of Portion(s)	Rosen, Milton J.; Kunjappu, Joy T.
Volume / Edition	4	Publication Date of Portion	2012-04-03
Page or Page Range of Portion	Pages 39,40 and 41		

John Wiley & Sons - Books Terms and Conditions

No right, license or interest in any trademark, trade name, service mark or other branding ("Marks") of WILEY or its licensors is granted hereunder, and you agree that you shall not assert any such right, license or interest with respect thereto. You may not alter, remove or suppress in any manner any copyright, trademark or other notices displayed by the Wiley material. This Agreement will be void if the Type of Use, Format, Circulation, or Requestor Type was misrepresented during the licensing process. In no instance may the total amount of Wiley Materials used in any Main Product, Compilation or Collective work comprise more than 5% (if figures/tables) or 15% (if full articles/chapters) of the (entirety of the) Main Product, Compilation or Collective Work. Some titles may be available under an Open Access license. It is the Licensor's responsibility to identify the type of Open Access license on which the requested material was published, and comply fully with the terms of that license for the type of use specified. Further details can be found on Wiley Online Library <http://olabout.wiley.com/WileyCDA/Section/id-410996.html>

Figure 9 from Ref [25]:

Adsorption of Anionic Surfactant on Alumina and Reuse of the Surfactant-Modified Alumina for the Removal of Crystal Violet from Aquatic Environment

Author: Asok Adak, Manas Bandyopadhyay, et al

Publication: Journal of Environmental Science & Health, Part A

Publisher: Taylor & Francis

Date: Jan 1, 2005

Rights managed by Taylor & Francis

Thesis/Dissertation Reuse Request

Taylor & Francis is pleased to offer reuses of its content for a thesis or dissertation free of charge contingent on resubmission of permission request if work is published.

[BACK](#)

[CLOSE](#)

Figure 10 from Ref [32]:

Adsorption of Zwitterionic Surfactant on Limestone Measured with High-Performance Liquid Chromatography: Micelle-Vesicle Influence

Author: David Aaron Nieto-Alvarez, Luis S. Zamudio-Rivera, Erick E. Luna-Rojero, et al

Publication: Langmuir

Publisher: American Chemical Society

Date: Oct 1, 2014

Copyright © 2014, American Chemical Society

PERMISSION/LICENSE IS GRANTED FOR YOUR ORDER AT NO CHARGE

This type of permission/license, instead of the standard Terms and Conditions, is sent to you because no fee is being charged for your order. Please note the following:

- Permission is granted for your request in both print and electronic formats, and translations.
- If figures and/or tables were requested, they may be adapted or used in part.
- Please print this page for your records and send a copy of it to your publisher/graduate school.
- Appropriate credit for the requested material should be given as follows: "Reprinted (adapted) with permission from (COMPLETE REFERENCE CITATION). Copyright (YEAR) American Chemical Society." Insert appropriate information in place of the capitalized words.
- One-time permission is granted only for the use specified in your RightsLink request. No additional uses are granted (such as derivative works or other editions). For any uses, please submit a new request.

If credit is given to another source for the material you requested from RightsLink, permission must be obtained from that source.

[BACK](#)

[CLOSE WINDOW](#)

Figure 11 from Ref [45]:

CCC | RightsLink

My Orders My Library My Profile Welcome pabloqui@aluno.puc-rio.br [Log out](#) | [Help](#) | [FAQ](#)

My Orders > Orders > All Orders

License Details

This Agreement between Mr. Pablo Godoy ("You") and Elsevier ("Elsevier") consists of your license details and the terms and conditions provided by Elsevier and Copyright Clearance Center.

[Print](#) [Copy](#)

License Number	5618260893388
License date	Aug 29, 2023
Licensed Content Publisher	Elsevier
Licensed Content Publication	Journal of Colloid and Interface Science
Licensed Content Title	Characterizing adsorption of associating surfactants on carbonates surfaces
Licensed Content Author	Guoqing Jian,Maura Puerto,Anna Wehowsky,Clarence Miller,George J. Hirasaki,Sibani L. Biswal
Licensed Content Date	Mar 1, 2018
Licensed Content Volume	513
Licensed Content Issue	n/a
Licensed Content Pages	9
Type of Use	reuse in a thesis/dissertation
Portion	figures/tables/illustrations
Number of figures/tables/illustrations	1
Format	electronic
Are you the author of this Elsevier article?	No
Will you be translating?	No
Title	Adsorption of cocamidopropyl betaine on analogue reservoir rocks under static and dynamic conditions
Institution name	PUC-Rio
Expected presentation date	Aug 2023
Order reference number	3389456
Portions	Figure 4 on page 688
Requestor Location	Mr. Pablo Godoy Av. Prefeito Dulcídio Cardoso
	Rio de Janeiro, RJ 22620-310 Brazil Attn: Mr. Pablo Godoy GB 494 6272 12
Publisher Tax ID	0.00 USD
Total	

[BACK](#)

Figure 12 from Ref [35]:



Comparative Study on the Static Adsorption Behavior of Zwitterionic Surfactants on Minerals in Middle Bakken Formation

Author: Xun Zhong, Hui Pu, Yanxia Zhou, et al

Publication: Energy & Fuels

Publisher: American Chemical Society

Date: Feb 1, 2019

Copyright © 2019, American Chemical Society

PERMISSION/LICENSE IS GRANTED FOR YOUR ORDER AT NO CHARGE

This type of permission/license, instead of the standard Terms and Conditions, is sent to you because no fee is being charged for your order. Please note the following:

- Permission is granted for your request in both print and electronic formats, and translations.
- If figures and/or tables were requested, they may be adapted or used in part.
- Please print this page for your records and send a copy of it to your publisher/graduate school.
- Appropriate credit for the requested material should be given as follows: "Reprinted (adapted) with permission from (COMPLETE REFERENCE CITATION). Copyright (YEAR) American Chemical Society." Insert appropriate information in place of the capitalized words.
- One-time permission is granted only for the use specified in your RightsLink request. No additional uses are granted (such as derivative works or other editions). For any uses, please submit a new request.

If credit is given to another source for the material you requested from RightsLink, permission must be obtained from that source.

BACK
CLOSE WINDOW

© 2023 Copyright - All Rights Reserved | Copyright Clearance Center, Inc. | Privacy statement | Data Security and Privacy | For California Residents | Terms and Conditions
Comments? We would like to hear from you. E-mail us at customercare@copyright.com

Figure 13 from Ref [48]:



My Orders
My Library
My Profile
Welcome pabloqui@aluno.puc-rio.br [Log out](#) | [Help](#) | [FAQ](#)

My Orders > Orders > All Orders

License Details

This Agreement between Mr. Pablo Godoy ("You") and Elsevier ("Elsevier") consists of your license details and the terms and conditions provided by Elsevier and Copyright Clearance Center.

Print
Copy

License Number	5618300788645
License date	Aug 29, 2023
Licensed Content Publisher	Elsevier
Licensed Content Publication	Applied Surface Science
Licensed Content Title	Adsorption of surfactants on sand surface in enhanced oil recovery: Isotherms, kinetics and thermodynamic studies
Licensed Content Author	Achinta Bera.T. Kumar,Keka Ojha,Ajay Mandal
Licensed Content Date	Nov 1, 2013
Licensed Content Volume	284
Licensed Content Issue	n/a
Licensed Content Pages	13
Type of Use	reuse in a thesis/dissertation
Portion	figures/tables/illustrations
Number of figures/tables/illustrations	1
Format	electronic
Are you the author of this Elsevier article?	No
Will you be translating?	No
Title	Adsorption of cocamidopropyl betaine on analogue reservoir rocks under static and dynamic conditions
Institution name	PUC-Rio
Expected presentation date	Aug 2023
Order reference number	5566
Portions	Figure 10, page 95
Requestor Location	Mr. Pablo Godoy Av. Prefeito Dulcídio Cardoso
	Rio de Janeiro, RJ 22620-310 Brazil
	Attn: Mr. Pablo Godoy GB 494 6272 12
Publisher Tax ID	
Total	0.00 USD

BACK

Copyright © 2023 Copyright Clearance Center, Inc. All Rights Reserved. Privacy statement. Data Security and Privacy. For California Residents. Terms and Conditions.
Comments? We would like to hear from you. E-mail us at customercare@copyright.com

Figure 14 from Ref [33]:

 **CCC RightsLink**

My Orders My Library My Profile Welcome pabloqui@aluno.puc-rio.br [Log out](#) | [Help](#) | [FAQ](#)

My Orders > Orders > All Orders

License Details

This Agreement between Mr. Pablo Godoy ("You") and Elsevier ("Elsevier") consists of your license details and the terms and conditions provided by Elsevier and Copyright Clearance Center.

[Print](#) [Copy](#)

License Number	5618311141526
License date	Aug 29, 2023
Licensed Content Publisher	Elsevier
Licensed Content Publication	Journal of Petroleum Science and Engineering
Licensed Content Title	Static and dynamic adsorption of anionic and amphoteric surfactants with and without the presence of alkali
Licensed Content Author	Weifeng Lv, Brigitte Bazin, Desheng Ma, Qingjie Liu, Dong Han, Kangyun Wu
Licensed Content Date	May 1, 2011
Licensed Content Volume	77
Licensed Content Issue	2
Licensed Content Pages	10
Type of Use	reuse in a thesis/dissertation
Portion	figures/tables/illustrations
Number of figures/tables/illustrations	2
Format	electronic
Are you the author of this Elsevier article?	No
Will you be translating?	No
Title	Adsorption of cocamidopropyl betaine on analogue reservoir rocks under static and dynamic conditions
Institution name	PUC-Rio
Expected presentation date	Aug 2023
Order reference number	5667
Portions	Figures 10 and 12 on pages 214 and 216
Requestor Location	Mr. Pablo Godoy Av. Prefeito Dulcídio Cardoso Rio de Janeiro, RJ 22620-310 Brazil Attn: Mr. Pablo Godoy GB 494 6272 12
Publisher Tax ID	
Total	0.00 USD

[BACK](#)

Figure 15 (a) from Ref [12]:

CCC Marketplace

Order Number: 1391464
Order Date: 29 Aug 2023

Payment Information

Pablo Godoy pabloalbgodoy@gmail.com Payment method: Invoice	Billing Address: Mr. Pablo Godoy Av. Prefeito Dulcildo Cardoso Rio De Janeiro, RJ 22620-310 Brazil +55 (21)996572727 pabloalbgodoy@gmail.com	Customer Location: Mr. Pablo Godoy Av. Prefeito Dulcildo Cardoso Rio De Janeiro, RJ 22620-310 Brazil
---	---	---

Order Details

1. Journal of applied polymer science Billing Status: Open

Article: Adsorption behavior of cocamidopropyl betaine under conditions of high temperature and high salinity

Order License ID	1391464-1	Type of Use	Republish in a thesis/dissertation
Order detail status	Completed	Publisher	JOHN/WILEY & SONS, INC.
ISSN	0021-8995	Portion	Image/photo/illustration

0.00 USD
Republishing Permission

LICENSED CONTENT

Publication Title	Journal of applied polymer science	Publication Type	Journal
Article Title	Adsorption behavior of cocamidopropyl betaine under conditions of high temperature and high salinity	Start Page	n/a
Date	01/01/1959	End Page	n/a
Language	English, French, German	Issue	12
Country	United States of America	Volume	131
Rightsholder	John Wiley & Sons - Books		

REQUEST DETAILS

Portion Type	Image/photo/illustration	Distribution	Worldwide
Number of Images / Photos / Illustrations	3	Translation	Original language of publication
Format (select all that apply)	Electronic	Copies for the Disabled?	No
Who Will Republish the Content?	Academic institution	Minor Editing Privileges?	No
Duration of Use	Life of current edition	Incidental Promotional Use?	No
Lifetime Unit Quantity	Up to 499	Currency	USD
Rights Requested	Main product		

NEW WORK DETAILS

Title	Adsorption of cocamidopropyl betaine on analogue reservoir rocks at static and dynamic conditions	Institution Name	PUC-Rio
Instructor Name	Prof. Aurora Perez Gramatges	Expected Presentation Date	2023-09-09

ADDITIONAL DETAILS

The Requesting Person/Organization to Appear on the License: Pablo Godoy

REQUESTED CONTENT DETAILS

Title, Description or Numeric Reference of the Portion(s)	Figures 1, 4 and 6	Title of the Article/Chapter the Portion is From	Adsorption behavior of cocamidopropyl betaine under conditions of high temperature and high salinity
Editor of Portion(s)	Da, Cai; Zhao, Jianhui; Yan, Lipeng; Zhao, Mingwei	Author of Portion(s)	Da, Cai; Zhao, Jianhui; Yan, Lipeng; Zhao, Mingwei
Volume / Edition	131	Publication Date of Portion	2014-06-15
Page or Page Range of Portion	Pages 2, 4 and 5		

John Wiley & Sons - Books Terms and Conditions

No right, license or interest in any trademark, trade name, service mark or other branding ("Marks") of WILEY or its licensors is granted hereunder, and you agree that you shall not assert any such right, license or interest with respect thereto. You may not alter, remove or suppress in any manner any copyright, trademark or other notices displayed by the Wiley material. This Agreement will be void if the Type of Use, Format, Circulation, or Requestor Type was misrepresented during the licensing process. In no instance may the total amount of Wiley Materials used in any Main Product, Compilation or Collective work comprise more than 5% (if figures/tables) or 15% (if full articles/chapters) of the (entirety of the) Main Product, Compilation or Collective Work. Some titles may be available under an Open Access license. It is the Licensors' responsibility to identify the type of Open Access license on which the requested material was published, and comply fully with the terms of that license for the type of use specified. Further details can be found on Wiley Online Library <http://olabout.wiley.com/WileyCDA/Section/Id-410895.html>.

Figure 15 (b) from Ref [52]:

 **CCC RightsLink**

[My Orders](#) [My Library](#) [My Profile](#) Welcome pabloqui@aluno.puc-rio.br [Log out](#) | [Help](#) | [FAQ](#)

My Orders > Orders > All Orders

License Details

This Agreement between Mr. Pablo Godoy ("You") and Elsevier ("Elsevier") consists of your license details and the terms and conditions provided by Elsevier and Copyright Clearance Center.

[Print](#) [Copy](#)

License Number	5618331113680
License date	Aug 29, 2023
Licensed Content Publisher	Elsevier
Licensed Content Publication	Colloids and Surfaces A: Physicochemical and Engineering Aspects
Licensed Content Title	Surface properties and adsorption behavior of cocamidopropyl dimethyl amine oxide under high temperature and high salinity conditions
Licensed Content Author	Jianhui Zhao,Caili Dai,Jichao Fang,Xuan Feng,Lipeng Yan,Mingwei Zhao
Licensed Content Date	May 20, 2014
Licensed Content Volume	450
Licensed Content Issue	n/a
Licensed Content Pages	6
Type of Use	reuse in a thesis/dissertation
Portion	figures/tables/illustrations
Number of figures/tables/illustrations	3
Format	electronic
Are you the author of this Elsevier article?	No
Will you be translating?	No
Title	Adsorption of cocamidopropyl betaine on analogue reservoir rocks under static and dynamic conditions
Institution name	PUC-Rio
Expected presentation date	Aug 2023
Order reference number	5668
Portions	Figures 1, 4 and 5 on pages 94 and 97
Requestor Location	Mr. Pablo Godoy Av. Prefeito Dulcídio Cardoso Rio de Janeiro, RJ 22620-310 Brazil Attn: Mr. Pablo Godoy GB 494 6272 12
Publisher Tax ID	
Total	0.00 USD

[BACK](#)

Copyright © 2023 Copyright Clearance Center, Inc. All Rights Reserved. [Privacy statement](#). [Data Security and Privacy](#). For California Residents. [Terms and Conditions](#).
Comments? We would like to hear from you. E-mail us at customer@copyright.com

Figure 16 from Ref [62]:

CCC RightsLink

My Orders My Library My Profile Welcome pabloqui@aluno.puc-rio.br [Log out](#) | [Help](#) | [FAQ](#)

My Orders > Orders > All Orders

License Details

This Agreement between Mr. Pablo Godoy ("You") and Elsevier ("Elsevier") consists of your license details and the terms and conditions provided by Elsevier and Copyright Clearance Center.

[Print](#) [Copy](#)

License Number	5618340862525
License date	Aug 29, 2023
Licensed Content Publisher	Elsevier
Licensed Content Publication	Microchemical Journal
Licensed Content Title	Analytical applications of admicelle and hemimicelle solid phase extraction of organic analytes
Licensed Content Author	Sriatha Gangula, Shing-Yi Suen, Eric D. Conte
Licensed Content Date	May 1, 2010
Licensed Content Volume	95
Licensed Content Issue	1
Licensed Content Pages	3
Type of Use	reuse in a thesis/dissertation
Portion	figures/tables/illustrations
Number of figures/tables/illustrations	1
Format	electronic
Are you the author of this Elsevier article?	No
Will you be translating?	No
Title	Adsorption of cocamidopropyl betaine on analogue reservoir rocks under static and dynamic conditions
Institution name	PUC-Rio
Expected presentation date	Aug 2023
Order reference number	55669
Portions	Figure 1 on page 3
Requestor Location	Mr. Pablo Godoy Av. Prefeito Dulcídio Cardoso Rio de Janeiro, RJ 22620-310 Brazil Attn: Mr. Pablo Godoy GB 494 6272 12
Publisher Tax ID	
Total	0.00 USD

[BACK](#)

Figure 17 from Ref [64]:

CCC | RightsLink

My Orders My Library My Profile Welcome pabloqui@aluno.puc-rio.br [Log out](#) | [Help](#) | [FAQ](#)

My Orders > Orders > All Orders

License Details

This Agreement between Mr. Pablo Godoy ("You") and Elsevier ("Elsevier") consists of your license details and the terms and conditions provided by Elsevier and Copyright Clearance Center.

[Print](#) [Copy](#)

License Number	5618341164761
License date	Aug 29, 2023
Licensed Content Publisher	Elsevier
Licensed Content Publication	Chemical Engineering Science
Licensed Content Title	Modelling dynamic adsorption of an anionic surfactant on Berea sandstone with radial flow
Licensed Content Author	W. Kwok, R.E. Hayes, H.A. Nasr-El-Din
Licensed Content Date	Mar 1, 1995
Licensed Content Volume	50
Licensed Content Issue	5
Licensed Content Pages	15
Type of Use	reuse in a thesis/dissertation
Portion	figures/tables/illustrations
Number of figures/tables/illustrations	1
Format	electronic
Are you the author of this Elsevier article?	No
Will you be translating?	No
Title	Adsorption of cocamidopropyl betaine on analogue reservoir rocks under static and dynamic conditions
Institution name	PUC-Rio
Expected presentation date	Aug 2023
Order reference number	55670
Portions	Figure 7 on page 778
Requestor Location	Mr. Pablo Godoy Av. Prefeito Dulcídio Cardoso Rio de Janeiro, RJ 22620-310 Brazil Attn: Mr. Pablo Godoy GB 494 6272 12
Publisher Tax ID	0.00 USD
Total	

[BACK](#)

Copyright © 2023 Copyright Clearance Center, Inc. All Rights Reserved. [Privacy statement](#). [Data Security and Privacy](#). For California Residents. [Terms and Conditions](#).
Comments? We would like to hear from you. E-mail us at customer@copyright.com

Figure 18 from Ref [75]:

CCC | RightsLink

My Orders My Library My Profile Welcome pabloqui@aluno.puc-rio.br Log out Help FAQ

My Orders > Orders > All Orders

License Details

This Agreement between Mr. Pablo Godoy ("You") and Elsevier ("Elsevier") consists of your license details and the terms and conditions provided by Elsevier and Copyright Clearance Center.

[Print](#) [Copy](#)

License Number	5618360831471
License date	Aug 29, 2023
Licensed Content Publisher	Elsevier
Licensed Content Publication	Journal of Colloid and Interface Science
Licensed Content Title	A Surface Structural Approach to Ion Adsorption: The Charge Distribution (CD) Model
Licensed Content Author	T. Hiemstra,W.H. Van Riemsdijk
Licensed Content Date	May 10, 1996
Licensed Content Volume	179
Licensed Content Issue	2
Licensed Content Pages	21
Type of Use	reuse in a thesis/dissertation
Portion	figures/tables/illustrations
Number of figures/tables/illustrations	1
Format	electronic
Are you the author of this Elsevier article?	No
Will you be translating?	No
Title	Adsorption of cocamidopropyl betaine on analogue reservoir rocks under static and dynamic conditions
Institution name	PUC-Rio
Expected presentation date	Aug 2023
Order reference number	55677
Portions	Figure 2 on page 491
Requestor Location	Mr. Pablo Godoy Av. Prefeito Dulcídio Cardoso Rio de Janeiro, RJ 22620-310 Brazil Attn: Mr. Pablo Godoy GB 494 6272 12
Publisher Tax ID	
Total	0.00 USD

[BACK](#)

Copyright © 2023 Copyright Clearance Center, Inc. All Rights Reserved. Privacy statement Data Security and Privacy For California Residents. Terms and Conditions. Comments? We would like to hear from you. E-mail us at customercare@copyright.com

Figure 19 from Ref [82]:

CCC | RightsLink ? Help ▾ Live Chat



Electrokinetic behavior of artificial and natural calcites: A review of experimental measurements and surface complexation models
 Author: María Bonto,Ali A. Eftekhari,Hamidreza M. Nick
 Publication: Advances in Colloid and Interface Science
 Publisher: Elsevier
 Date: March 2022
 © 2022 The Authors. Published by Elsevier B.V.

Creative Commons

This is an open access article distributed under the terms of the [Creative Commons CC-BY](#) license, which permits unrestricted use, distribution, and reproduction in any medium, provided the original work is properly cited.

You are not required to obtain permission to reuse this article.

To request permission for a type of use not listed, please contact [Elsevier Global Rights Department](#).

Are you the [author](#) of this Elsevier journal article?

© 2023 Copyright - All Rights Reserved | Copyright Clearance Center, Inc. | Privacy statement | Data Security and Privacy
 | For California Residents | Terms and ConditionsComments? We would like to hear from you. E-mail us at customercare@copyright.com